

# Imaging and Photodynamic Therapy: Mechanisms, Monitoring, and Optimization

Jonathan P. Celli,<sup>†</sup> Bryan Q. Spring,<sup>†</sup> Imran Rizvi,<sup>†,‡</sup> Conor L. Evans,<sup>†</sup> Kimberley S. Samkoe,<sup>‡</sup> Sarika Verma,<sup>†</sup> Brian W. Pogue,<sup>†,‡</sup> and Tayyaba Hasan<sup>\*,†</sup>

Wellman Center for Photomedicine, Massachusetts General Hospital and Harvard Medical School, Boston, Massachusetts 02114, and Thayer School of Engineering, Dartmouth College, Hanover, New Hampshire 03755

Received September 4, 2009

## Contents

1. Introduction	2795	4.5. Optical Coherence Tomography in Photodynamic Therapy	2819
1.1. Photodynamic Therapy and Imaging	2795	4.5.1. Optical Coherence Tomography Background	2819
1.2. Photochemical and Photophysical Basis of Photodynamic Therapy and Related Imaging	2799	4.5.2. Noninvasive Visualization of Photodynamic Therapy in Ophthalmology	2819
2. Imaging of Photosensitizer Fluorescence for Detection of Disease and Optimization of Surgical Resection	2800	4.5.3. Doppler Optical Coherence Tomography Monitors the Vascular Response to Photodynamic Therapy	2820
2.1. Overview of Photosensitizer Fluorescence Detection	2800	4.5.4. In Vitro Model Treatment Response Imaging with Optical Coherence Tomography	2820
2.2. Early PS Fluorescence Studies	2801	5. Molecular Imaging of Dynamic Molecular Mechanisms Induced by PDT	2821
2.3. $\delta$ -Aminolevulinic Acid-Induced Protoporphyrin IX	2802	5.1. Overview	2821
2.4. Photosensitizer Fluorescence Detection for Disease-Specific Applications	2804	5.2. Imaging Molecular Pathways Involved in PDT-Induced Apoptosis	2822
2.4.1. Bladder Cancer	2804	5.2.1. Green Fluorescent Protein Sensors for Visualizing Proapoptotic Factor Activation and Trafficking	2822
2.4.2. Brain Cancer	2804	5.2.2. Caspase-Activated Fluorescent Reporter of Apoptosis	2823
2.4.3. Ovarian Cancer	2807	5.3. Imaging Biomarkers of Therapeutic Responses to PDT	2824
2.4.4. Photosensitizer Fluorescence Detection in Skin Cancer	2808	5.3.1. Heat Shock Protein 70	2824
2.4.5. Photosensitizer Fluorescence Detection in Oral Cancer	2810	5.3.2. Matrix Metalloproteinase	2825
2.4.6. Other Applications of Photosensitizer Fluorescence Detection	2810	5.3.3. Vascular Endothelial Growth Factor	2825
2.5. Perspective and Future Outlook for PFD	2811	5.4. PET and MRI for Molecular Imaging of Biological Responses to PDT	2827
3. Targeted Photosensitizers as Selective Therapeutic and Imaging Agents	2811	5.5. Summary of Molecular Imaging To Elucidate Biological Mechanisms Induced by PDT	2828
3.1. Overview	2811	6. Perspective and Future Directions	2828
3.2. Site-Specific Delivery	2811	6.1. In Vivo Tracking of Cell Migration in Response to Photodynamic Therapy	2829
3.3. Site-Activated Constructs	2813	6.2. Multiphoton Excitation for Deep Tissue Imaging	2831
4. Imaging for Planning, Assessment, and Monitoring of Photodynamic Therapy Response	2815	6.3. Monitoring Molecular Oxygen for Photodynamic Therapy Dosimetry	2831
4.1. Imaging Methods for Optimization and Dosimetry of Photodynamic Therapy	2815	7. List of Abbreviations	2832
4.2. Online Monitoring of Photodynamic Therapy Response	2815	8. Acknowledgments	2833
4.3. Imaging Techniques for Assessment of the Photodynamic Therapy Outcome	2816	9. References	2833
4.4. Monitoring Oxygen and Dose Rate Effects in PDT	2817		
4.4.1. Oxygen Measurement	2817		
4.4.2. Dose Rate Effects upon the Outcome	2818		
4.4.3. Vascular Response and Tissue Oxygen	2818		

## 1. Introduction

### 1.1. Photodynamic Therapy and Imaging

The purpose of this review is to present the current state of the role of imaging in photodynamic therapy (PDT). For the reader to fully appreciate the context of the discussions embodied in this paper we begin with an overview of the PDT process, starting with a brief historical perspective

\* To whom correspondence should be addressed. E-mail: thasan@partners.org.

<sup>†</sup> Massachusetts General Hospital and Harvard Medical School.

<sup>‡</sup> Dartmouth College.



Jonathan Celli is a postdoctoral fellow in the laboratory of Dr. Tayyaba Hasan at the Wellman Center for Photomedicine at Massachusetts General Hospital and Harvard Medical School. He received his B.S. in Physics from the University of Massachusetts (2002) and his Ph.D. in Physics from Boston University (2007). There, under the mentorship of Professors Shyamsunder Erramilli and Rama Bansil, he studied the pH-dependent rheology and microrheology of gastric mucin and motility of the ulcer-causing bacterium *Helicobacter pylori*. In his current research, he draws upon his training in microscopy and quantitative imaging to study PDT treatment response in pancreatic and ovarian tumor models toward the goal of designing combination treatments to enhance outcomes.



Imran Rizvi is a Doctoral Candidate at the Thayer School of Engineering at Dartmouth College and a Graduate Research Fellow at the Wellman Center for Photomedicine at Massachusetts General Hospital. His thesis research, co-advised by Professors Tayyaba Hasan and Brian Pogue, draws on concepts from tissue engineering and tumor biology to create in vitro 3D models for human tumors that can be used to design and evaluate PDT-based combination regimens for cancer. Imran received a B.A. in Natural Sciences—Biology from Johns Hopkins University (1997) and an M.S. in Tumor Biology from Georgetown University (2003).



Bryan Quilty Spring is a postdoctoral fellow in the Wellman Center for Photomedicine at Massachusetts General Hospital and Harvard Medical School. He received a B.S. in Physics from Iowa State University in 2002 and a Ph.D. in Biophysics and Computational Biology from the University of Illinois at Urbana—Champaign in 2008. His doctoral work with Robert M. Clegg focused on developing video-rate fluorescence lifetime imaging and quantitative measurements of Förster resonance energy transfer. Since joining Tayyaba Hasan's laboratory in 2008 he has become immersed in tumor biology, animal models of cancer, and translational research. His current research aims to develop online microendoscopic molecular imaging for monitoring tumor cell signaling during treatment towards the rational design of combination treatments for pancreatic and ovarian cancer.

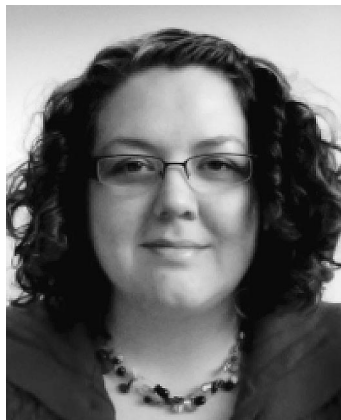
followed by detailed discussions of specific applications of imaging in PDT. Each section starts with an overview of the specific topic and, where appropriate, ends with a summary and future directions. The review closes with the authors' perspective of the areas of future emphasis and promise. The basic premise of this review is that a combination of imaging and PDT will provide improved research and therapeutic strategies.

PDT is a photochemistry-based approach that uses a light-activatable chemical, termed a photosensitizer (PS), and light of an appropriate wavelength to impart cytotoxicity via the generation of reactive molecular species (Figure 1A). In clinical settings, the PS is typically administered intrave-



Conor Evans received his B.S. in chemical physics from Brown University in 2002 and completed his Ph.D. in physical chemistry in 2007 at Harvard University under the instruction of Prof. X. Sunney Xie. He worked on coherent anti-Stokes Raman scattering (CARS) microscopy during his doctoral work and became fascinated in applying advanced imaging approaches for solving critical problems in cancer. He moved to the Wellman Center for Photomedicine at Massachusetts General Hospital and joined the groups of Drs. Tayyaba Hasan and Johannes de Boer to pursue a translational cancer imaging research program. His current research interests include fighting treatment-resistant ovarian cancer, spectroscopic and interferometric imaging technologies, and photodynamic therapy. He was recently selected to join the Wellman faculty through a competitive search and holds an appointment at Harvard Medical School.

nously or topically, followed by illumination using a light delivery system suitable for the anatomical site being treated (Figure 1B). The time delay, often referred to as the drug–light interval, between PS administration and the start of illumination with currently used PSs varies from 5 min to 24 h or more depending on the specific PS and the target disease. Strictly speaking, this should be referred to as the PS–light interval, as at the concentrations typically used the PS is not a drug, but the drug–light interval terminology seems to be used fairly frequently. Typically, the useful range of wavelengths for therapeutic activation of the PS is 600–800 nm to avoid interference by endogenous chromophores within the body and yet maintain the energetics necessary for the generation of cytotoxic species (as discussed below) such as singlet oxygen ( $^1\text{O}_2$ ). However, it is



Kimberley S. Samkoe is a postdoctoral fellow at the Thayer School of Engineering at Dartmouth College (Hanover, NH, U.S.A.). She obtained her B.Sc. (Hons) in Biochemistry from the University of Regina (Regina, SK, Canada) in 2001 and her Ph.D. from the University of Calgary (Calgary, AB, Canada) in Biophysical Chemistry in 2007. Her Ph.D. thesis demonstrated proof-of-principle concepts for two-photon excitation photodynamic therapy, and she continues to have an interest in photodynamic therapy for the treatment of solid tumors. She also has particular interest in medical imaging with the integration of optical spectroscopy, specifically fluorescence, for cancer diagnosis and therapy monitoring.



Sarika Verma, Ph.D., is a Research Scientist and Program Manager at the Wellman Center for Photomedicine and a Research Associate at Harvard Medical School. She received her B.Sc. Honors degree and M.Sc. organic chemistry degree from Delhi University, India, in 1998 and 2000, respectively. She completed her Ph.D. in polymer chemistry from the University of Massachusetts, Lowell, in 2005 and worked as a postdoctoral research fellow at Wellman Center for Photomedicine in 2006–2007. Her research work is focused on target-specific photosensitizers for photodynamic therapy.

important to note that photosensitizers can also serve as fluorescence imaging agents for which activation with light in the 400 nm range is often used and has been extremely useful in diagnostic imaging applications as described extensively in section 2 of this review. The obvious limitation of short-wavelength excitation is the lack of tissue penetration so that the volumes that are probed under these conditions are relatively shallow.

Historically, the concept of combining light with a chemical agent has ancient beginnings. Records of the therapeutic effect of sunlight activation of psoralens dates back to approximately 3000 years ago when this early photochemotherapy was used for repigmentation of vitiligo in both ancient Egypt and India.<sup>1</sup> The therapeutic effect of sunlight itself (in the absence of an exogenous chemical agent) can be traced back over 5000 years ago, to India, Egypt, and China, and later became the underpinning of the

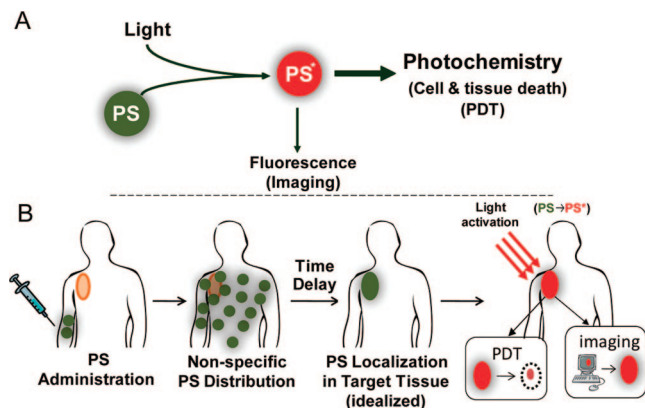


Brian W. Pogue, Ph.D., received his B.Sc. Honors degree and M.Sc. degree from York University, Canada, in 1989 and 1991, respectively. He completed his Ph.D. in Physics from McMaster University in 1995 and a postdoctoral research at the Wellman Center for Photomedicine at the Massachusetts General Hospital from 1995–1996. He joined the Thayer School of Engineering in 1996 and is currently Professor of Engineering Sciences, with adjunct appointments in Surgery and Physics and Astronomy at Dartmouth. He is currently Dean of Graduate Studies at Dartmouth and directs research in the areas of optical spectroscopy of cancer, imaging research, and imaging cancer pathobiology. He is Deputy Editor of *Optics Letters* and Associate Editor for *Medical Physics*, the *Journal of Biomedical Optics*, and the *Journal of Photochemistry and Photobiology B*.



Tayyaba Hasan, Ph.D., is a Professor of Dermatology at Harvard Medical School and Professor of Health Sciences and Technology at Harvard–MIT. She is based at the Wellman Center for Photomedicine, Massachusetts General Hospital (MGH). She is also the Director of the Office for Research Career Development at MGH. She completed her Ph.D. in Physical Organic Chemistry from University of Arkansas in 1980 and a postdoctoral research at the University of Pennsylvania from 1980–1982. She started at the Wellman Center as an Assistant Biochemist in 1982, and her research is in photobiology and photodynamic therapy with over 200 publications and inventions. Dr. Hasan is an inventor of the FDA-approved photodynamic treatment of Age-Related Macular Degeneration. She is a recipient of William Silen Lifetime Achievement in Mentoring Award from Harvard Medical School and Pioneer award in Biomedical Optics for Bench to Bedside Translation from the National Institute of Health.

practice of heliotherapy, associated with the famous Greek physician Herodotus.<sup>2</sup> A timeline starting with these ancient developments and leading into more recent milestones in the evolution of PDT is presented in Figure 2. PDT, as we know it currently, may be attributed to the observations of Raab in 1900 of the cytotoxicity to paramecia exposed to acridine orange and light. The more recent era of PDT application arose following the discovery by Schwartz and Lipson that the acid treatment of hematoporphyrin (HP) yielded a mixture of chemicals, termed hematoporphyrin derivative (HpD),



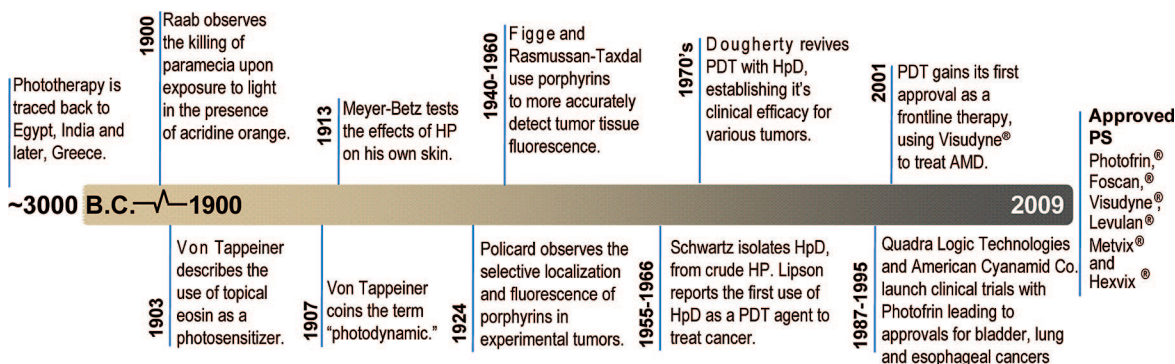
**Figure 1.** (A) Schematic representation of PDT where PS is a photoactivatable multifunctional agent, which upon light activation can serve as both an imaging agent and a therapeutic agent. (B) Schematic representation of the sequence of administration, localization, and light activation of the PS for PDT or fluorescence imaging. Typically the PS is delivered systemically and allowed to circulate for an appropriate time interval (the “drug–light interval”), during which the PS accumulates preferentially in the target lesion(s) prior to light activation. In the idealized depiction here the PS accumulation is shown to be entirely in the target tissue; however, even if this is not the case, light delivery confers a second layer of selectivity so that the cytotoxic effect will be generated only in regions where both drug and light are present. Upon localization of the PS, light activation will result in fluorescence emission which can be implemented for imaging applications, as well as generation of cytotoxic species for therapy. In the former case light activation is achieved with a low fluence rate to generate fluorescence emission with little or no cytotoxic effect, while in the latter case a high fluence rate is used to generate a sufficient concentration of cytotoxic species to achieve biological effects.

which had tumor-localizing properties.<sup>3</sup> It was also found that this mixture could be activated with red light, resulting in the PDT effect. Although the exact characterization of the constituents was not clear then and remains somewhat of a mystery even now, Kessel did confirm that HpD was primarily a mixture of esters and ethers of HP.<sup>4</sup> Efforts led by Dougherty in the 1970s resulted in the development of PDT as the viable clinical modality that we know today when he established the clinical efficacy of HpD in various tumors.<sup>5</sup> Despite the fact that PDT was known for its tumoricidal and antimicrobial properties for over a century, and that thousands of patients had been treated with some version of HpD, controlled clinical trials did not commence until the late 1980s and early 1990s when QLT Photo Therapeutics (Vancouver, British Columbia, Canada) and Lederle Laboratories (American Cyanamid, Pearl River, NY) formed a partnership to achieve approvals for the clinical use of PDT. The first approval of PDT by a regulatory authority occurred

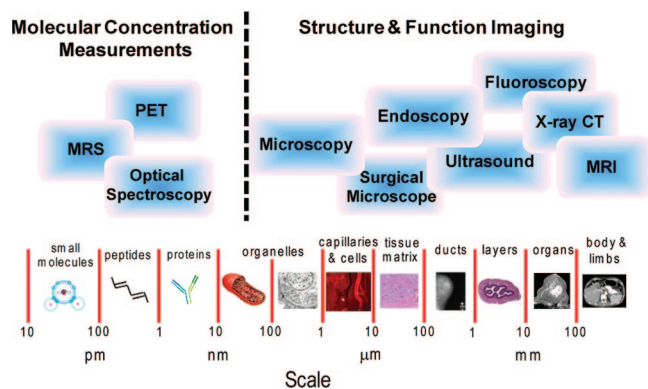
in 1993 in Canada using a more purified and better characterized version of HpD called Photofrin (PF) for the treatment of specific cases of bladder cancer.<sup>6</sup> The first FDA approval of PDT in the United States, also with PF, was obtained in 1995 for palliation of obstructive esophageal cancer.<sup>6</sup> The success of treatments with PF in the early 1960s and subsequent approvals generated worldwide interest in this treatment modality, and the number of papers increased from a modest 112 in the first half of the century (1900–1955) to more than 15 000 in the second half (1955–2009), with more than 6000 papers in the past 5 years (source: “photodynamic” on Web of Science) (<http://apps.isiknowledge.com>).

Figure 2 presents a summary of approvals for PDT to date; in addition there are numerous ongoing clinical investigations and trials for several indications. The use of PDT in cancer treatment is usually palliative and typically for advanced disease. In ophthalmology, the demonstrated clinical success of PDT for treatment of choroidal neovascularization<sup>7</sup> led to FDA approval in 2000 of PDT as a first-line treatment for age-related macular degeneration (AMD), the leading cause of blindness in the eye among the elderly in the Western world. Currently over 2 million treatments have been performed for this indication, and it still represents the only first-line therapeutic application of PDT. In the context of this review, the integration of imaging for assessment of outcomes from PDT treatment of AMD has also had noted success as described in section 4.

The timeline in Figure 2 shows that the first indication of PDT-related imaging via fluorescence appeared in the 1920s with the report by Policard on the localization of tumors via HP imaging.<sup>8,9</sup> A detailed history of the emergence of fluorescence imaging with HP and related derivatives, as well as more recent applications with other PSs, is presented in section 2 on PS fluorescence detection (PFD). In section 2 the demonstrated utility of photosensitizer fluorescence for improving tumor margin resection and other clinical applications is described in detail for a variety of human diseases. Furthermore, the loss of fluorescence as the PS is photobleached during irradiation has also proved to be a valuable tool for treatment monitoring and dosimetry<sup>8–10</sup> as discussed in section 4. In the context of imaging and PDT, imaging can be used as both a research and a clinical tool. In the laboratory, imaging is useful for studying basic PDT mechanisms, for understanding PDT tissue interactions, for developing models of disease,<sup>10,11</sup> and as a marker of response to therapy.<sup>12</sup> In addition, imaging can provide a basis for establishing the likelihood of success of new therapeutic approaches.<sup>13–16</sup> Clinically, the use of imaging in PDT is similar to that in other therapeutic modalities, with a unique difference and advantage in the case of PDT: the



**Figure 2.** Timeline of selected milestones in the historical development of PDT.



**Figure 3.** Imaging platforms for molecular structural and functional imaging across a broad range of size scales. For molecular concentration imaging (left side of the figure), optical spectroscopy and magnetic resonance spectroscopy (MRS) are primarily employed, but positron emission tomography (PET) can be used for imaging at these length scales. For structural and molecular imaging at length scales greater than tens of nanometers (right side of the figure) a variety of imaging techniques can be employed including various types of microscopy, endoscopy, X-ray CT, and MRI depending on the size and composition of the structure being imaged.

same entity (PS) can act as both the therapeutic and the image contrast agent due to the PS's ability to fluoresce. To date, the only known exception is Tookad, a PS with a negligible fluorescence quantum yield.<sup>17,18</sup> The potential of PS fluorescence used in PDT lies in diagnosis, therapy monitoring, and guidance of surgery or other therapies. However, this does not preclude the use of other exogenous or endogenous contrast agents. The therapeutic outcome can be made more robust by including all forms of appropriate imaging platforms, with the choice of imaging modalities and contrast agents based on the question being addressed. In fact, it is likely that, in the long term, combinations of multiple imaging modalities and contrast agents will turn out to be most useful. Therefore, the current emphasis on efforts at multiplexing many aspects of imaging and treatment strategies<sup>19–22</sup> will greatly enhance the use of imaging in PDT.

This review covers the significance of imaging as it pertains to PDT and enhancing treatment outcome. A section on fundamental photochemical and photophysical principles that underlie PDT and much of PDT-related imaging follows this introduction (section 1.2). Figure 3 presents an overview of several imaging modalities that can be used in conjunction with PDT on the basis of their spatial scale and source of contrast. For example, as described in section 4, the quantification, detection, and characterization at the molecular level requires spectroscopy-based technologies, as is the case with efforts at imaging of <sup>1</sup>O<sub>2</sub>, which is believed to be a key species that leads to PDT cytotoxicity. Microscopic and endoscopic techniques are used in surgical guidance, therapy monitoring, and dosimetry. As questions arise at the organ level, tomographic techniques such as magnetic resonance imaging (MRI) and computed tomography (CT) (including optical tomography) become appropriate.

As pointed out earlier, imaging in PDT has multiple points of significance including diagnostics, therapy guidance, monitoring, treatment assessment, and mechanistic studies. Each of these topics is covered in a separate section below, and each section presents an overview of the particular topic. The uniqueness of PDT, in that the same molecule may serve as both the therapeutic agent and the imaging contrast agent,

has resulted in the development of the application of PS fluorescence for guidance of surgery and other interventions and is discussed in detail in section 2. Targeted fluorophore/PS imaging, summarized in section 3, is currently in a fairly nascent state and requires further development if imaging and treatment of occult disease are to become part of the PDT domain. Assessment of the treatment outcome is key to therapeutic success and is summarized for PDT applications in section 4. In this context, both optical and nonoptical imaging have been used to assess PDT outcomes. As with other therapies and PDT, these treatment outcomes are typically assessed somewhat later in time when the disease may have progressed due to incomplete response. The challenge currently, taken up by several laboratories, lies in developing online or early monitoring approaches so that strategies to combat poor response can be developed in a timely fashion. These concepts are discussed in sections 2–5.

For example, optical coherence tomography (OCT) has been used only minimally in conjunction with PDT so far, but the authors view OCT as a potential natural partner with PDT for detecting structural alterations resulting from treatment response and anticipate increasing development and use of OCT following PDT. Furthermore, considering that PDT can target the vasculature, current advances in OCT using Doppler techniques hold promise for online monitoring of vascular responses. For this reason a discussion of OCT imaging in PDT is included as section 4.5 of this review. A far less developed but promising application of OCT for PDT is in investigations of basic tumor biology, which is also discussed in section 4.5.

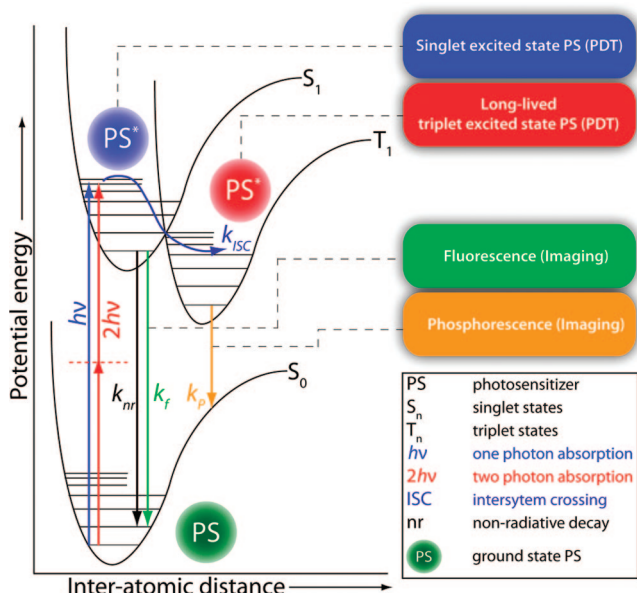
An understanding of the mechanisms involved in cell death following treatment is key to improving the treatment outcome, as this understanding could provide the rationale for combination therapies. Often treatment responses are dynamic, so that molecular-imaging-based real-time monitoring, often of secreted molecules, becomes important and presents a particular challenge. This forms the substance of section 5. This exciting area of imaging as it relates to PDT (and perhaps other therapies) has captured the interest of many investigators and is emerging as a promising field of development. We conclude with section 6, which provides a perspective and discusses future directions.

## 1.2. Photochemical and Photophysical Basis of Photodynamic Therapy and Related Imaging

All processes relevant to PDT, as currently practiced, can be initiated with visible light in the wavelength range of 400–800 nm. The relationship between the wavelength,  $\lambda$ , of light and the energy content,  $E$ , is governed by the equation

$$E = h\nu = hc/\lambda \quad (1)$$

where  $h$  is Planck's constant ( $6.63 \times 10^{-34}$  J s),  $\nu$  is the frequency, and  $c$  is the speed of light in a vacuum ( $2.98 \times 10^8$  m/s). Each unit represented by  $h\nu$  is referred to as a quantum of energy for the specific wavelength. Upon absorption of a quantum of energy, there are several possible pathways by which this energy can be dissipated, each with an associated probability of occurrence. For those pathways that involve radiation of the absorbed energy (such as fluorescence emission) this can be described in terms of the quantum yield of the system, the ratio of photons (quanta) emitted by a particular process to photons absorbed.



**Figure 4.** Perrin–Jablonski energy diagram for a PS molecule. Various processes during the excited-state lifetime of the PS and resulting from its relaxation back to its ground state are highlighted. While in its long-lived triplet excited state the PS may undergo excited-state reactions to generate cytotoxic species such as singlet molecular oxygen (via energy transfer from the PS to ground-state, triplet oxygen). While both the excited singlet state and triplet state are involved in photosensitized cell killing, photodynamic killing comes primarily from the triplet manifold. PS fluorescence and phosphorescence may be used to image PS localization in tissue, and time-resolved imaging techniques may be applied to monitor the PS's interactions with its microenvironment.

A simplified energy level diagram showing the possible pathways of energy absorption and dissipation is presented in Figure 4. Using conventional light sources, a single quantum of light is typically absorbed, causing the absorbing molecule to be electronically excited. The electronic states are represented by the singlet states,  $S_n$ , and the triplet states,  $T_n$ . (The singlet and the triplet excited states arise as a quantum mechanical consequence of electron spin.) The singlet excited states are rather short-lived, with typical values for PDT-related PS singlet-state lifetimes,  $\tau_S$ , being in nanoseconds, while the triplet-state lifetimes,  $\tau_T$ , are in the microsecond to millisecond range. With the absorption of a single photon of light, the molecule is promoted to an excited singlet state, for example,  $S_1$ . Other higher excited states can be populated depending on the photosensitizer and the excitation wavelength used. From this excited state, it may initiate photochemistry (depending on its chemical structure and lifetime) or undergo intersystem crossing to an electronically different excited state, for example, the first triplet state,  $T_1$ , with a rate constant of  $k_{isc}$ . From  $S_1$ , the excited molecule may also relax back to  $S_0$  by nonradiative decay (rate constant  $k_{nr}$ ) and generate heat or may re-emit radiation as fluorescence with a rate constant of  $k_f$ , which forms the basis of fluorescence imaging described in the sections below. In general,  $T_1$  is longer lived than the first excited singlet state, so that the biologically relevant photochemistry is often mediated by this state.  $T_1$  can initiate photochemical reactions directly, giving rise to reactive free radicals, or transfer its energy to the ground-state oxygen molecules ( $^3O_2$ ) to give rise to  $^1O_2$  molecules. The relatively longer lifetimes for the triplet excited states make the collisional transfer of energy to surrounding oxygen molecules possible. The electronic excitation to produce  $^1O_2$

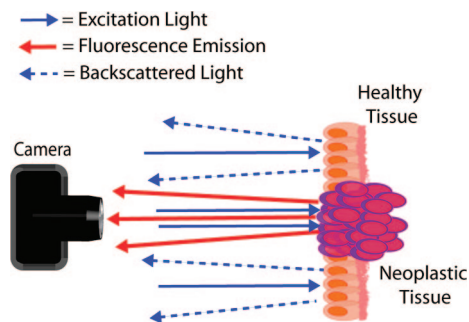
requires at least 20 kcal/mol, which places limits on the longest absorption wavelength of the PS. If the energetics are appropriate, photo-oxidative reactions may occur by  $^1O_2$  mediation. This  $^1O_2$ -mediated photodynamic mechanism of cytotoxicity is a generally accepted mode of action for most PSs currently under investigation, although other competing mechanisms exist.  $T_1$  can also potentially relax to  $S_0$  by radiationless decay or by radiative decay as phosphorescence,  $k_p$ . Under the special circumstance of multiphoton absorption (short pulse, high intensities of irradiation), the upper excited states may be populated and complex photophysical and photochemical processes can occur,<sup>23,24</sup> resulting in changes in phototoxicity, including oxygen-independent mechanisms.<sup>24</sup> Studies of radical-mediated PSs and PSs which are specifically activated by multiphoton absorption mechanisms are ongoing,<sup>25,26</sup> although the potential for these pathways in imaging is not well developed in relation to PDT (section 6).

## 2. Imaging of Photosensitizer Fluorescence for Detection of Disease and Optimization of Surgical Resection

### 2.1. Overview of Photosensitizer Fluorescence Detection

As described above, the electronic excitation of a PS can result not only in a cytotoxic effect but also in the emission of fluorescence due to relaxation of the excited-singlet-state PS back to the ground state. Hence, in addition to being therapeutic agents for PDT, PSs can readily serve as imaging agents that fluoresce in the visible region upon excitation with the appropriate wavelength (albeit with a lower quantum yield than traditional fluorescent dyes that are not also therapeutic agents). As PSs have a propensity for preferential accumulation in neoplastic tissues, this approach, often termed photodynamic diagnosis (PDD) in the literature, is inherently well-suited for selective visualization of tumors by using fluorescence contrast to demarcate the boundaries of cancerous and healthy tissues. The ability to accurately define tumor margins is a crucial aspect in optimization of surgical interventions and constitutes a major subset of the applications of this fluorescence imaging technique. In general, the ability to obtain cancer-free margins around cancerous tissue being excised is a major predictive factor in whether the disease will recur. On the other hand, resection of excess healthy tissue can have severe implications for the patient's quality of life. For example, in neurosurgical applications, excision of even one extra millimeter of eloquent brain can significantly interfere with vital functions such as speech or motor skills. The inherent capability of PS to selectively detect disease for use as a tool to optimize therapy has led to significant improvements in quality of life for patients with several human diseases, as described in the following subsections.

With regard to the terminology typically used to describe this approach in the literature, we suggest an alternative to the phrase “photodynamic diagnosis”, which we feel is somewhat misrepresentative of both the underlying physical process and its application. The production of fluorescence by a PS involves only radiative decay from the excited singlet state of the PS, while the term “photodynamic” implies the generation of toxic species via photoreactions. Furthermore, although fluorescence imaging of PSs can play a role in



**Figure 5.** Schematic representation of the basic principles of photosensitizer fluorescence detection. The photosensitizer accumulates preferentially in neoplastic tissue (depicted as purple cells), which upon excitation with light of the appropriate wavelength (blue arrows) emits red fluorescence emission (red arrows). The contrast generated by this fluorescence emission against backscattered illumination (blue arrows with dashed lines) can be used to demarcate the boundaries of neoplastic tissues for sensitive detection of a variety of human cancers and optimization of surgical resection. The backscattered illumination can be useful to observe surrounding nonfluorescent tissue, though in many applications an emission filter is placed before the observer or detector to exclude the backscattered light.

diagnosis of disease, this technique has been more developed as a tool for optimizing surgical resection, rather than actually grading and staging of tumors as the term “diagnosis” suggests. For these reasons, we suggest the more general phrase “photosensitizer fluorescence detection” (PFD). Going forward in this review, we use this term in reference to all applications in which a photosensitizing species is used to generate fluorescence contrast for the selective identification of diseased tissue.

The implementation of PFD requires only a source of illumination (generally blue or blue-violet light) such as a lamp or a laser to excite the PS and appropriate optics to image the longer wavelength (typically red) fluorescence emission, as shown schematically in Figure 5. In porphyrins, the Soret band in the 400 nm range is typically excited for diagnosis, taking advantage of the large Stokes shift between excitation and emission bands. In general, standard diagnostic imaging equipment such as laparoscopes, endoscopes, cystoscopes, and neurosurgical microscopes can be adapted for fluorescence imaging by implementing the appropriate illumination with minimal modification to the optical instrumentation. This suitability for clinical translation has allowed the use of PFD for selective identification of cancerous lesions in a broad range of anatomical sites including the bladder, brain, skin, lungs, breast, abdomen, female reproductive tract, and others. In contrast to other imaging techniques such as PET, MRI, conebeam CT, etc. that can be used in capacities similar to those in which diagnostic imaging modalities are used, it is important to note that PFD is inherently a surface-sensitive technique (with the exception of fluorescence tomography implementations as described later in this review). While the aforementioned volume-sensitive techniques provide structural details not achieved with fluorescence imaging, the sensitivity of detection decreases during the process of resection as the volume of nonresected disease diminishes. In contrast, the sensitivity of fluorescence imaging is not impacted. In this section, we review clinical and preclinical studies in which this basic premise is applied to the detection of cancer or precancerous growths, guidance of surgical resection, and monitoring of treatment response.

## 2.2. Early PS Fluorescence Studies

The history of early studies and observations that provided the basis for the modern field of PDT and associated fluorescence imaging applications were reviewed comprehensively in 2001 by Ackroyd et al.<sup>8</sup> Here, we highlight some key findings, with an emphasis on the past two decades, that paved the way for the widespread application of PFD for the identification of cancerous tissues. The original studies of PS fluorescence used the substance that came to be known as HP, first produced by Scherer in 1841 from the precipitate of dried blood heated with sulfuric acid and washed of iron.<sup>27</sup> The first published account that HP accumulates preferentially in malignant tumors is attributed to Policard, who reported the observation in 1924 of red HP fluorescence emission from a rat sarcoma illuminated with ultraviolet light from a Woods lamp.<sup>9</sup> This finding was corroborated in the 1940s by Auler and Banzer<sup>28</sup> and later by Figge, Weiland, and Manganiello, who more comprehensively characterized the tumor-localizing properties of several porphyrins and metalloporphyrin chemical species in a large-scale mouse model study.<sup>29</sup> Figge et al. found that all porphyrin species tested produced localized red fluorescence upon ultraviolet activation in tumors but not in normal tissues, with the exception of lymphatic, omental, fetal, placental, and traumatized regenerating tissues. This exciting finding laid the groundwork for a clinical PFD study by Rassmussen-Taxdal et al., who injected HP hydrochloride intravenously to patients prior to the excision of benign and malignant lesions.<sup>30</sup> Not only was the red fluorescence emission evident in a higher percentage of malignant tumors compared with benign tumors, but the intensity increased with increasing HP concentration, and solid tumors could be detected even through intact skin.

These first studies of PS fluorescence had low potential for clinical translation due to their reliance on the crude form of HP, which required administration of large doses to produce a detectable fluorescence signal. Indeed, in their first clinical tests in humans with head and neck malignancies, Manganiello and Figge were unable to detect HP fluorescence, presumably due to the much lower dose of HP that was used relative to that in previous animal studies. Further chemical analysis of HP by Schwarz et al. revealed the substance to be a mixture of porphyrin compounds with variable uptake and fluorescent properties.<sup>31</sup> This observation led Schwartz et al. to conduct a series of additional purification steps on crude HP which led to the derivative substance, HpD, with stronger affinity for tumor localization and higher phototoxicity.

HpD, although still a complex mixture of porphyrins and other species, represented a major step forward for both therapeutic and imaging applications of PDT, achieving greater phototoxicity with a lower dose than its less refined predecessor, HP. In preclinical studies, Lipson and Baldes demonstrated that HpD accumulated in neoplastic tissues with greater efficiency than crude HP.<sup>32</sup> This finding paved the way for the first application of HpD fluorescence detection of malignancy by Lipson and colleagues, who devised an endoscopic fluorescence imaging procedure for clinical use at the Mayo Clinic.<sup>33</sup> Over the next two decades, HpD-based fluorescence detection was evaluated for several clinical applications including the detection of cervical cancer,<sup>34,35</sup> lung cancer by fluorescence bronchoscopy,<sup>36–39</sup> and head and neck tumors<sup>40</sup> and identification of various malignancies in the bladder.<sup>41</sup> Although promising results were obtained, the

majority of these HpD-based PFD studies were conducted with small groups of patients or in preclinical models that did not lead to larger scale clinical studies. In the one large clinical trial of PFD that was conducted in this era, the results were somewhat disappointing. In this study, Gregorie and colleagues at the Medical College of South Carolina evaluated HpD fluorescence detection for identification of malignant neoplasms in a broad range of anatomical sites in 226 patients.<sup>42</sup> Only 76.3% of patients with confirmed malignant neoplasms exhibited positive tumor fluorescence. Although correctable factors were identified as responsible for false-negative results in 10.5% of patients, the approach was determined at that time to be too unreliable for clinical identification of tumors.

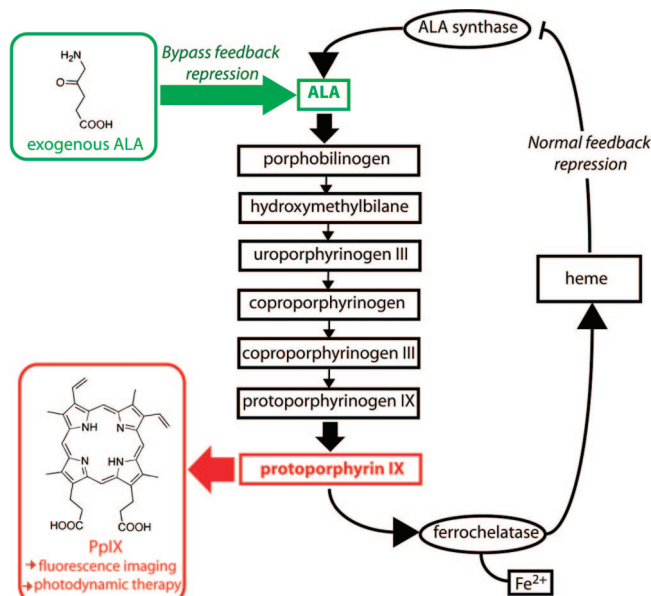
The nonoptimal results obtained in early PFD studies may have been partly due to the lack of characterization of the uptake and pharmacokinetics of PS in vivo. In the late 1970s, Gomer and Dougherty conducted the most detailed quantitative study to date of the timing and distribution of HPD in normal and malignant tissues using <sup>3</sup>H-labeled and <sup>14</sup>C-labeled HpD.<sup>43</sup> Following intraperitoneal injection of labeled HpD into mammary carcinoma mouse models, they made measurements of HpD concentration in the blood, tumor, liver, kidney, spleen, lung, skin, and muscle at time points up to 72 h. While the measured HpD concentration in tumor reached a higher maximum value than in skin or muscle, the highest concentrations were observed in the liver, kidney, spleen, and lung (in that order). Furthermore, the temporal profile of concentrations at each site was comparable, in that high levels of HpD in the tumor occurred at the same time as high levels in normal tissues. Nevertheless, it was argued that a time window of 24 h existed, at least in murine models, during which the higher accumulation of HpD in the tumor relative to surrounding tissues allowed for tumor destruction with minimal toxicity to surrounding normal tissue. A similar study of HpD distribution in tissue reported by Jori et al. in the same year using a rat ascites hepatoma model concluded that, relative to that in the liver, only small amounts of HpD were metabolized by tumor cells. A time window was found to occur at 12 h after injection with a high tumor to liver ratio, which was optimal for selectivity in PFD or PDT.<sup>44</sup>

These tissue distribution studies brought to light crucial pharmacokinetic considerations pertinent to HpD-based PFD and PDT. In a study published in 1982, Kessel reported a detailed reversed-phase thin layer chromatography analysis of HpD. Although partially purified from the crude HP form, HpD comprised a complex mixture of porphyrin species, including HP, protoporphyrin, (hydroxyethyl)vinyldeuteroporphyrin, and other fluorescent species, with different tumor-localizing properties.<sup>45</sup> Kessel's findings were consistent with results from an in vivo study of HpD pharmacodynamics conducted by Unsold et al.<sup>46</sup> This study reported that the timing of maximum HpD fluorescence emission from the tumor and optimal therapeutic efficacy were completely asynchronous in their murine model. The maximum therapeutic effect was achieved 24 h following administration of HPD, while fluorescence intensity from the tumor at that time was at a minimum. In addition to the noted side effects of HPD, including prolonged cutaneous toxicity, the problem of substance impurity was clearly a limiting factor in its ability to accurately and reliably identify the boundaries of diseased tissue for diagnosis or surgical guidance. Another partially purified derivative, PF, which emerged in the mid-1980s and ultimately achieved widespread therapeutic ap-

plication, was also a composite of oligomers formed by linkages of up to eight porphyrin units, and thus also was of dubious suitability for use as an imaging agent. It was not until the introduction of a new photosensitizing strategy introduced by Kennedy and Pottier, which enhanced endogenous protoporphyrin IX (PpIX) production in the heme cycle of tumors themselves, that PFD would enjoy more widespread and successful implementation.

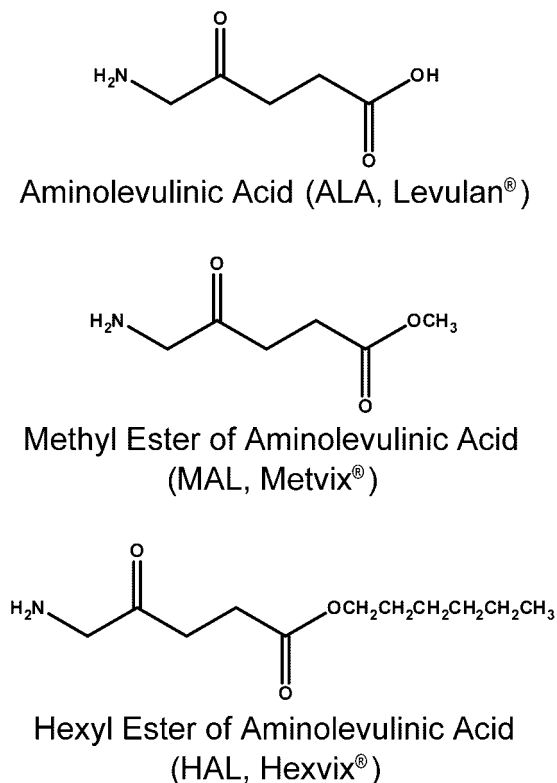
### 2.3. $\delta$ -Aminolevulinic Acid-Induced Protoporphyrin IX

The traditional implementation of PDT involves the administration of a synthetic PS followed by a period of delay, in which the PS accumulates in the tumor or tissue of interest, before light activation. An alternative approach, which can be implemented for both PDT and PFD, was first described by Kennedy and Pottier in the early 1990s. This approach leverages the in situ synthesis of  $\delta$ -aminolevulinic acid (ALA), a nonphotoactivatable precursor, into PpIX, a naturally occurring photosensitizing species via the cellular heme biosynthesis pathway.<sup>47,48</sup> In its naturally occurring context, the formation of ALA is the first compound in the porphyrin synthesis pathway (shown schematically in Figure 6) that ultimately leads to the production of heme-containing compounds in mammalian cells.<sup>49</sup> In this pathway, two molecules of ALA react in the cytosol to form porphobilinogen, four molecules of which then combine via deamination to produce (hydroxymethyl)bilane. This product is hydrolyzed to form uroporphyrinogen III, which undergoes several subsequent modifications in the cytosol, resulting in the formation of coproporphyrinogen. Coproporphyrinogen oxidase, which is localized in the intermembrane space of mitochondria, catalyzes the stepwise oxidative decarboxylation of coproporphyrinogen III, yielding protoporphyrinogen IX in the mitochondria, where PpIX is ultimately produced.



**Figure 6.** Schematic representation of the heme synthesis pathway which leads to synthesis and accumulation of protoporphyrin IX in vivo. Under normal physiological conditions, synthesis of PpIX is regulated by negative feedback control of free heme on ALA synthase. This feedback is bypassed by addition of exogenous ALA, which, due to the relatively low rate of iron insertion by the enzyme ferrochelatase, leads to accumulation of excess PpIX that can be used either therapeutically, for PDT, or to generate fluorescence contrast, for PFD.





**Figure 7.** Structures of ALA (Levulan), MAL (Metvix), and HAL (Hexvix).

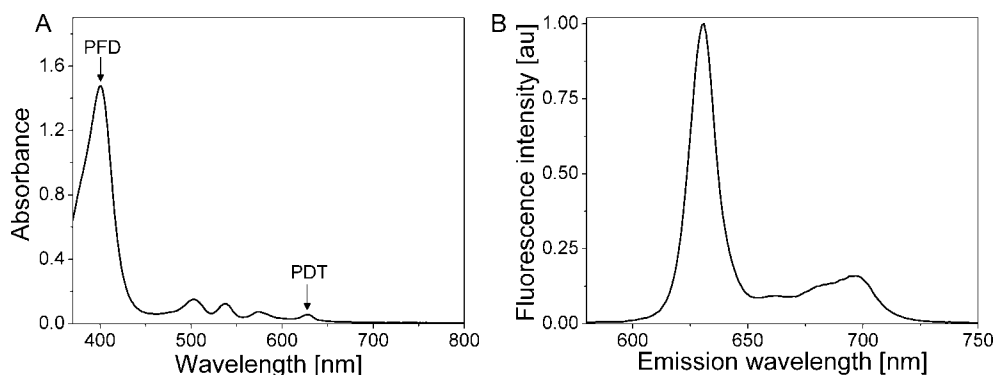
Ferrochelatase then catalyzes the insertion of iron into PpIX to form heme, which in turn triggers a feedback repression of ALA synthase, which reinitiates the cycle and is the rate-limiting step in the process under physiological conditions. Addition of exogenous ALA bypasses this control mechanism, allowing excess synthesis of downstream metabolites. As iron is inserted by ferrochelatase (which is down-regulated in many tumors) at a relatively low rate, it is unable to compensate for the excess PpIX formed, allowing for significant accumulation in neoplastic tissues following administration of exogenous ALA.<sup>48</sup>

The actual rates of uptake of ALA in normal versus malignant tissue are believed to be comparable, while differential rates of ALA conversion and accumulation of PpIX are believed to be the primary driving force of the favorable tumor selectivity.<sup>50</sup> An improved understanding of the relative importance of the enzymes involved in PpIX conversion could provide valuable insight, allowing manipulation of the process to further enhance both fluorescence

contrast and therapeutic efficacy. The picture is further complicated by the fact that the relative importance of the enzymes involved seems to vary depending on the tissue and tumor type. Regardless of the mechanism, a time delay of 1–4 h following administration of ALA is generally required for localization of PpIX in the target tissue prior to imaging (or treatment). The specific time delay depends on the route of delivery (intravenous, oral, intravesical instillation, topical, or inhalation) and the tissue in question,<sup>51–54</sup> with PpIX levels dependent upon the cellular differentiation status.<sup>55</sup> Other studies described below reveal that, for certain applications, the hexyl and/or methyl ester derivatives of ALA (HAL and MAL, respectively, Figure 7) result in similar PpIX production but with improved penetration and more homogeneous distribution in malignant tissue as discussed below.

PpIX absorbs light strongly at 409 nm with several weaker absorption bands, including one at 635 nm, and, as seen in the absorption spectrum in Figure 8, produces characteristic dual-peaked red fluorescence emission at 635 and 700 nm. For PDT treatments, longer wavelength activation of the PS is favored to achieve deeper penetration into tissue with reduced scattering and absorption. Hence, for ALA-induced PpIX, therapeutic light activation is generally accomplished with illumination at 635 nm. However, for imaging applications, it is often not feasible to excite the PS with red light as the Stokes-shifted spectral peak of the fluorescence emission has significant overlap with the excitation peak and is challenging to separate. Furthermore, in many PFD implementations, an emission filter to block the illumination light is intentionally not employed, so as to retain the capability of visualizing the landscape of healthy tissues surrounding the malignant regions of more intense fluorescence. For these reasons, the 409 nm excitation of PpIX (which is close to the 405 nm emission of commonly available blue-violet laser diodes) is often used to generate fluorescence emission. This is true of other PSs as well, which are generally excited at wavelengths in the 400 nm range for imaging applications but also have strong absorption bands in the 600 nm range that are advantageous for PDT treatment.

The specific PFD implementation depends on the clinical application and generally mirrors the conventional white-light imaging instrumentation suitable for that application. Endoscopy procedures for diagnostic imaging of the gastrointestinal tract can easily be adapted for fluorescence imaging using the endoscope to both deliver fluorescence excitation and collect emission. For detecting bladder cancer, transurethral endoscopy or cystoscopy is used to image the interior of the bladder in the same manner. For intraoperative



**Figure 8.** Absorption (A) and fluorescence emission (B) spectra obtained from PpIX in methanol. Positions of absorption maxima typically (although not exclusively) used for PFD and therapeutic PDT applications are marked with arrows.

imaging during brain surgery, a standard neurosurgical microscope, which typically operates in white-light mode, can be adapted for fluorescence imaging.

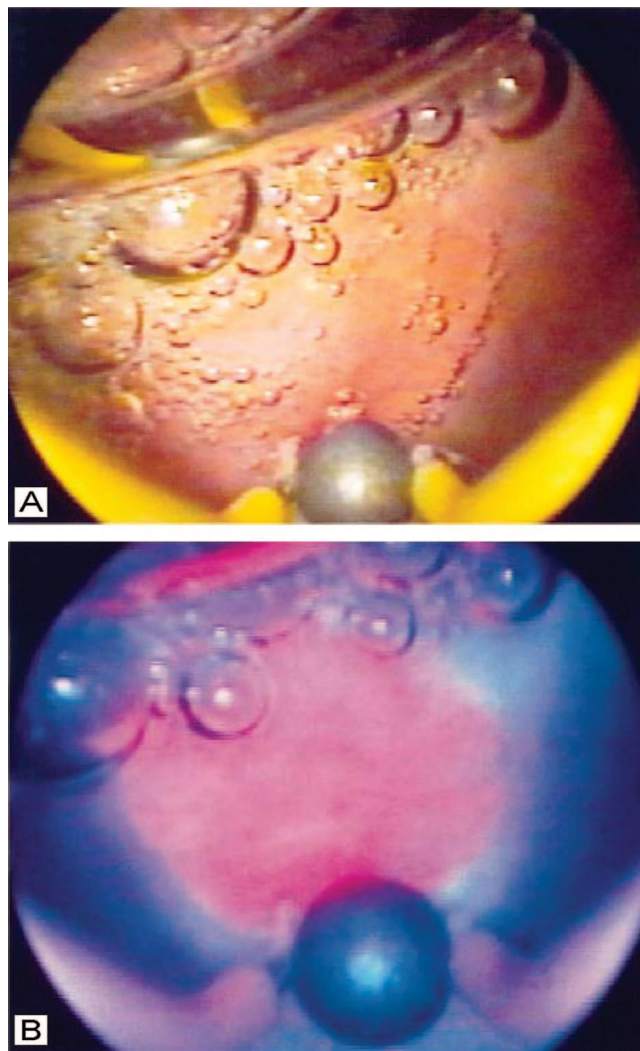
## 2.4. Photosensitizer Fluorescence Detection for Disease-Specific Applications

### 2.4.1. Bladder Cancer

PFD is a powerful tool in the detection and guided resection of bladder cancer, as recently reviewed by Witjes and Douglass.<sup>56</sup> Bladder cancer is the fourth most common malignancy among men in the Western world, and due to high rates of recurrence, it is an extremely costly disease to treat and monitor over the lifetime of the patient.<sup>57–59</sup> The current front-line diagnostic tool for confirmation of the presence and type of disease is visual examination by white-light cystoscopy. While this approach is effective for identifying larger tumors that protrude from the surface, many other manifestations of the disease are challenging to detect, including flat carcinomas, dysplasia, multifocal growth, and microscopic lesions. Of these flat lesions, the detection of carcinomas in situ (CIS), which is a critical factor in predicting the recurrence of disease, generates particularly poor contrast for white-light imaging.<sup>58</sup>

In 1994, Kriegmair et al. demonstrated that intravesical instillation of ALA (Levulan, DUSA Pharmaceuticals Inc., Tarrytown, NY) enabled the fluorescence detection of numerous lesions in the bladder that were not recognized by routine white-light cystoscopy.<sup>60</sup> Furthermore, the sensitivity for the detection of cancerous lesions was confirmed to be 100% by histological validation. The high diagnostic efficiency of ALA-induced PpIX PFD was supported in subsequent studies comparing this approach with conventional white-light imaging.<sup>61–63</sup> In these studies, it was also noted that CIS, the very lesions that escaped detection by white-light cystoscopy, were clearly discernible by ALA-induced PpIX fluorescence. Figure 9 (from Koenig et al.<sup>62</sup>) illustrates this point, with white-light and fluorescence images of the same cystoscopic field of view showing an intermediate grade cancerous lesion in the fluorescence image not evident in the white-light image. In the Riedl et al. study, follow-up assessment of patients in the fluorescence endoscopy group revealed that the superior sensitivity of fluorescence imaging led to a reduced rate of early recurrence of superficial bladder cancer, compared with white-light imaging.<sup>64</sup> In a phase III trial comparing transurethral guided resection using ALA-induced PpIX versus white-light cystoscopy, 61.5% of patients in the PpIX fluorescence endoscopy group were tumor-free at the time of follow-up, compared with only 40.6% in the white-light group, with no noted difference in side effects from the procedure.<sup>65</sup>

While ALA as a PS precursor for PFD produced very promising results, several drawbacks pertaining to the bioavailability of ALA in the malignant tissue prompted Lange et al. to explore the use of the lipophilic HAL for diagnostic imaging of bladder cancer.<sup>66</sup> In this application, HAL achieved deeper penetration into the urothelial layers and a more homogeneous distribution in malignant tissue. In addition, HAL produced higher fluorescence emission intensity with a lower dose following a shorter incubation period in the subject. Since 2003, studies of fluorescence cystoscopy for detection of bladder cancer using HAL instead of free ALA reported a similar marked improvement in sensitivity over white-light imaging.<sup>67–71</sup> Very few recent



**Figure 9.** Comparison of white-light and PpIX fluorescence images of an intermediate grade malignant lesion in the bladder of a human patient, obtained via cystoscopy. In the white-light image (A), the lesion is not evident, while, in the PpIX fluorescence image obtained under blue illumination (B), the lesion is readily visible as a pink region just above the large air bubble in the lower middle part of the field. Reprinted with permission from ref 62. Copyright 1999 BJU International.

bladder cancer detection studies have employed PSs other than HAL. However, one recent study using hypericin explored the interesting possibility that analysis of PS fluorescence data could be used not only for the detection of disease but also for pathological grading.<sup>72</sup> This work suggests that the full potential of such an approach is yet to be achieved. With further development of image processing routines for quantitative analysis of fluorescence data, it may be possible to glean considerably more information into the disease state beyond simply identifying the presence of malignancy and demarcating the boundaries of diseased tissues.

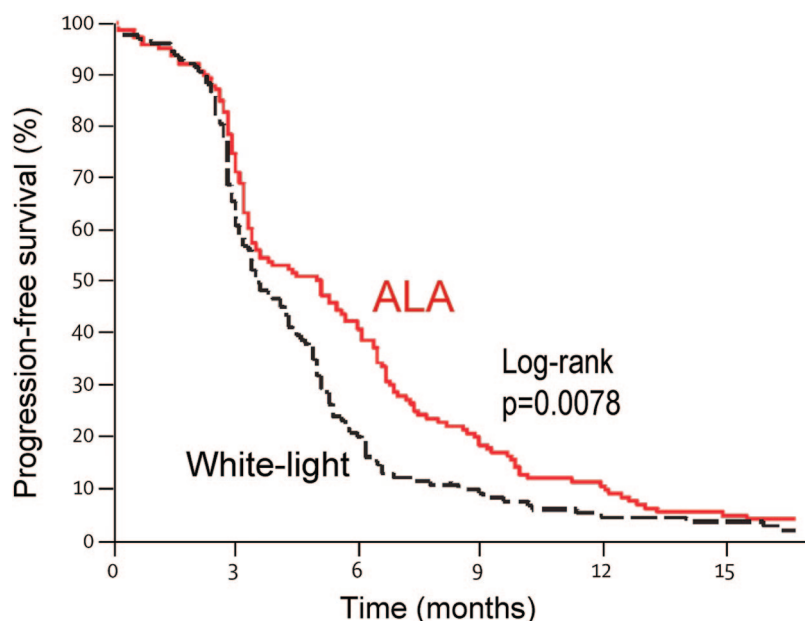
### 2.4.2. Brain Cancer

Fluorescence-guided resection (FGR) using PS precursors has received considerable attention in the treatment of brain cancer. The ability to optimally resect malignant tissue with minimal damage to surrounding normal areas is a critical determinant of meaningful improvement in progression-free survival and quality of life for patients with brain cancer.<sup>73,74</sup>

**Table 1. Results of FGR versus White-Light Resection for Patients with Malignant Glioma in a Multicenter Randomized Trial<sup>a</sup>**

	FGR ( <i>n</i> = 139)	white-light resection ( <i>n</i> = 131)	OR (95% CI)	<i>p</i>
all patients	90 (65%)	47 (36%)	3.28 (1.99–5.40)	<0.0001 <sup>*</sup>
age (years)			3.42 (2.06–5.70) <sup>†</sup>	<0.0001 <sup>‡</sup>
≤55	35/45 (78%)	20/43 (47%)	4.03 (1.60–10.14)	0.0025 <sup>*</sup>
>55	55/94 (59%)	27/88 (31%)	3.19 (1.73–5.87)	0.0002 <sup>*</sup>
Karnofsky performance scale			3.27 (1.98–5.40) <sup>†</sup>	0.0001 <sup>‡</sup>
70–80	13/28 (46%)	9/31 (29%)	2.12 (0.72–6.20)	0.1676 <sup>*</sup>
>80	77/111 (69%)	38/100 (38%)	3.70 (2.09–6.54)	<0.0001 <sup>*</sup>
tumor location			3.26 (1.97–5.40) <sup>†</sup>	<0.0001 <sup>‡</sup>
noneloquent	45/65 (69%)	26/55 (47%)	2.51 (1.19–5.30)	0.351 <sup>‡</sup>
eloquent	45/74 (61%)	21/76 (28%)	4.06 (2.05–8.07)	0.0148 <sup>*</sup>

<sup>a</sup> Data adapted with permission from ref 78. Copyright 2006 Elsevier Ltd. <sup>\*</sup>Crude *p*-value based on  $\chi^2$  test. <sup>†</sup>Common odds ratio (OR), adjusted for variable; *p*-value based on Cochran–Mantel–Haenszel test. <sup>‡</sup>Breslow–Day test for homogeneity of OR within variable.

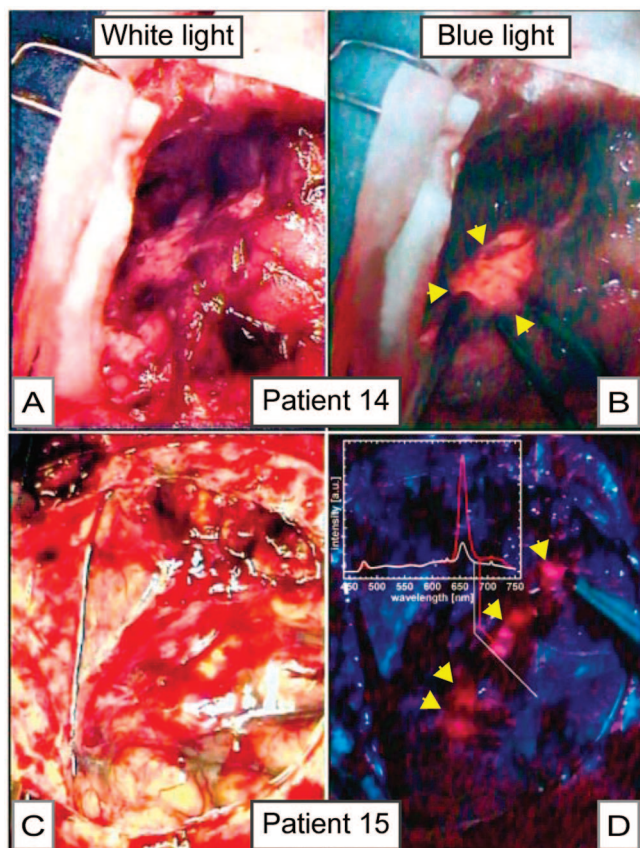


**Figure 10.** Progression-free survival data by treatment group for the large multicenter trial reported by Stummer et al. in 2006, which compared white-light and fluorescence-guided resection for treatment of malignant glioma. After 6 months there is a significant enhancement in progression-free survival in the 5-ALA group as compared to white light, while the two curves collapse after 15 months. Reprinted with permission from ref 78. Copyright 2006 Elsevier Ltd.

However, as with other malignancies, the tumor margins are often not sufficiently defined by white-light imaging alone. The feasibility of fluorescence imaging for this application was suggested by Stummer et al., who observed high levels of porphyrin accumulation in malignant glioma cells exposed to ALA<sup>75</sup> and corroborated this finding in a small group of patients.<sup>76</sup> Motivated by these promising results, the same group initiated a clinical study evaluating the use of intraoperative fluorescence imaging in 52 patients with glioblastoma multiforme.<sup>77</sup> As with bladder cancer, the value of ALA-induced PpIX for guided resection allowed for a high percentage of patients (63%) to achieve complete resection through contrast enhancement. This work led to a large phase III multicenter trial in which patients were randomly assigned to receive either traditional white-light microsurgery or oral administration of ALA for PpIX FGR, followed in both cases with standard adjuvant radiotherapy.<sup>78</sup> This highly successful trial was terminated at the interim analysis of the first 270 patients, when 65% of those in the FGR group were without residual disease at postoperative MRI, compared with 36% in the white-light group (Table

1). It is important to note, however, that while this dramatic improvement in progression-free survival, and hence quality of life, was achieved at the 6 month follow-up, the survival curves for the FGR and white-light resection groups converged at about 15 months (Figure 10). Nevertheless, considering the significant clinical challenges posed by the surgical resection of malignant gliomas, this improvement in progression-free survival was a major advancement in improving the clinical management of the disease.

The clinical value of this large-scale trial was put into perspective in an editorial letter written by Barker and Chang.<sup>79</sup> They pointed out that numerous technologies designed to improve surgical resection of gliomas have been widely adopted in the clinic without evidence that they actually have any impact on the efficacy or safety of surgery. In contrast, Barker and Chang describe the study by Stummer and co-workers<sup>78</sup> as “a step forward in the study of surgery for malignant glioma”.<sup>79</sup> It is also noted that, due to the nature of FGR, the surgeons in the Stummer et al. study were not blinded to the treatment group, a consideration which could have introduced bias and confounded the results. However,



**Figure 11.** Intraoperative images of a partially resected brain tumor (A, B) and the surface of the brain (C, D), comparing images obtained by white-light imaging (A, C) and mTHPC fluorescence imaging under blue light (B, D). In (A), a partially resected tumor is difficult to discern, while it is readily apparent in the blue-light mTHPC fluorescence image of the same tissue. Similarly, in (C) (a white-light image of the surface of the brain), there is no apparent tumor, while the mTHPC fluorescence image, which is complemented by spectroscopy (inset) of the same field, reveals the presence of malignancy. Reprinted with permission from ref 80. Copyright 2001 Wiley.

the methods that would have allowed blinded randomization are difficult to apply. Another inherent difficulty in this study, as with image-guided resection in general, is of course the inherent subjectivity in interpretation of regions of fluorescence contrast corresponding to diseased tissues. Despite these confounding factors, Barker and Chang suggest that FGR provides a promising new technique for neurosurgical oncologists to achieve meaningful improvements in progression-free survival for patients with malignant glioma.

While the most comprehensive clinical evaluations of FGR for glioma have been carried out using ALA-induced PpIX as the photosensitizing strategy, there may be benefits to exploring other PSs. An earlier phase II study by Zimmermann et al. evaluated the use of tetrakis(*m*-hydroxyphenyl)-chlorin (mTHPC or Foscan) for FGR of malignant glioma.<sup>80</sup> mTHPC produces red fluorescence with a maximum intensity at 652 nm upon excitation by blue-violet illumination. Zimmermann et al. evaluated 138 specimens from 22 patients with malignant brain tumors in this study and achieved a sensitivity and specificity of 87.9% and 95.7%, respectively.<sup>80</sup> Furthermore, the authors noted that, in 10 of the patients, tumors that were not visible by white light were identified correctly by mTHPC fluorescence exclusively (Figure 11). These results were comparable to those reported by Stummer et al. using ALA-PpIX in their first clinical PFD study to

identify gliomas in 89 biopsies (from 9 patients) with a sensitivity and specificity of 85% and 100%, respectively.<sup>76</sup> Although ALA-induced PpIX had, by this point, gained widespread acceptance for imaging, Zimmermann et al. suggested that since mTHPC offers a higher quantum efficiency for the production of cytotoxic species, with greater light penetration, it is better suited for treatment of brain tumors with significant bulk. They also noted that, even during the several minutes of illumination of mTHPC brain tissues during FGR, there was no observable photobleaching, a concern with ALA-induced PpIX that had been previously reported by Stummer and colleagues.<sup>76</sup>

Prompted by the noted success of FGR in improving malignant glioma tumor resection, studies by others explored the possibility of further improving the efficacy of this approach. To help overcome the challenge of subjectivity in assessment of diseased tissue encountered in previous clinical studies, Bogaards et al. introduced a new ratiometric 2D quantification approach and tested it experimentally and demonstrated its feasibility in a clinical setting.<sup>81</sup> Another avenue toward improving the outcome that has been explored in both preclinical and clinical settings is that of using the PS as both an imaging and a therapeutic agent simultaneously.<sup>82–87</sup> In the standard treatment protocol, surgical resection of malignant tissue is followed by adjuvant radiation therapy. However, when FGR is used instead of white-light resection, the PS is already present in the tissue at the time of resection, and a logical extension of this protocol would be to use PDT to selectively destroy any residual disease in the resection bed. In an effort led by Kostron and colleagues mTHPC-guided FGR with adjuvant PDT was evaluated in 26 patients with malignant brain tumors with results similar to those previously reported by Zimmermann et al.<sup>80</sup> Additionally, Kostron et al. reported an increase in median survival from 3.5 months in the matched pair control group to 9 months in the FGR-PDT group.<sup>82</sup> Light was delivered either superficially or interstitially for adjuvant PDT with no difference in median survival, and the treatment was tolerated well by all patients.

In 2007 Stepp and co-workers published a report evaluating combined FGR and adjuvant PDT for the treatment of malignant glioma.<sup>83</sup> ALA-induced PpIX was used for both FGR and PDT, with light irradiation delivered via microlens fibers or interstitial fibers, placed to generate the optimal fluence rate in positions determined from Monte Carlo calculations used for light propagation calculations. In this study, Stepp et al. compared spectroscopic measurements of PpIX fluorescence from the tumor border and infiltrating region of 19 patients to establish PpIX selectivity for tumor. As expected, they found that the fluorescence intensity was significantly lower at the infiltrating zone as compared to the border and determined that normal brain was practically free of any PpIX accumulation.

Extensive work has been performed by the Wilson group at the University of Toronto for image-guided resection and PDT for glioma.<sup>84–87</sup> Their custom-built, intraoperative, high-resolution, multispectral fluorescence imaging system was first described in 2003 by Yang et al.<sup>84</sup> This user-friendly “point-and-shoot” system provided a long working distance, large field of view, and depth-of-view imaging capabilities, in addition to point fluorescence spectroscopy. Initial studies were performed with PF in both tissue phantoms and humans. Subsequent studies used ALA-induced PpIX for blood-brain barrier penetration studies in normal brain and tumor tissue<sup>85</sup>

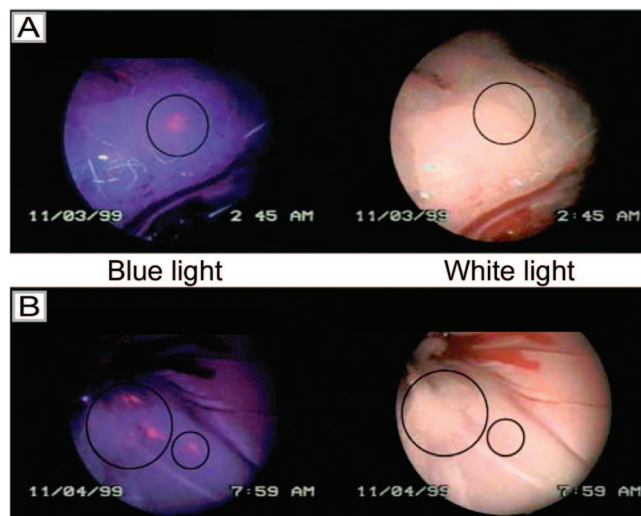
as well as FGR of brain tumors,<sup>87</sup> all in a rabbit model. Bogaards et al. also explored the combination of FGR with so-called “metronomic” PDT using ALA-induced PpIX in a rabbit model of glioblastoma multiforme.<sup>86</sup> In this approach, low light doses were delivered over an extended period of time via intracranially implanted light-emitting diodes, rather than the conventional methodology of using a single dose of irradiation at a higher fluence rate. Through these studies, the Wilson group has successfully demonstrated that an intraoperative fluorescence imaging system not only improves tumor resection but allows for PDT of the residual tumor.

Although the application of ALA-induced PpIX for FGR of brain tumors represents one of the highest impact clinical applications of PFD to date, new innovations continue to refine this approach and offer the potential for further enhancement of therapeutic outcomes. To improve specificity for both imaging and PDT treatment of brain tumors, Reddy and colleagues at the University of Michigan conducted a preclinical study in a 9L rat glioma model using multifunctional vascular targeted nanoparticles loaded with PF, Alexa Fluor 594 for fluorescence imaging, iron oxide to provide contrast for MRI, and a targeting peptide for molecular specificity.<sup>22</sup> For the latter function, they chose a 31-amino acid peptide called F3 to selectively target angiogenic vasculature. The details of this nanoparticle construct are discussed further in section 3.2. Using this multifunctional nanoparticle platform, Reddy et al. were able to obtain time-resolved sequences of MRI to monitor the pharmacokinetics and distribution of nanoparticles within the tumor. In a comparison of survival across the treatment groups of untreated, light-only control, free PF, and targeted and nontargeted nanoparticles, Reddy et al. reported a pronounced increase in survival in animals in the targeted nanoparticle therapy group. This group demonstrated a survival probability of approximately 0.4 at 60 days after treatment, compared with all other groups in which survival dropped to 0 within 20 days.

While PFD has made a significant clinical impact as an intraoperative brain-imaging modality for guidance of surgical resection, it has not been extensively explored as a noninvasive approach. In a recent study by Gibbs-Strauss et al., the fluorescence to transmission ratio of PpIX fluorescence was measured through the cranium using a single-channel fluorescence spectroscopy system in malignant glioma in a murine model.<sup>16</sup> If optimized, this low-cost and noninvasive approach could provide a valuable complement to the more established intraoperative PFD protocol, allowing for more frequent screenings and, when called for, timely intervention. However, to establish the utility of this approach for use in a clinical setting, there may be additional challenges to be addressed as the human skull is significantly thicker than the mouse skull and there is potential for tumors to be buried much more deeply by surrounding brain tissue. Gibbs-Strauss et al. also explored the technique of intentionally photobleaching the skin-accumulated PpIX with 635 nm light as a means to increase contrast between tumor and control mice.

### 2.4.3. Ovarian Cancer

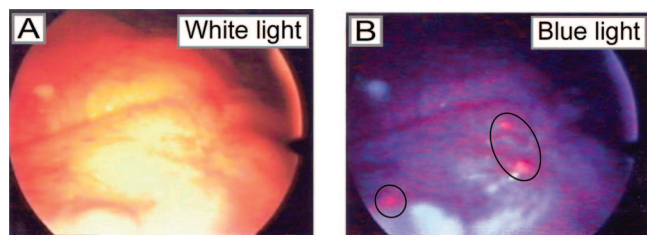
PS-based fluorescence imaging has also been applied with promising results for the detection of ovarian cancer. The high overall mortality for this disease is largely due to the large proportion (70%) of patients who present with late-stage disease at the time of diagnosis. The treatment options for these patients are limited to surgical debulking and cycles



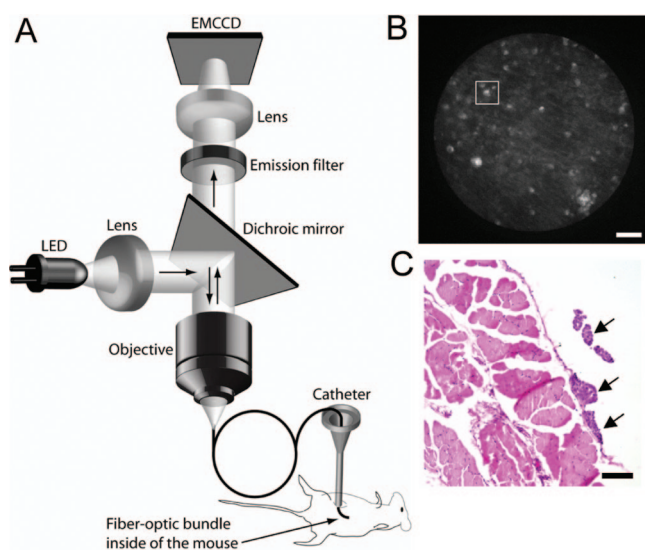
**Figure 12.** Laparoscopic images of peritoneal metastases in a rat model of ovarian cancer obtained by white-light imaging (right) and HAL-induced PpIX fluorescence imaging under blue-light illumination (left). Image A shows a lesion that is only visible in the blue-light mode, but not by white light (position marked by a circle) (8 mM HAL after 2 h). Image B shows three lesions visible by both blue and white light (big circle) and one only detectable by fluorescence (small circle) (8 mM HAL after 2 h). Reprinted with permission from ref 94. Copyright 2003 Nature Publishing Group.

of chemotherapy and have a high likelihood of recurrence, resulting in 5 year survival of 31% that has only marginally improved over the past few decades.<sup>88</sup> The prognosis for the relatively small subgroup of patients who are diagnosed with early-stage disease, which has not yet spread to regional and distant sites, is much better, with a 5 year survival rate of 93%. Ovarian cancer presents special challenges for diagnostic imaging due to the characteristic pattern of the disseminated disease, with microscopic tumor nodules implanted throughout the peritoneal cavity.<sup>89</sup> This microscopic disease frequently remains after surgical debulking procedures and escapes detection by traditional surgical and laparoscopic second-look procedures as well as other non-optical imaging approaches.<sup>90–92</sup> The urgent need for sensitive detection of this problematic microscopic disease suggests that PFD could be of value in this application.

Preclinical studies using Fischer 344 rats conducted by Chan et al. in 2002 and Ludicke et al. in 2003 using ALA-induced and/or HAL-induced PpIX to image ovarian cancer were successful in detecting lesions not evident by white-light imaging (Figure 12), with a fluorescence intensity ratio of neoplastic to normal tissues of approximately 4:1.<sup>93,94</sup> The average size of the optically biopsied metastatic lesions measured by Chan et al. was 1.0 mm (range 0.3–2.5), compared with 1.5 mm (range 0.5–2.9) with standard white-light illumination.<sup>93</sup> In a clinical study using ALA-induced PpIX in 29 patients, the ovarian cancer nodule detection sensitivity was 92%, a marked improvement over that of white-light imaging.<sup>95</sup> Loning and colleagues also reported in this clinical study that, of the 13 patients in whom disease was confirmed either histologically or cytologically, 4 patients had lesions that were detectable only by PpIX fluorescence emission (Figure 13). In these studies, however, the absence of suitable instrumentation for high-resolution, *in vivo* microscopy limited the investigators' capability to detect only those nodules larger than 300  $\mu\text{m}$ .



**Figure 13.** Laparoscopic images comparing metastatic ovarian carcinoma lesions in human patients under white- and blue-light illumination following intraperitoneal instillation of ALA in human patients. As observed in preclinical studies for detection of micrometastatic ovarian cancer using PFD, lesions are visible. Tumor was detected on tissue specimens by strong red fluorescence in lesions measuring  $<0.5$  mm. Reprinted with permission from ref 95. Copyright 2004 American Cancer Society.



**Figure 14.** (A) Schematic of the prototype fiber-optic fluorescence microendoscope imaging system. Fluorescence excitation is provided by a light-emitting diode (LED) which is directed through the objective via a dichroic mirror. Excitation light is directed into the mouse through a flexible submillimeter imaging fiber which also collects fluorescence emission. The longer wavelength emission passes the dichroic mirror and is registered on a CCD camera with on-chip multiplication gain. (B) Fluorescence image of microscopic tumor nodules (tens of micrometers in size) detected on the peritoneal wall of an ovarian cancer mouse by the fluorescence microendoscope using BPD as the contrast agent. The scale bar is  $100\ \mu\text{m}$ . (C) Hematoxylin-eosin (H & E) stain of a  $5\ \mu\text{m}$  section from the same region. Arrows indicate tumor nodules. Reprinted with permission from ref 15. Copyright 2009 Nature Publishing Group.

Motivated by these promising results using PS fluorescence for detection of ovarian cancer nodules, Zhong and Celli et al. recently combined PFD with high-resolution fluorescence microendoscopy to achieve minimally invasive detection of nodules *in vivo* on the order of a few tens of micrometers (Figure 14),<sup>15</sup> an order of magnitude smaller than the nodules detected in previous experiments.<sup>93</sup> In this study, which used the photosensitizer benzoporphyrin derivative monoacid ring A (BPD, or Visudyne, QLT Inc.), a flexible imaging fiber coupled to a fluorescence microscope was used to achieve the higher spatial resolution while conducting minimally invasive imaging inside the peritoneal cavity of mice with a model of disseminated ovarian cancer.

The inherent ability of a PS to serve in the dual capacity as an imaging agent and a light-activated therapeutic agent has not been extensively developed for this application. The

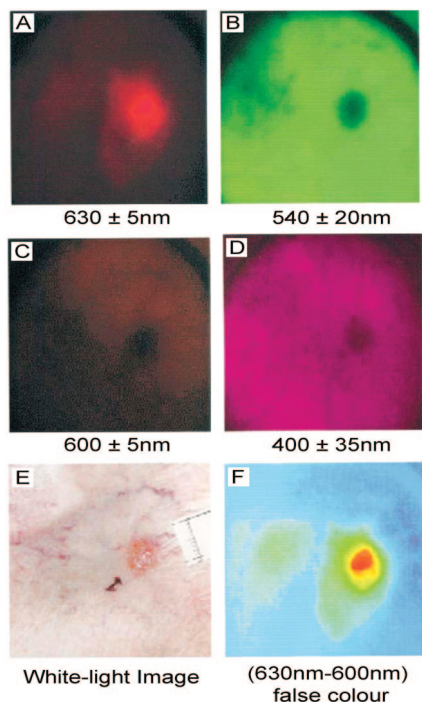
possibility of seamless integration of therapy and online monitoring of the treatment response is of particular interest for ovarian cancer, a disease for which PDT has shown promise in phase I and II trials with minimal peripheral toxicity.<sup>96–98</sup> In the study of Zhong and Celli et al. using BPD, PFD was used to conduct baseline imaging to assess the disease state immediately before intraperitoneal therapeutic irradiation. The PS was then activated and the treatment response was assessed in a follow-up imaging session conducted several days later.<sup>15</sup> Using BPD fluorescence to quantitatively report the acute treatment response, the study found that the tumor nodules continued to grow unchecked in untreated mice, while in the treatment group there was a significant reduction in mean tumor volume. This finding indicates the promise of PS-based fluorescence microendoscopy for monitoring PDT response, as well as the potential of this approach to fulfill a broader clinical need for improved outcome assessment following therapeutic intervention. Further studies are warranted to correlate feedback from imaging with long-term outcomes to evaluate the capability of this approach for early reporting following treatment and, by extension, as a tool to aid in rational treatment planning.

#### 2.4.4. Photosensitizer Fluorescence Detection in Skin Cancer

The integration of PFD and PDT is readily accomplished in dermatological applications due to the accessibility of skin-based lesions, as well as the simplicity of topical drug administration. PFD and PDT have been used for imaging and treatment of basal cell carcinoma (BCC),<sup>99</sup> squamous cell carcinoma (SCC),<sup>42,100–104</sup> Bowen's disease,<sup>103,105–108</sup> Paget's disease,<sup>105,109</sup> guidance of Mohs surgery,<sup>110</sup> and other dermatological indications. The original demonstration of exogenous ALA administration for PDT was for the treatment of superficial BCC and SCC by Kennedy, Pottier, and Pross in 1989.<sup>48</sup> In this study, the authors noted that the topical application of ALA was well suited to delineating dermatological malignancies due to the propensity of ALA to penetrate abnormal but not normal keratin, further enhancing PpIX fluorescence contrast in abnormal tissue.

Andersson-Engels and colleagues in Lund, Sweden, attempted to increase this PpIX-based fluorescence tissue contrast in normal skin in seven patients with nodular BCC, SCC *in situ*, or cutaneous T-cell lymphoma. A multichannel fluorescence imaging system developed in an earlier study<sup>111</sup> was used to collect PpIX (635 nm), autofluorescence (470 and 600 nm), and photobleached product (670 nm) emission from both cancerous lesions and surrounding normal skin before and after PDT. This imaging-based approach was complemented by a fiber-based, point-measuring system<sup>111</sup> that provided spectra from tissue sites. This information was then used to unmix background autofluorescence from tumor-based PpIX fluorescence on a pixel-by-pixel basis.<sup>112</sup> This was a promising and insightful attempt to use PS fluorescence to distinguish normal skin from malignant lesions, as well as to track the accumulation of photodegraded products during PDT. As the authors themselves point out, however, there was no independent verification of the tumor margins or of treatment response following PDT, which would have enhanced the interpretation of the results in this early investigation of multichannel PFD.

A later study by Hewett et al. used a multispectral fluorescence imaging system with an integrated excitation



**Figure 15.** Multispectral images (A–D) taken pre-PDT of a superficial BCC on the ankle and the corresponding white-light image (E) taken before ALA application. Real-time image processing displays the difference between the 630 and 600 nm images displayed with a false-color scale (F) showing clearly the extent of the lesion and the differential accumulation of PpIX in the SBCC compared with the application site and surrounding healthy tissue. Scale bars for these images were not available. Reprinted with permission from ref 113. Copyright 2001 Wiley.

source to monitor the kinetics of PpIX photobleaching before, during, and after PDT of superficial skin cancer *in vivo*.<sup>113</sup> The rate of light delivery and fractionation schedule were varied to optimize the treatment outcome. Specifically, rapid photobleaching early in the treatment suggested that the light dose either should be given more slowly or should be fractionated to achieve a more consistent therapeutic effect over the time course of the treatment. In the same study, Hewett et al. used information from multispectral fluorescence images, collecting the fluorescence signal from not only the PpIX emission but also surrounding tissue autofluorescence in an effort to more accurately delineate the margins of the lesions. Emission at 540 nm was found to decrease in the lesion relative to surrounding tissue. This contrast was further enhanced by applying a false-color map that displayed each pixel value in a different color (Figure 15).

An important consideration in using PFD and PDT to improve treatment efficiency and outcome is understanding PpIX production and distribution in diseased tissue as well as adjacent normal skin. Martin and colleagues<sup>114</sup> examined microscopic heterogeneities in the distribution of PpIX following topical application of 20% ALA in 16 patients with BCC and found that macroscopic imaging correlated well with the presence and gross margins of BCC. Microscopic examination of the tissue, however, revealed significant heterogeneities in the ALA-induced PpIX fluorescence patterns and “showed no inherent selectivity for BCC over normal epidermal structures”.<sup>114</sup> The authors suggested that any macroscopic selectivity could be attributed to increased penetration of ALA into the compromised stratum corneum surrounding the tumor as well as tumor thickness effects.

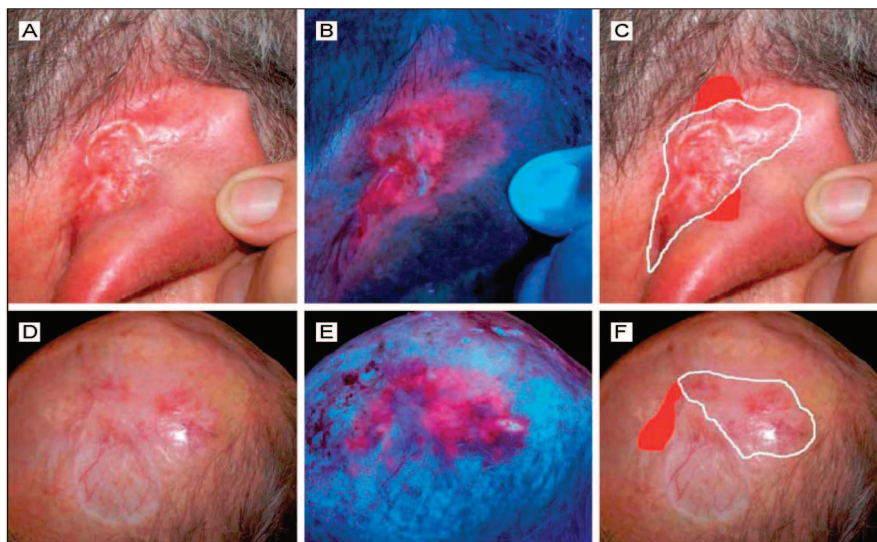
These findings indicated that PpIX fluorescence could be useful for treating malignant cutaneous lesions or superficial BCC, but optimizing the formulation and delivery of ALA will be important for deeper lesions.

Motivated by the need to improve the selectivity and homogeneity of porphyrins accumulated in diseased dermatological tissue, Fritsch and colleagues compared ALA-induced versus MAL-induced porphyrin production in human solar keratoses (SK) and adjacent normal skin.<sup>115</sup> Incubation with ALA was found to lead to higher levels of total porphyrin accumulation than incubation with MAL in both SK and normal skin. Selectivity for SK versus adjacent normal skin, however, was significantly better with MAL than with ALA. The study found that, after 6 h of incubation, the ratio of total porphyrin enrichment in SK versus adjacent normal skin was 8.7 for MAL in contrast to 5.1 for ALA. A distribution analysis of the porphyrin metabolites following MAL incubation revealed that 82% of the porphyrins in SK were specifically composed of PpIX, in contrast to 89% in normal skin, while ALA-induced porphyrin metabolites consisted of 90% PpIX in both normal skin and SK. These results demonstrated that MAL provided better selectivity for SK than ALA, due, in part, to the preferential penetration of MAL into damaged skin. However, the lower total porphyrin production and lower proportion of PpIX levels observed with MAL are important factors to consider in designing future PDT-based strategies for SK.

In another study comparing ALA and its hexyl and methyl esters for dermatological applications, Moan and colleagues<sup>116</sup> evaluated PpIX production in normal skin following topical administration of 0.2%, 2.0%, or 20% (w/w) ALA, MAL, or HAL. The group found that the concentrations required to induce half the maximum PpIX fluorescence were 2% for ALA, 8% for MAL, and 1% for HAL, confirming the need for higher concentrations of topical MAL to reach comparable levels of PpIX in normal skin.

Clinical studies evaluating the impact on treatment response for ALA versus MAL PDT of dermatological lesions have also been conducted, but at this time it is not clear as to whether any decisive conclusion can be drawn. Kuijpers et al. and Wiegell et al. examined the response rates for ALA and MAL PDT for BCC<sup>117</sup> and acne vulgaris,<sup>118</sup> respectively, with both studies finding that there was no significant difference between the two agents. The adverse effects associated with ALA PDT of acne vulgaris were more severe than those associated with MAL PDT,<sup>118</sup> whereas the pain scores were comparable for the two modalities during treatment of BCC.<sup>117</sup> This ambiguity is in contrast to the situation in bladder cancer PFD, where HAL became widely accepted, with essentially all recent studies favoring HAL over free ALA for PFD in the bladder.

One recent study conducted by Redondo and colleagues at the University Clinic of Navarra in Spain using MAL-induced PpIX for delineation of BCC demonstrated promise in using PFD for the guidance of Mohs micrographic surgery. In this clinical pilot study, Redondo et al. retrospectively compared the margins as determined by white light and MAL-induced PpIX PFD with the “real margins” determined by histopathology (Figure 16).<sup>110</sup> In 14 of 20 patients, the margins determined by PFD corresponded exactly to the gold-standard histopathologic evaluation, where stepwise excision of tumor tissue was performed until the presence of normal tissue was verified by hematoxylin–eosin staining. In half of these patients, the diseased regions determined

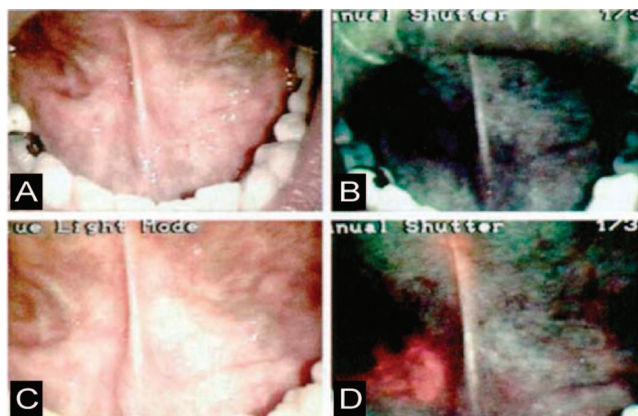


**Figure 16.** MAL-induced PpIX fluorescence images of two patients (A–C and D–F) who received Mohs micrographic surgery (MMS). Images were obtained 3 h following administration of MAL. Clinical pictures showing the outlines of the first MMS excision (white lines) were conducted without respect to the fluorescence images. The real margins of the tumors confirmed by histopathologic analysis are also included (red areas) and were already delineated by the fluorescence seen in panels B and E. The agreement between the fluorescence and histopathology margins suggests that the use of PFD may speed Mohs surgery by reducing the number of stepwise excisions necessary. Reprinted with permission from ref 110. Copyright 2008 American Medical Association.

from PFD (and in agreement with histopathology) were larger than predicted by white light. The results of PFD included three false-negative results and three false-positive results, two from recent scar tissue. The authors of this study concluded that PFD has the potential for guidance of Mohs micrographic surgery by reducing the number of necessary excisions. However, the authors themselves noted the inherently limited ability of PFD to determine the depth of BCC.

#### 2.4.5. Photosensitizer Fluorescence Detection in Oral Cancer

The prognosis of oral cancer is largely dependent on the stage presented at the time of diagnosis. For those with early disease, the 5 year survival rate is 82%, while for those diagnosed with advanced disease, the prognosis is considerably worse, at 53% for patients with regional spread and 28% for patients with distant spread.<sup>88</sup> As such, a minimally invasive, routine screening technique for the oral cavity with minimal side effects could have a dramatic clinical impact. As with other cancers, small and/or early-stage lesions often escape routine visual inspection by white light, indicating the potential of another application where PFD could be of value. Motivated by this promise, Leunig et al. studied patients with suspected oral cancer using topical application of ALA.<sup>119,120</sup> As with other cancer detection applications, fluorescence imaging provided superior diagnostic efficacy over white-light imaging, revealing a subgroup of patients with dysplasia, carcinoma in situ, primary tumor, secondary carcinoma, and tumor branches that were not evident by white-light inspection (Figure 17). In a subsequent study, Betz et al. systematically compared diagnosis by white light, ALA-induced PpIX fluorescence, autofluorescence, and a combination of PpIX fluorescence and autofluorescence, termed combined fluorescence diagnosis (CFD).<sup>121</sup> CFD was the most effective diagnostic approach, with spectral analysis of histology-validated cancerous tissue revealing both the expected increased PpIX fluorescence accompanied by a concomitant decrease in autofluorescence intensity. The ability to demarcate neoplastic regions was found to be



**Figure 17.** Comparison of white-light and ALA-induced PpIX fluorescence imaging (excitation wavelengths 375–440 nm) for identification of oral cancer: (A) white-light image of a tumor in the right floor of the mouth, (B) autofluorescence imaging under excitation with blue-violet light of the same region, (C) same region imaged again under ordinary white light, 1.5 h after application of ALA, (D) PpIX fluorescence image of the same region. Reprinted with permission from ref 120. Copyright 2000 Wiley.

independent of the disease stage. A subsequent study by Ebihara et al. indicated that fluorescence emission following ALA administration can also differentiate between the different stages of premalignancy and malignancy in a hamster cheek pouch model of oral cancer.<sup>122</sup>

#### 2.4.6. Other Applications of Photosensitizer Fluorescence Detection

In this review, we have focused on a subset of PFD applications that have particular scientific interest and/or have made the most dramatic clinical impact. However, the principal of PS fluorescence imaging for detection of diseased tissue can be applied to any situation in which the PS can be delivered to the tissue of interest and where an imaging device can access the tissue to image fluorescence emission. Since varied routes of drug delivery can be employed to access different anatomical sites and advances in fiber-optic



fluorescence imaging allow the use of submillimeter-diameter probes to maneuver through narrow internal luminal spaces, there is clearly a broad range of applications, and the full potential of this approach is yet to be explored. For example, the potential for fluorescence imaging of early-stage lung cancer was demonstrated in a clinical study in which patients were administered ALA via inhalation.<sup>123</sup> Similarly, fluorescence endoscopy using exogenously administered ALA has been used extensively to detect dysplasia in Barrett's esophagus.<sup>124,125</sup> Imaging of ALA-induced PpIX fluorescence has been evaluated for detection of cervical cancer by both topical<sup>126–128</sup> and oral<sup>129</sup> administration of ALA. In the study by Duska et al., oral administration overcame the tumor penetration and distribution inhomogeneity previously reported with topical delivery of ALA for cervical malignancies.<sup>117</sup>

## 2.5. Perspective and Future Outlook for PFD

Having noted many clinical successes and promising preclinical studies using PFD, this approach has certain limitations that are common to any fluorescence-imaging-based detection strategy. Fluorescence emission is generally collected through a lens or fiber en face, generating a two-dimensional projection of the tumor and surrounding normal tissue. Because fluorescence excitation is generally accomplished with blue light, which is highly scattered as it propagates through tissue, the depth of penetration may be as low as a few hundred micrometers. For flat lesions, such as carcinomas in situ, this approach is highly successful at delineating disease margins, while lesions which may have a considerable subsurface cannot be observed without the capability for depth-resolved imaging. This inherent limitation suggests the implementation of a multimodality imaging approach based on PFD for identification of neoplastic regions that is complemented by a depth-resolved structural imaging modality, such as OCT, that can reveal structures up to 2 mm deep inside tissue. This multimodal imaging strategy would increase the specificity of PFD by improving the clinician's ability to reject fluorescence false-positive results on the basis of a more detailed picture of the underlying structure.

Notwithstanding the limitations of this approach, the potent capability offered by PFD to combine sensitive imaging with selective destruction of diseased tissues has not been exploited to its full potential as a tool for treatment monitoring and for "search and destroy" treatment approaches. Virtually all therapeutic applications of PDT could benefit from the integration of PFD as a routine tool for feedback and dosimetry. For in situ PFD applications, an endoscope could be inserted into the patient alongside a light delivery fiber using PFD to obtain feedback on the disease margins while using photobleaching as a real-time dosimetry tool to monitor the extent of PS activation at particular sites. In this manner, light and PS dose could be modulated online to achieve a truly consistent PDT dose (although this can only be predictive for sufficiently thin lesions and if there is in fact excess photosensitizer present in the tissue to make a fluorescence measurement). Furthermore, by utilizing the PS already present in tissue following FGR, adjuvant postresection PDT could be more broadly applied for the selective destruction of residual disease for other clinical intraoperative applications in which PFD is used for surgical guidance.


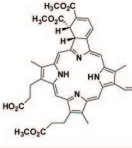
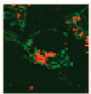

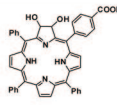
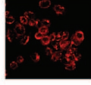
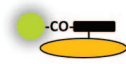
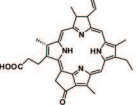
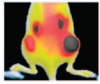

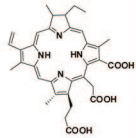
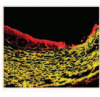


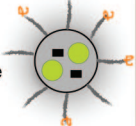
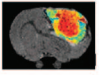
## 3. Targeted Photosensitizers as Selective Therapeutic and Imaging Agents

### 3.1. Overview

Nonspecific localization of imaging and therapeutic agents often leads to suboptimal treatment outcomes and unintended toxicity to normal tissues following exposure to light irradiation during PDT. Numerous attempts have been made to alter the structure of photosensitizers by moderating physiochemical properties such as hydrophilicity, hydrophobicity, log *P*, charge, and delivery strategies to achieve optimum activity for photodynamic action, but even the high accumulation of photosensitizer at the target tissue in vitro does not warrant an ideal outcome in vivo.<sup>130,131</sup> A number of target-specific strategies for PDT have been developed to avoid these problems and improve PS specificity for diseased tissue.<sup>132</sup> PS fluorescence has been used as a reporter of PS accumulation via spectroscopy and microscopy<sup>133</sup> and has also been combined with other imaging agents to obtain a multimodal platform for imaging and treatment,<sup>19,20,134–136</sup> as described in section 5.4. Section 3 focuses on two key strategies to enhance PS selectivity: (i) the utilization of site-specific delivery agents that carry PSs to target tissue (e.g., nanoparticles, antibodies, aptamers, or peptides)<sup>19,20,137</sup> or (ii) the synthesis of target-activated PDT agents that remain optically and photodynamically inactive until encountering the molecular target for selective activation and retention at the site of interest.<sup>138</sup> We discuss examples of the implementation of both of these strategies in the following sections.

### 3.2. Site-Specific Delivery

A number of PS conjugates have been developed for site-specific delivery in the context of both PDT and imaging applications. These constructs for targeted delivery often make use of the PS as a dual fluorescence imaging and PDT agent, but a separate imaging moiety can be added when desired. As an example of the former case, Soukos et al.<sup>14</sup> used a monoclonal antibody conjugated to Ce6 as a tumor-specific targeting agent for imaging and therapy in a hamster cheek pouch carcinogenesis model. This type of construct, defined as a "photoimmunoconjugate" (PIC), allows for the specific delivery of a photosensitizer by targeting a protein, such as an enzyme or receptor, that is overexpressed or overactive in diseased tissue. The targeted molecule in the study by Soukos et al.<sup>14</sup> was the EGFR, which is overexpressed in a number of human tumors. The authors used an anti-EGFR monoclonal antibody (C225) conjugated to Ce6 to detect and treat premalignant lesions and demonstrated the potential of the PIC to be used both as a diagnostic platform and monitoring tool to evaluate therapeutic response.<sup>14</sup> Recently, another PIC was assembled using the same antibody (C225) conjugated to the PS BPD (verteporfin). The uptake and localization of the BPD–C225 PIC has been characterized in live cells by confocal imaging (Figure 18A),<sup>139</sup> and BPD–C225 has been applied for target-specific destruction of EGFR-positive ovarian cancer cells.<sup>140</sup> In another study, pyropheophorbide a (Pyro) and verteporfin were conjugated to a single-chain antibody fragment (scFv) specific to the human EGFR2 (HER2). Fluorescence imaging of the two immunoconjugates demonstrated the improved specificity of both conjugates for HER2-positive cancer cell lines.<sup>141</sup>

Targeting Agent	Imaging Agent	Application
A  Antibody	BPD 	 Subcellular localization of BPD in human ovarian cancer cells <i>in vitro</i> <sup>139</sup>
B  Peptide	TPC 	 Peptide-mediated delivery of TPC to human breast carcinoma cells <i>in vitro</i> <sup>142</sup>
C  Small Molecule	Pyro 	 Folate receptor-targeted delivery of Pyro in a subcutaneous murine model for human epidermoid carcinoma <sup>143</sup>
D  Antibody	Ce6 	 PFD of aortic plaques <i>ex vivo</i> with an antibody-Ce6 conjugate in a rabbit model <sup>146</sup>
E  Antibody	Alexa Fluor 680	 Real-time post-PDT imaging of secreted VEGF using an antibody-fluorophore conjugate in a subcutaneous murine model for prostate cancer <sup>147</sup>
F  Peptide	Alexa Fluor 594 Iron oxide	 Peptide-targeted nanoparticle for PFD, PDT, and MRI in an orthopic rat glioma model <sup>24</sup>

**Figure 18.** Disease-targeted constructs for PFD and PDT, showing the targeting moiety, imaging agent, and biological application. (A) Ovarian cancer cells incubated for 15 h with 140 nM equivalent BPD–C225 construct. A confocal laser scanning fluorescence microscope is used to monitor the subcellular localization of the PS with high spatial resolution. Fluorescence from the mitochondrial markers is shown in false color as green, and BPD is shown in false color as red. Reprinted with permission from ref 139. Copyright 2006 The International Society for Optical Engineering (SPIE). (B) Confocal microscopy shows that TPC conjugated to a membrane-penetrating arginine oligopeptide (R7) enters MDA-MB-468 (human breast carcinoma) cells efficiently where red represents fluorescence signal from TPC. Reprinted with permission from ref 142. Copyright 2006 Wiley. (C) Monitoring the fluorescence signal distribution after intravenous injection of 100 nmol of Pyro–GDEVGSGK–folate conjugate to double-tumor-bearing mice (with an FR-positive tumor on the right side and FR-negative one on the left side) indicates preferential accumulation of construct in the receptor-positive tumor, establishing the NIR imaging ability of the targeted PS construct. Reprinted from ref 143. Copyright 2007 American Chemical Society. (D) Fluorescence from aortic segments 24 h postinjection of Ce6–maleylated albumin conjugate indicates the construct's ability to detect and/or photodynamically treat inflamed plaques. Red represents Ce6, and yellow is tissue autofluorescence from the elastic fibers. Reprinted with permission from ref 146. Copyright 2008 The Royal Society of Chemistry and Owner Societies. (E) Post-PDT changes in VEGF expression are monitored with the molecular imaging strategy, where an Avastin–Alexa Fluor construct was imaged in PDT-treated subcutaneous PC-3 (prostate cancer) tumors, 6 h following laser irradiation, and the fluorescence image of tumor labeling is pseudocolored in gold. Reprinted with permission from ref 147. Copyright 2008 American Association for Cancer Research. (F) T2-weighted magnetic resonance images at day 8 after PDT treatment from F3-targeted Photofrin-containing nanoparticles in a 9L brain tumor showing imaging and monitoring of therapeutic efficacy post-treatment. Reprinted with permission from ref 22. Copyright 2006 American Association for Cancer Research.

In addition to antibody-based PICs, small molecules and peptides can also be used to target cancer cells. For example, Choi et al.<sup>142</sup> designed a PS conjugate with a membrane-penetrating arginine oligopeptide (R7), R7–TPC, to enhance the cellular uptake of the PS 5-(4-carboxyphenyl)-10,15,20-triphenyl-2,3-dihydrochlorin (TPC). Confocal imaging of the uptake of this conjugate into a human breast cancer cell line (MDA-MB-468) is shown in Figure 18B.<sup>142</sup> Stefflova et al.<sup>143</sup> designed and synthesized a folate receptor (FR)-targeted, water-soluble, and pharmacomodulated PDT agent that selectively detects and destroys the targeted cancer cells while sparing normal tissue. As shown in Figure 18C, this construct consists of three parts: (1) the PS (Pyro), for near-infrared (NIR) imaging and PDT, (2) a folate moiety, serving as a tumor-homing molecule that guides the PS to FR-overexpressing cancer cells, and (3) a short peptide sequence

between the PS and folate that improves the stability, solubility, and specificity of the probe. Notably, Pyro possesses a long-wavelength absorption peak (665 nm), red fluorescence emission approaching the NIR wavelengths (peaks at 675 and 720 nm) for deeper tissue imaging, and a singlet oxygen quantum yield of over 50%, making it an efficient PDT agent.<sup>143</sup> An *in vivo* imaging study established preferential accumulation of the targeted construct in FR-positive tumors post intravenous injection with rapid clearance from normal tissues.<sup>144</sup>

Site-specific PDT and PS conjugate imaging has also been applied to a number of non-neoplastic diseases. For example, a targeted PS conjugate has been used in the intravascular detection and treatment of inflamed atherosclerotic plaques.<sup>145,146</sup> A Ce6–maleylated albumin construct (MA–Ce6) showed specific accumulation in plaques via surface spectrofluoro-

rometry, fluorescence extraction of Ce6 from aortic segments, and confocal microscopy (Figure 18D). These studies demonstrated the ability of a PDT agent to detect and selectively treat inflamed plaques.<sup>145,146</sup>

As mentioned above, an imaging moiety that is not a PS can be used to enhance imaging contrast and to facilitate multimodal imaging of PS conjugates. Since fluorescence emission and the production of singlet oxygen (via energy transfer) are competing de-excitation pathways, there is inevitably a trade-off between the fluorescence and singlet oxygen quantum yields of the PS (Figure 4). This means that highly efficient singlet oxygen-generating PS molecules are often weak fluorophores. A simple alternative to the use of PS fluorescence for imaging PICs is to add a fluorescent probe with a high fluorescence quantum yield. Figure 18E gives an example of a fluorophore–antibody conjugate that has been applied successfully for molecular imaging of vascular endothelial growth factor (VEGF) secretion dynamics following PDT, which represents a challenging imaging application.<sup>147</sup> Section 5.3.3 describes the application of this molecular imaging strategy for monitoring secreted factors in detail. We are not aware of a PIC that also has a dedicated fluorophore for imaging, but this is a probable direction for future development of site-targeted, dual fluorescence contrast and PDT agents.

A second example of the use of a non-PS imaging moiety is a nanoconstruct loaded with both PS molecules and additional imaging agents. In a recent example of site-specific targeting using a multimodal nanoplatfrom, Reddy et al.<sup>22</sup> conjugated a tumor vasculature-targeting F3 peptide on a multifunctional, polymeric, nanoparticle-encapsulating PF as a PDT agent and iron oxide as an MR imaging agent. This approach, while inherently more complex than using a single molecule to serve multiple functions, offers the advantage that each selected agent can provide optimal performance in a single function. For example, PF, although it yields excellent phototoxicity, has not been favored as a PS due to its high systemic toxicity and prolonged cutaneous toxicity and, as noted above, the asynchronous localization of fluorescent and phototoxic components. However, when delivered with high specificity to the target tissue, a small concentration can produce the desired tumor destruction with minimal peripheral toxicity. Furthermore, rather than using the relatively low fluorescence quantum yield of the PS to provide contrast, nanoparticles can be loaded with a brightly fluorescent imaging agent such as the Alexa Fluor dye chosen in this study. *In vitro* and *in vivo* studies confirmed that the attachment of the F3 homing peptide on the nanoparticle surface significantly improved tumor nanoparticle localization and retention and improved the efficacy of PDT as evidenced by an enhanced overall survival in the animals.<sup>22</sup> Figure 18F is a schematic of the nanoconstruct and a corresponding *in vivo* MRI image. Nanotechnology has already begun to play a major role in biomedical applications, and these targeted multimodal platforms represent a new venue for simultaneous detection, treatment, and monitoring of PDT treatment therapeutic effects.

### 3.3. Site-Activated Constructs

The application of fluorescence imaging to PDT can be immensely enhanced by devising methods to specifically activate the PS molecules themselves within the site of interest. It is possible, through careful chemical design, to energetically quench a PS by placing it in close proximity

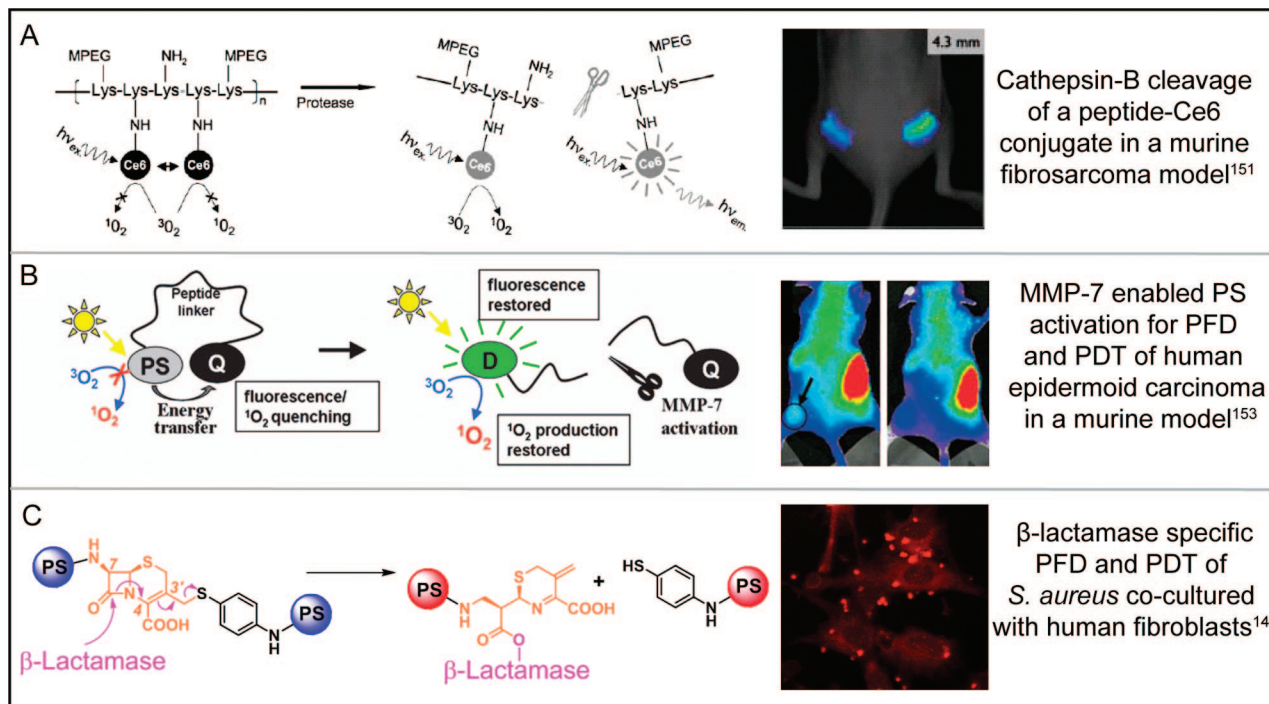
to another identical PS (self-quenching) or to another dye molecule (energy transfer).<sup>148–150</sup> If the chemical bonds holding the PS and quencher in contact (self-quenching or energy transfer) are broken, the PS will become unquenched and fully activated. A targeted delivery mechanism is not needed in this approach, as the specificity is achieved by selective activation of the construct in the diseased tissue. Applications of quenched, site-activated PS constructs to PDT and imaging have been reviewed in detail by Stefflova et al.<sup>138</sup> The authors introduced the term “killer beacons” to define a customizable construct composed of a fluorescent PS, responsible for both imaging and therapy, attached to energetic quenchers through a functional linker.

Some of the early work in this area was done by Weissleder et al. to develop protease-activated NIR fluorescent probes for cancer imaging.<sup>151</sup> Later, the same group conjugated numerous Ce6 molecules (a PDT agent) onto a polylysine backbone<sup>152</sup> (Figure 19A). The PS molecules were held in a close geometry for efficient self-quenching, prohibiting energy transfer between the PS and ground-state molecular oxygen, thus inhibiting the generation of <sup>1</sup>O<sub>2</sub>. In the presence of tumor-associated enzymes (such as cathepsins), the peptide linkages of the polylysine backbone were cleaved, and the degraded probes became highly phototoxic and fluorescent. The authors validated the construct, not only in terms of *in vivo* PDT efficacy but also for imaging by using fluorescence molecular tomography to determine the distribution of Ce6 in tumors. This work allowed not only visualization of the target but also quantification of the local drug concentration before selective therapy. These site-activated dual PDT agents and probes hold promise for future tailored treatments to avoid unnecessary side effects.

In the PDT community, many papers have focused on using the quenched fluorescence of a PS as a reporter for the PS's quenched singlet oxygen efficiency. Recently, Lovell et al.<sup>153</sup> established the correlation between PS fluorescence quenching and singlet oxygen quenching, implying that the fluorescence intensity can be used as a convenient indicator for the singlet oxygen production status of a PS. In this study, Förster resonance energy transfer (FRET) quenching of Pyro fluorescence and singlet oxygen production was demonstrated with partner FRET-acceptor molecules, with a maximum of 90% fluorescence and singlet oxygen quenching observed, depending upon the distance between Pyro and the FRET-acceptor molecules and the extent of spectral overlap between the FRET-acceptor absorption spectrum and the Pyro fluorescence emission spectrum.

Putting this concept into practice, Zheng et al.<sup>154</sup> have introduced several FRET-based target-activatable constructs consisting of a PS and quencher held together by functional linkers, which the authors have termed “photodynamic molecular beacons” (PMBs). The feasibility of the PMB construct was first demonstrated using an apoptotic factor-cleavable linker, which carries implications for molecular imaging of PDT-induced apoptosis as discussed in detail in section 5.2.2. While this construct is not selective for tumor cells, it has paved the way for the development of a tumor-site-selective design based on optical and photodynamic activation of the PS by matrix metalloproteinase 7 (MMP-7),<sup>154</sup> an important tumor biomarker as discussed in section 5.3.2.

This MMP-7-activated PMB, which used a dark FRET quencher for the purpose of quenching both the PS fluorescence and singlet oxygen quantum yields (Figure 19B), was



**Figure 19.** Concept design and application of PS fluorescence in site-activated constructs. (A) Release of Ce6 for PFD and PDT following cleavage of a cathepsin B-specific construct in a subcutaneous murine model for human fibrosarcoma. Three-dimensional fluorescence-mediated tomography was used to image the HT1080 fibrosarcomas following 24 h of incubation with a poly-L-lysine–Ce6 construct (0.125 mg of Ce6 equiv/kg). Reprinted with permission from ref 152. Copyright 2006 American Association for Cancer Research. (B) Proof-of-concept study demonstrating the cleavage of a peptide linker by MMP-7 for PFD and PDT in a subcutaneous murine model for human epidermoid cancer. The PP<sub>MMP-7</sub>B construct (drug) was injected intravenously (80 nmol) in a single mouse bearing two KB tumors on each hind leg. Only one tumor, left leg, was treated, and this mouse was monitored by white-light and fluorescence imaging before treatment (left image, 3 h after drug injection) and 1 h after PDT (right image, 5 h after drug injection) on one hind flank. Right image: The treated tumor on the left leg became edematous 1 h post-PDT, while no fluorescence change is observed in the untreated right tumor. Reprinted with permission from ref 154. Copyright 2007 National Academy of Sciences of the U.S.A. (C) Mechanism for the cleavage of an enzyme-activated prodrug where the blue balls represent the inactive PSs in the uncleaved construct and the red balls represent the photoactive PSs. The image shows PS fluorescence in cellular cocultures of *Staphylococcus aureus* with human foreskin fibroblasts (HFFs) where significantly greater fluorescence intensity is observed in bacterial cells than in the neighboring fibroblasts, indicating cleavage of construct only at the site of infection. Reprinted with permission from ref 13. Copyright 2009 Wiley.

designed to demonstrate exquisite PDT selectivity for MMP-7-positive tumors. In this construct, Pyro was conjugated to BHQ via an eight-amino acid linker sequence that serves as a substrate for MMP-7 cleavage (Pyro–GPLGLARK–BHQ).<sup>154</sup> The PS fluorescence and singlet oxygen production is effectively turned “on” following MMP-7 cleavage of the linker sequence. Live cell fluorescence images suggest selective activation of this PMB in MMP-7-positive tumor cell lines, compared with MMP-7-negative tumor cell lines (Figure 19B).

The PMB concept is a promising approach to develop tumor-selective PDT agents, independent of the selectivity of PS delivery to cancer cells. That is, the imaging and therapeutic specificity of PMBs is determined by the activity of the targeted biomarker in cancer cells and on the degree of interaction of the PMB with the biomarker. Moreover, this same principle can be applied to other activation schemes to generate a wide range of clinically useful strategies to enhance the specificity and efficacy of PDT to treat cancer and other pathologies. For example, Zheng et al.<sup>13</sup> have developed a phenothiazinium-based, target-activated construct selective for  $\beta$ -lactam-producing phenotypes of pathogens (Figure 19C). The authors used a  $\beta$ -lactamase-sensitive cephalosporin linker attached to two phenothiazinium PSs, such that the PSs are quenched in their ground state and activated by cleavage of the  $\beta$ -lactam ring only in the presence of the  $\beta$ -lactamase enzyme produced by resistant

bacteria.<sup>13</sup> This work has potential for differentiating human cells from microbial cells and also for selectively targeting  $\beta$ -lactamase-producing phenotypes. The authors demonstrated the selective cleavage of the construct by visualizing an increase in PS fluorescence in the presence of infected human cells, compared with noninfected healthy controls. This design is an ideal example of the “see and treat” approach, where a PS construct is cleaved and activated for photodestruction only in the presence of  $\beta$ -lactamase-positive infections, preventing any collateral damage to healthy host cells.

To summarize, the use of targeted imaging for in vivo PDT applications is not yet well developed, and many challenges still remain in determining the most appropriate target to discriminate diseased cells from healthy human cells. One major hurdle is the lack of tumor-specific biomarkers, which means that “selective targeting” of tumor cells typically relies on exploiting modest differences in the expression levels of molecular targets in normal versus diseased tissue. Therefore, the design and synthesis of appropriate disease-targeted PS constructs, capable of discriminating and localizing only in tumor tissue, is a challenging task. In contrast, the targeting of enzymes specific to antimicrobial resistant microbes appears ripe for the application of target-activated constructs. A promising future direction is the use of nanotechnology, which provides a platform for the development of multimodal carriers<sup>21,155</sup> by

combining different imaging, targeting, and treatment modalities to further enhance the imaging capabilities in conjugation with PDT treatment. However, as currently practiced there are numerous hurdles in translation of nanotechnology to targeted multimodal treatment, such as transport barriers, drug distribution, and drug uptake. For the constructs to be tested in a high-throughput manner, so that several nanoagents can be evaluated rapidly, there is a need for appropriate models for rapid initial testing. In this context, the emergence of biologically relevant, three-dimensional (3D) models of disease is an exciting prospective.<sup>10</sup> These 3D platforms restore critical tissue architectural cues absent from monolayer cultures and overcome many of the limitations of animal models, which are time intensive and expensive. In vitro models are well-suited for high-throughput imaging and in combination with nanotechnology will complement the development, and expedite the evaluation, of targeted and site-activated constructs.

#### 4. Imaging for Planning, Assessment, and Monitoring of Photodynamic Therapy Response

##### 4.1. Imaging Methods for Optimization and Dosimetry of Photodynamic Therapy

Imaging prior to the use of PDT is an essential step in therapeutic planning where the tissue of interest, normally a tumor, lesion, or type of diseased tissue or other organs at risk, should be assessed as noninvasively as possible. For cases such as skin cancers or lesions, visual assessment may be possible. However, in most cases, locating the diseased tissue by visual assessment is difficult, if not impossible, and therefore, a method of imaging is typically used. In addition to locating the tissue of interest, it is often possible to discern vascular patterns, areas of pre-existing necrosis, and areas of disease infiltration by choosing from a variety of techniques or contrast agents. The structural and functional information gathered through pretreatment imaging can be used in treatment planning, light delivery, and even treatment dose assessment. Molecular imaging techniques are now emerging to complement structural and functional imaging data to obtain more complete information regarding biological response to treatment, including protein expression and receptor binding data. This exciting category of imaging will be detailed below in section 5. The relationship between these imaging approaches and their roles in pretreatment planning, therapy monitoring, and outcome assessment are summarized schematically in Figure 20.

Some of the most common modalities for PDT treatment planning are endoscope-coupled systems for imaging hollow-tube organs, such as the esophagus, bronchial tube, and colon. Fluorescence bronchoscopy, developed by Xillix Technologies<sup>156,157</sup> and improved upon in an experimental system,<sup>158</sup> is used for the detection of abnormal tissue autofluorescence in laryngeal, lung, and esophageal cancers. Endoscopic ultrasound, developed for detecting dysplasia of the bronchial system, has been extensively tested in humans in detection and treatment guidance for esophageal cancers<sup>159,160</sup> and more recently in the guidance of fiber placement for pancreatic cancer.<sup>175</sup> There have been many endeavors in the detection of cancerous or dysplastic tissue of the colon, with several experimental systems utilizing autofluorescence<sup>161</sup> and other optical techniques, including fluorescence, Raman, and OCT.<sup>162</sup>

	Pre-treatment Planning	Monitoring Therapy	Outcomes Assessment
Structural Imaging	Organs Surrounding tissue Vascular patterns	Light Delivery  Necrosis	Necrosis Blood Flow Tissue Loss Color Changes
Functional Imaging	Photosensitizer Blood Flow Oxygenation	Light Delivery Photosensitizer Blood Flow Oxygenation	PS bleaching  Blood flow changes
Molecular Imaging	Receptor / protein expression PS Binding	Singlet O <sub>2</sub> Pre-treatment modulation PS Bleaching	Signaling / receptor changes

**Figure 20.** Schematic diagram depicting the intersecting roles of imaging in key steps of pretreatment planning, therapy monitoring, and outcome assessment.

Diagnosis and treatment planning for PDT of choroidal neovascularization (CNV) in AMD, which may be one of PDT's greatest success stories, is performed with fluorescein angiography.<sup>163–170</sup> Extravasation of fluorescein from the retinal blood vessels is indicative of the newly formed, leaky blood vessels that are the targets for verteporfin PDT, as occlusion of leaky blood vessels slows the progress of AMD and hence vision loss. Interpretation of the fluorescein angiograms is important for making critical treatment decisions (laser spot size, etc.).<sup>166</sup> OCT imaging of CNV in AMD for treatment planning and therapy is ever increasingly becoming more popular and is discussed further in section 4.5.2.

The proper placement of light delivery fibers in tumors of solid organs is another essential parameter in treatment planning. CT has been used for the identification and treatment planning of cancers located in both solid organs (e.g., the pancreas<sup>171</sup>) and hollow organs (e.g., bladder<sup>172,173</sup> and bronchi<sup>174</sup>). Bown et al<sup>171</sup> reported PDT of 16 patients with inoperable tumors, in which fiber placement occurred under CT guidance. Optical fibers for PF PDT of recurrent malignant brain tumors have been placed under CT guidance prior to surgery.<sup>175</sup> In this example, patients were anesthetized, with CT performed with the base ring of a stereotactic frame already in place. The location and implantation paths of the fibers were determined from the CT imagery and fibers were placed in the surgical suite. Similar techniques have also been used with <sup>31</sup>P MRI to determine tumor location. Chan et al.<sup>176</sup> demonstrated the use of endoscopic ultrasound for optical fiber placement in the normal pancreas, liver, spleen, and kidney of the swine.

##### 4.2. Online Monitoring of Photodynamic Therapy Response

Specific dosimetry for PDT is challenging due to the nonlinear interplay among light dose, irradiation time, and concentration of both the PS and molecular oxygen. Although there are several imaging techniques for PDT dosimetry, as discussed in the previous section, many efforts have been made to develop online measurement techniques to guide the effective dose–response relationship during treatment. Throughout light administration in PDT, there are many photophysical, metabolic, and molecular changes occurring within the treated tissue, each providing a unique signal that

can be monitored. Several different techniques for measuring effective dose–response relationships online involve the detection of the fluorescence signal, blood flow dynamics, blood perfusion, glucose metabolism, and oxygen monitoring.

Perhaps the most well developed and easily accessible method for imaging the effective dose–response relationship during PDT is measurement of the fluorescence and dynamics of photobleaching of the PS itself. Several studies that used this approach for monitoring the response have been described in section 2. However, numerous other imaging techniques and approaches have also been employed as a means of providing online feedback of the treatment response. A fluorescence imaging system originally described by Cubeddu et al. in 1997<sup>177</sup> and subsequently reported in 2000<sup>178</sup> detected cancerous tissue and monitored the emission of disulfonated aluminum phthalocyanine (AlS2Pc) during PDT of MS-2 fibrosarcomas. The time-gated fluorescence imaging system (red-light excitation and 3 ns gated detection) allowed for the online visualization of fluorescence in the tissue of interest, while offline software provided a means for quantifying the fluorescence intensities.<sup>177</sup> During AlS2Pc PDT of the MS-2 fibrosarcomas, there was a spatial variation in response, with some mice displaying a decrease in the fluorescence intensity, while a fluorescence enhancement occurred in others.<sup>178</sup> Although more studies are required to further investigate these dynamic fluorescence changes, this technique further demonstrates the complexity of online PDT imaging.

Online changes in tumor metabolism have been demonstrated at the University of Sherbrooke, Quebec, Canada, using dynamic PET in both rat and mouse mammary tumors.<sup>179,180</sup> Initially demonstrated in 1999,<sup>180</sup> and further investigated in 2006,<sup>179</sup> the Lecomte group established that continual perfusion of radiolabeled fluoro-2-deoxy-D-glucose showed dynamic changes in both perfusion rates and metabolic activity due to PDT. PDT performed with phthalocyanine-based photosensitizers was illuminated for 30 min<sup>178,179</sup> or 2 h<sup>179</sup> during PET imaging. There appears to be three distinct phases of cellular metabolism that can be related to therapeutic or biological factors. First, within the first 3 min of fluoro-2-deoxy-D-glucose administration, the scans indicated tumor perfusion, confirmed with blood samples. Second, the next 3–15 min of the fluoro-2-deoxy-D-glucose time course was correlated with the type of tumor necrosis, either direct cell killing or indirect cellular necrosis. Finally, the tumor uptake after 15 min was attributed to cellular metabolism and reflected the efficacy of PDT drugs, especially when more than one drug is compared as in these cases.<sup>179,180</sup> Although still in the developmental phase, dynamic PET during PDT could allow visualization of real-time changes in the treatment parameters to provide an optimal therapeutic outcome.

Blood flow dynamics during PDT have been studied with laser speckle imaging,<sup>181</sup> fluorescence imaging, and Doppler OCT<sup>182–188</sup> to predict vascular occlusion as a signal for a therapeutic end point. Laser speckle imaging is a noninvasive optical imaging technique that uses the coherent nature of the PDT-illuminating laser to collect information regarding blood flow dynamics in the tissue of interest, without interrupting the treatment.<sup>181</sup> A study by Khurana et al. used confocal microscopy for intravital imaging to assess cellular changes and molecular events in an *in vivo* mouse dorsal skin-fold window model.<sup>189</sup> Fluorescently labeled antibodies against CD31 (endothelial cells) and CD41 (platelet ag-

gregation), in addition to SYTOX Orange nucleic acid stain (a cell permeability/viability indicator), were imaged immediately before and after the 6 min illumination period of verteporfin PDT. Complementary flow dynamics were obtained using Doppler OCT, a technique that is being more extensively explored for this application, as described below in the subsection on OCT imaging and PDT.

The ability to measure therapeutic signals online during light application has the potential to allow the physician to alter the therapeutic course as it progresses; however, some of the signals measured online will only be indicators of the therapeutic outcome. For instance, monitoring the fluorescence signal of the photosensitizer may allow immediate changes to be made to the PDT protocol if the fluorophore is being bleached too quickly or too slowly. Contrarily, in PET scanning the fluoro-2-deoxy-D-glucose metabolism is a direct resultant of the PDT, and final results (i.e., cellular death) may not be known until hours or days later, providing predictive information on the therapeutic outcome and possibly the need for retreatment.

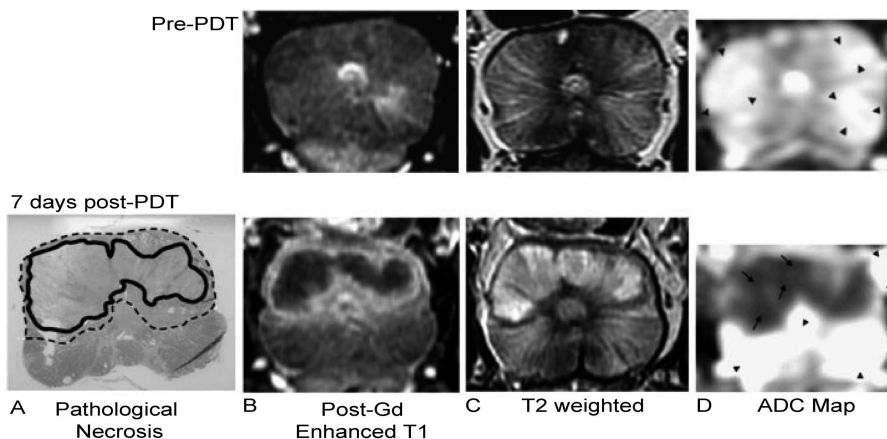
### 4.3. Imaging Techniques for Assessment of the Photodynamic Therapy Outcome

Assessment of the therapeutic outcome has routinely been performed by comparing images of tissue before and after PDT for evidence of necrosis, apoptosis, and blood vessel occlusion. Imaging techniques that have been successfully demonstrated and often clinically implemented for PDT outcome assessment include CT, PET,<sup>190</sup> angiography, MRI, fluorescence imaging, and OCT.

There has been significant progress in the use of MRI for PDT outcome assessments in tumors including contrast-enhanced MRI,<sup>175,191–195</sup> analysis of T1-weighted and T2-weighted relaxation times,<sup>196–198</sup> apparent diffusion coefficient maps,<sup>192</sup> and longitudinal changes in tumor volume (Figure 21).<sup>192,196,199–201</sup> There is good spatial correlation between MRI-determined necrosis and histopathological analysis when images are obtained a short time after PDT. However, the correlation is inconclusive when images are obtained a longer time after PDT due to the onset of fibrosis.<sup>191,192,198</sup> Jiang et al.<sup>197</sup> and Fei et al.<sup>196</sup> have shown that the T1-weighted<sup>197</sup> and T2-weighted<sup>196,197</sup> relaxation times increase within the treated tissue at short time intervals following treatment ( $\leq 48$  h). Additionally, changes in vascular perfusion and permeability can be seen as early as 1 h after PDT,<sup>194</sup> and a change in permeability has been found to be indicative of treatment success.<sup>194,195</sup>

Tumor necrosis and the absolute volume of surviving tumor tissue can be followed by using radioisotopes with either PET imaging or autoradiography. In 1998, Moore et al.<sup>190</sup> used fluorine-18-labeled fluoro-2-deoxy-D-glucose to demonstrate that PET can be used to follow both tumor volume and surviving fractions at short time periods with the same degree of accuracy as high-resolution MRI. Necrosis and surviving tumor volume have also been successfully followed with pre-PDT and post-PDT contrast CT in the pancreas,<sup>171</sup> bladder,<sup>172,173</sup> lung, and bronchial tube.

PDT-induced vascular changes can be monitored with laser Doppler perfusion imaging,<sup>202–206</sup> blood flow dynamics in laser speckle imaging,<sup>207,208</sup> angiography,<sup>164–166,209</sup> and, as further described in the following subsection, Doppler OCT.<sup>210</sup> In all cases, both vascular perfusion and the velocity of blood flow increased immediately after PDT and returned to baseline values within several hours to months post-PDT.<sup>202,203,207,208</sup>



**Figure 21.** Example of structural imaging for PDT outcome assessment. PDT of the prostate was monitored with MRI before (top panel) and 7 days after (bottom panel) PDT. The results of Tookad PDT in the prostate are evident. (A) The pathological necrosis is circled with a bold black line, while the transition region showing signs of inflammation and edema is indicated with a dotted line. Postgadolinium contrast-enhanced T1-weighted MRI (B) shows that the necrotic region does not enhance while the transition region strongly enhances. The opposite is seen in the T2-weighted image (C). (D) The apparent diffusion coefficient map indicates that the necrotic region (arrows) has a diffusion rate ( $1000 \times 10^{-6} \text{ mm}^2/\text{s}$ ) different from that of the remaining prostate (arrow heads,  $2500 \times 10^{-6} \text{ mm}^2/\text{s}$ ). Reprinted with permission from ref 178. Copyright 2006 Wiley.

These examples used superficial tissue samples including skin cancers<sup>202,203</sup> and dorsal skin-fold chambers.<sup>207,208</sup> Angiography has long been used to monitor choroidal neovascularization from age-related macular degeneration.<sup>164–166,209</sup> While fluorescein angiography is the most common, indocyanine green has often been used, and lutetium texaphyrin (Lu-Tex) has also been proposed.<sup>166</sup> The treatment of AMD with PDT (TAP) investigation and the verteporfin in PDT (VIP) trial published fluorescein angiographic guidelines for the evaluation and treatment of CNV from AMD.<sup>166</sup>

#### 4.4. Monitoring Oxygen and Dose Rate Effects in PDT

The complex role of oxygen in PDT has been an area of significant research and gains in theoretical understanding, and yet arguably has led to fairly subtle clinical improvement. This is despite the widespread recognition of the essential role that tissue oxygen plays in the therapy.<sup>211,212</sup> The role of oxygen is ubiquitous, in that type II photosensitization is largely thought to dominate the process of photodamage. The quenching of the excited-state PS leads to singlet-state oxygen, which rapidly oxidizes molecules, and in a biological environment lipid peroxidation is thought to occur on the microsecond time scale.<sup>213</sup> Thus, as singlet oxygen,  $^1\text{O}_2$ , is produced by quenching of ground-state (triplet-state) molecular oxygen,  $^3\text{O}_2$ , with the excited-triplet-state photosensitizer, the singlet oxygen reacts rapidly in vivo and is consumed as part of an oxidized product.<sup>214–216</sup> Since a single photosensitizer molecule can cycle through many quenching steps before it is likely to be photobleached, the deletion of oxygen can occur, dependent upon the concentration of PS and the fluence rate of the light field. The probability of loss of an oxygen molecule for each photon absorbed is high, and the PS can cycle to lead to a high depletion rate of molecular oxygen. In vitro, in the absence of lipids and proteins, the singlet oxygen lifetime is in the range of microseconds up to near 1 ms; yet, in a biological environment, the reaction probability is several orders of magnitude higher, leading to a lifetime below 1  $\mu\text{s}$ . These values vary considerably with the solvent and microenvironment, and many studies have examined this kinetics and the interplay

between singlet oxygen luminescence and the ability to detect singlet oxygen.<sup>217</sup>

All clinically used photosensitizers lack efficacy in the absence of oxygen, and the importance of oxygen has been known for over 30 years in PDT.<sup>218</sup> In more recent studies, it has been shown that higher light dose rates can lead to rapid oxygen consumption and local depletion of the oxygen.<sup>219–221</sup> A theoretical and experimental analysis of this effect was first demonstrated in the early 1990s by Foster et al.<sup>222,223</sup> This phenomenon of oxygen depletion from a dose rate increase has been studied substantially in vitro and in vivo, as it clearly indicates that lower dose rates, or fractionated light dose delivery, can lead to superior treatments in some situations. Additionally there is some evidence that increased delivery of oxygen during therapy could improve efficacy.<sup>224</sup> The major complexity in this issue is that the tumor “oxygen level” is a challenging parameter to measure with high spatial and temporal accuracy, and the dose rate effect varies strongly with different sensitizers and different tissues. Indeed, there are few good ways to image oxygen; however, tumors are well-known to have heterogeneous blood flow and regions of preexisting and transient hypoxia.<sup>225</sup> Therefore, the PDT process can easily consume all available oxygen if the excitation rate, i.e., optical fluence, and PS concentration lead to high rates of oxygen consumption, and thereby, the efficacy is inherently limited by our ability to know the oxygenation of tissue spatially and temporally. Systems to image oxygenation would be extremely useful from this perspective.

##### 4.4.1. Oxygen Measurement

There are several different measurement systems that can be applied to quantify tissue oxygen, but a key factor to set this stage is that the oxygen pressure ( $p\text{O}_2$ ) in tissue varies considerably between capillaries and can be near or at zero in large regions of a tumor and quite high in other regions. While global measurements have been made with good repeatability, using large surface  $p\text{O}_2$  sensors,<sup>219,220</sup> these values do not provide the full data set to interpret what transients are ongoing at the microscopic scale. Indeed, the temporal kinetics of these systems are typically related to

the size and the electrical readout circuit and so often can be temporally slower than the actual kinetics. Nichols and Foster demonstrated careful use of Clarke electrodes in tumor spheroids to methodically examine the issues of oxygen diffusion into tissue and the effect that PS quenching has on the consumption of oxygen.<sup>221,226</sup> They showed that this phenomenon was directly dependent upon the PS concentration, molecular extinction coefficient, and light fluence in the tissue, using Photofrin, PpIX, and mTHPC.<sup>221,227–229</sup> The fundamental insight in this case was that oxygen diffuses out into tissue from the vessels, and this diffusion takes a finite time. If the molecular oxygen is being consumed by PDT faster than it is being supplied by diffusion, then a transient oxygen depletion can occur in that region of tissue.<sup>223</sup> This phenomenon is especially dominant when the optical irradiance is high.<sup>230</sup> There can also be periods of semipermanent or permanent hypoxia induced when vessels constrict or occlude, thereby shutting off the supply of oxygen to regions of the tissue. These transients have also been well documented using window chamber studies, microelectrode studies,<sup>231</sup> Doppler blood flow studies, and more recently global near-infrared oximetry and blood flow.<sup>232</sup>

These observations were utilized in planning clinical studies, and measurements with the Eppendorf electrode were in agreement with the model predictions.<sup>233–236</sup> This latter electrode system requires stepping the needle in tracks through the tumor and provides a histogram of microscopic data about the oxygenation of the tissue. It is conventionally accepted as perhaps the best approach to quantifying a tumor oxygenation, but has obvious logistical and morbidity concerns associated with multiple needle tracks through the tumor each time a measurement is needed. Other systems applied to methodically study the role of oxygen have been the smallest pipet microelectrodes, allowing a 10  $\mu\text{m}$  sampling size, fiber-optic oxygen sensors, providing larger region sampling, and electron paramagnetic resonance spectroscopy of implanted charcoal.

The use of oxygen-sensitive luminescence dyes has long been in development, and in experimental studies, these dyes have been used to show the preponderance of oxygen depletion in an imaging geometry. In recent years, singlet oxygen detection has also become feasible,<sup>217,237</sup> and despite some early concerns that this was not a detectable signal,<sup>217</sup> newer photocathode materials with appropriate amplification have been used to show that singlet oxygen can be detected in vitro and in vivo, leading to recent human clinical trials.<sup>238–242</sup> Much of this early work has been with single photomultiplier tubes, and now imaging photomultiplier tubes are also available. While they are still expensive, they open up the opportunity to image the production of singlet oxygen, as was recently demonstrated by Lee et al.

#### 4.4.2. Dose Rate Effects upon the Outcome

In the absence of widespread direct oxygen measurements or imaging, the theory of oxygen depletion in PDT has been supported by many phenomenological observations that PSs have lower efficacy when high optical fluence rates are used.<sup>233</sup> This has been nicely demonstrated with biological outcomes such as skin photosensitivity, clonogenic assay, tumor regrowth assay, and tumor cure rates.<sup>243,244</sup> The phenomenon is very dominant in Photofrin and ALA–PpIX PDT, where dramatic improvements in therapy outcome have been shown in lowering the irradiance<sup>245,246</sup> from 200 mW/

$\text{cm}^2$  to values below 10 mW/ $\text{cm}^2$  in some cases.<sup>247</sup> The practicality of lowering the fluence rate below 50 mW/ $\text{cm}^2$  has limited most studies to this lower limit, as the time needed to complete a treatment increases linearly with decreasing irradiance. Fractionated delivery of the light was shown to be quite useful as well, with the hypothesized efficacy improvement being that the periods where the tissue is not being irradiated allow the oxygen diffusion back into the tissue.<sup>223,248,249</sup>

This area of dose rate effects has been studied most extensively with ALA PDT, because of the curious interplay between the PS photobleaching and the dose rate phenomenon.<sup>250</sup> When photobleaching occurs during the treatment, the complexity of this process increases, but largely photobleaching will lead to a loss in PDT efficacy, because the PS is being depleted along with the tissue oxygen, and this is again especially problematic when high irradiances are used. Dose fractionation has been shown to have dramatic effects, and fractionation on the time scale of hours appears to have even more of an effect, which has recently been attributed to allowing PS replenishment during the fractionation period. Several strategies have been examined to use photobleaching as a measure of photodamage in vivo, and pilot studies are compelling.<sup>251,252</sup>

The concept of low-dose-rate delivery to optimize both the drug concentration and the oxygen delivery was taken to the most extreme case, by Bisland et al., who proposed the use of continuous ultralow-dose-rate light delivery with continuous or low-dose ALA delivery.<sup>253</sup> This approach, termed metronomic PDT, follows the convention of metronomic chemotherapy has been studied for potential use in glioma tumor treatment.

#### 4.4.3. Vascular Response and Tissue Oxygen

The confounding feature of vascular constriction, dilation, and occlusion has always made it very difficult to definitively demonstrate the beneficial effects of low-dose-rate PDT for photosensitizers that have high vasoreactive treatment.<sup>254</sup> Indeed some studies have shown oxygen increases, oxygen decreases, and later oxygen increases all in the same tumor, using a fixed irradiation value. Recently a very systematic approach to monitoring the combination of vascular flow and oxygenation has been through near-infrared spectroscopy, with correlation flow measurements to track the temporal response to Photofrin PDT.<sup>232</sup> This has been used in humans to show that optimal treatment occurs when the rate of change of blood flow is greatest during therapy delivery.

Many photosensitizers act specifically upon the vasculature, and by far the largest clinical success in AMD has been in this biological effect, using irradiance values of 600 mW/ $\text{cm}^2$ . At these rates, there would definitely be oxygen depletion in the tissue if photosensitizer was present, but the delivery was to the vasculature, and so the oxygen supply by vascular perfusion is likely sufficient to keep oxygen delivery high in the vessels. A newer sensitizer, WST11, also is focused on vascular ablation for providing a highly controlled treatment,<sup>255</sup> with applications in retinal ablation or prostate tissue ablation.

Despite the focus on developing and analyzing vascular or nonvascular photosensitizers, most act in a dual role, where the effect is somewhat determined by the partitioning of the agent in and out of the vessels. This partitioning changes with time, and vascular targeting is induced by early irradiation shortly after injection, whereas nonvascular



therapy is induced by irradiation at longer times after injection of the drug.<sup>256</sup> Dual targeting can also be enhanced by a two-phase treatment, or by selective permeabilization of the vascular endothelium.<sup>257,258</sup> This is an area of ongoing study, and optimization of the temporal kinetics with the light irradiance must be done individually for each photosensitizer and each tumor/organ site to truly maximize the efficacy.

## 4.5. Optical Coherence Tomography in Photodynamic Therapy

OCT is a powerful noninvasive optical method that has recently emerged for both online monitoring of the response to PDT and assessment of the therapeutic outcome. The use of OCT as a nonperturbative imaging platform for PDT imaging began with its introduction in ophthalmology to visualize the treatment response of AMD and its associated neovascularization to PDT. This clinical success, which proved the utility of OCT for PDT imaging, set the stage for advances in visualizing PDT treatment response, including its use for monitoring vascular PDT effects. Applications of OCT for following treatment response have so far been limited, but the results of past and current studies described in this section show the great potential and impact of PDT imaging in the future. In the following sections we briefly introduce the background to OCT and several important studies from the literature, both preclinical and clinical, highlighting the use of OCT for monitoring and assessment of the PDT treatment response.

### 4.5.1. Optical Coherence Tomography Background

OCT is essentially the optical analogue of ultrasound imaging. As the speed of light is 5 orders of magnitude faster than the speed of sound, OCT makes use of interferometry to accurately measure the time delay of reflected photons. Light reflected off surfaces in a sample is collected and interfered in an interferometer with light from the reference arm, giving rise to an interferometric pattern containing the depth information.<sup>259,260</sup> Modern OCT systems operate in the so-called frequency domain,<sup>261–264</sup> where a spectral interferogram is collected and Fourier-transformed to retrieve the depth-resolved information. A three-dimensional tomogram of a sample is built by scanning the OCT beam across a sample and recording and Fourier transforming the interference pattern at each point. Newer OCT systems make use of swept-source laser sources. These optical frequency domain imaging (OFDI)<sup>265–267</sup> and Fourier domain mode-locked OCT (FDML)<sup>268</sup> systems make use of balanced detectors to record the interferogram as the wavelength is scanned. OCT has found extensive clinical applications in cardiology,<sup>269</sup> gastroenterology,<sup>270,271</sup> dermatology,<sup>272,273</sup> and especially ophthalmology.<sup>274–276</sup> OCT is a promising tool for PDT research due to its nonperturbative, structural volumetric imaging capabilities. OCT systems typically utilize wavelengths of light ranging from 850 to 1350 nm at light powers only in the hundreds of microwatts. As these wavelengths are far less energetic than those required to carry out PDT, OCT can be used to visualize a sample before, during, and after PDT without activating the PS. This differs from standard optical microscopy tools, which can suffer from sample perturbation due to photobleaching and phototoxicity. As the contrast in OCT comes from index of refraction changes at reflective surfaces, a potential drawback of

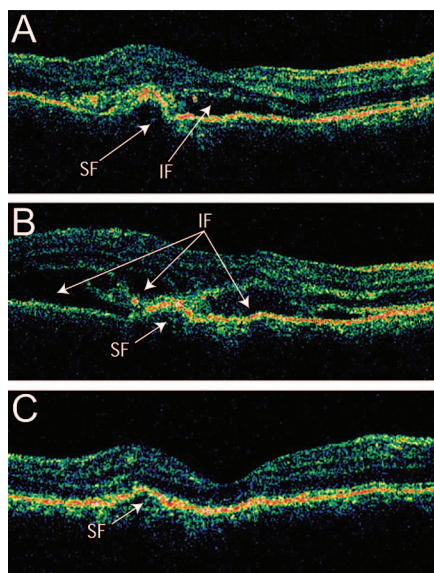
standard OCT systems is that they do not have molecular sensitivity, although there has been some pioneering work toward this goal.<sup>277,278</sup> This limitation, however, can be readily overcome in PDT studies by using OCT as part of a multimodality imaging suite, where rapid structural contrast is collected alongside fluorescence or luminescence. Unlike microscopic imaging methods used in PDT research, such as confocal and multiphoton microscopy, OCT is not limited to visualizing only one *xy* plane at a time. To collect a three-dimensional volume with a microscope, the objective or stage must be stepped to acquire individual *xy* images at different depths. In OCT, an entire depth scan is collected at each point, enabling OCT systems to capture a full three-dimensional tomogram of a sample in only one *xy* scan. This makes volumetric imaging with OCT almost an order of magnitude faster than even video-rate microscopy. By collecting backscattered NIR light, OCT is capable of penetrating beyond 1.5 mm deep into tissue, allowing for considerably greater imaging depths than standard microscopy approaches. This depth range is very advantageous for PDT imaging, as it is comparable to the depth of necrosis observed in tissue. Furthermore, due to the interferometric nature of OCT, the depth (axial) resolution is decoupled from the lateral resolution, allowing for subcellular, micrometer-resolution imaging deep in a sample. These three factors—speed, depth, and resolution—have made OCT an ideal imaging partner for following the detailed three-dimensional structural response to PDT in living systems.

### 4.5.2. Noninvasive Visualization of Photodynamic Therapy in Ophthalmology

Given its rapid, nonperturbative imaging capabilities, it comes as no surprise that OCT found initial success in imaging the PDT response in the field of ophthalmology. OCT is very effective in noninvasively visualizing the many layers of the retina with micrometer resolution. This has enabled OCT to facilitate the diagnosis of numerous retinal diseases including retinal detachment,<sup>279</sup> multiple sclerosis-related eye disease,<sup>280</sup> glaucoma,<sup>281</sup> and both types I and II AMD,<sup>266,281</sup> to name a few. Symptoms of the “dry” and “wet” forms of AMD, such as drusen, intraretinal fluid (IF), subretinal fluid (SF), and CNV, are all readily visualized with OCT.<sup>266,282</sup>

OCT has been used to follow the detailed changes in the retinal structure of patients with AMD immediately after PDT,<sup>282</sup> revealing complex dynamics in the days following treatment. In a study of 20 patients by Ozdemir et al., the retina was observed to swell following PDT due to an increase in subretinal and intraretinal fluid in the first 24 h after treatment. In the days following treatment OCT imaging revealed decreases in both subretinal and intraretinal fluid as the patients' retinas contracted. Figure 22 shows the retina of one patient before PDT and at 1 day and 7 days post-treatment. The initial state of the retina and its response to and subsequent recovery following PDT are clearly seen in the sequence of OCT scans, with more normal retinal morphology observed at 1 week post-treatment.

The nonperturbative imaging capability of OCT has also found use in both following disease recovery and evaluating the need for potential retreatment. In a study by Rogers et al.,<sup>210</sup> for example, OCT was used to visualize the retinal structure in patients with AMD in the weeks following PDT. On the basis of rodent experiments,<sup>283,284</sup> the study used both OCT contrast and fluorescein angiography to classify patients



**Figure 22.** Cross-section OCT B-scans of a patient with subfoveal CNV treated with PDT, pseudocolored for reflectance intensity. (A) One day before PDT, the presence of intraretinal and subretinal fluid AMD can clearly be seen with OCT. (B) One day after PDT, increased intraretinal and subretinal fluid can be seen. (C) After 1 week following treatment, OCT reveals a substantial decrease in both intraretinal and subretinal fluid. Reprinted with permission from ref 282. Copyright 2006 Elsevier.

into five distinct post-PDT stages and evaluate the ongoing response to treatment. OCT was particularly apt at visualizing the so-called post-PDT stage IV lesions where involution of the CNV accompanies the formation of cystoid macular edema. In fact, OCT was found to be particularly sensitive in detecting PDT-induced changes in CNV and may play a future role in post-PDT follow-up when fluorescein angiography results are poor or inconclusive.<sup>285</sup> Importantly, as a volumetric technique, OCT is capable of performing quantitative imaging in situ through segmentation and analysis. In a promising study by Sohni et al., quantitative OCT was used to compare improvements in visual acuity following multiple rounds of PDT with corresponding changes in retinal structure by computing measures of foveal thickness.<sup>286,287</sup> As PDT continues to be used to treat AMD, these studies underscore the potential of OCT for monitoring, optimizing,<sup>288</sup> and furthering our understanding of the treatment response.

#### 4.5.3. Doppler Optical Coherence Tomography Monitors the Vascular Response to Photodynamic Therapy

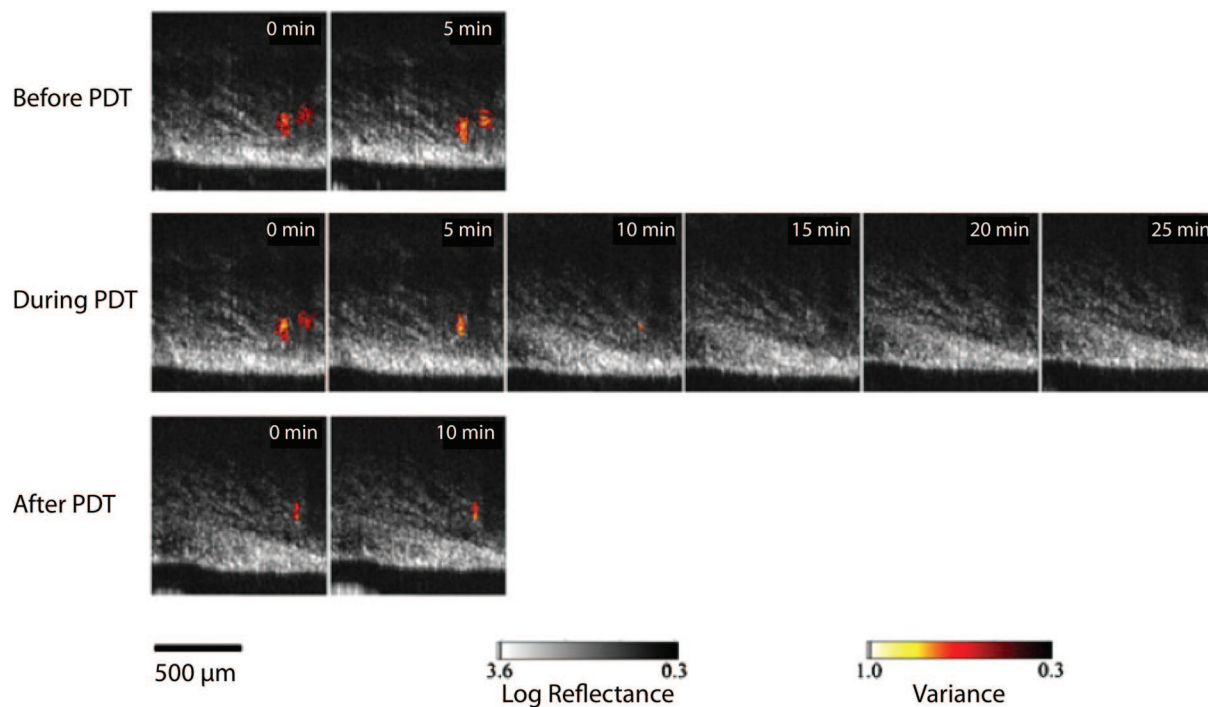
One of the key mechanisms of PDT-induced damage in the treatment of cancer is the impairment and destruction of the tumor vasculature. While techniques such as diffuse optical tomography,<sup>289</sup> reflectance tomography,<sup>290</sup> and laser Doppler<sup>291</sup> measurements have been used to detect changes in the tissue vasculature following PDT, a variant of OCT has the potential to play a large role in understanding the detailed treatment effects on the tumor vasculature. Doppler OCT is an extension of OCT where the small frequency shifts created by moving particles can be measured and used to quantitatively visualize flow.<sup>292,293</sup> Building on the many advantages of OCT, Doppler OCT enables high-resolution, noninvasive, deep optical measurements of the microvascular structure and flow dynamics. In a promising early study by Chen et al., a rodent mesentery artery model was treated

with BPD PDT at a dose of 12 J/cm<sup>2</sup>. Only 16 min after irradiation, a blood vessel was observed to undergo vasospasm and constricted to 81% of its original size. One hour after treatment, the same vessel was subsequently vasodilated to 120% of its original size, indicating that the artery might have expanded post-treatment to compensate for PDT-induced hypoxia.<sup>182</sup>

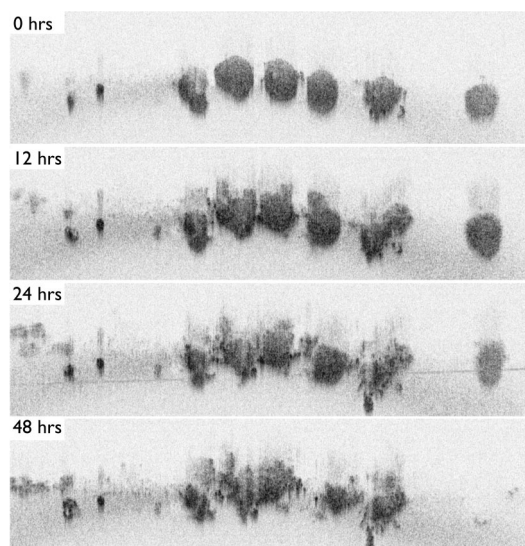
This direct quantitative visualization of the tumor microvasculature opens the door to visualizing and even optimizing the critical vascular treatment response dynamics for anticancer PDT.<sup>188</sup> Indeed, Doppler OCT has been recently used to visualize the effects of PF PDT on the vascular shutdown in an animal model of Barrett's esophagus.<sup>185</sup> Doppler OCT images acquired before, during, and after PDT show vasospasm leading to PDT-induced vessel constriction, a critical step in inducing hypoxia for treating tumors. For even deeper in situ imaging, needle probes can be used to access visceral targets, such as in a recent rat prostate cancer model, for interstitial Doppler OCT imaging.<sup>294</sup> In a study by Li et al., interstitial Doppler OCT revealed the differential shutdown kinetics and response between two closely spaced blood vessels during PDT (Figure 23). While one vessel (left) closed immediately and did not recover, its neighboring vessel constricted more slowly and fully recovered. Understanding the factors behind this differential treatment response will be critical for improving vascular-targeted PDT. In an ongoing study by Hasan and colleagues, Doppler OCT was used to visualize vascular destruction in the days and weeks following BPD PDT in a subcutaneous rat prostate model. While immediate vascular shutdown was observed, there was no correlation between successful treatment and rapid vascular response. Instead, the best predictor for treatment success was found to be the observation of vascular destruction three weeks following PDT. These early experiments show that blood vessel imaging with Doppler OCT has the potential to be used as a dosimetry methodology for PDT, but considerable work remains.

#### 4.5.4. In Vitro Model Treatment Response Imaging with Optical Coherence Tomography

Understanding tumor-based structural changes and molecular responses following PDT is critical in designing and optimizing effective therapeutic strategies. Three-dimensional in vitro models restore many of the cell–cell and cell–matrix interactions<sup>295–299</sup> missing from traditional monolayer cultures<sup>296</sup> and provide a promising platform to image the PDT response at the nodular, cellular, and subcellular level. A three-dimensional model for micrometastatic ovarian cancer has been developed by Hasan and colleagues on the basis of the pioneering work in breast cancer by Bissell et al.<sup>300</sup> The large size of these three-dimensional ovarian micronodules, which can grow to be 1 mm in diameter after 3 weeks, presents a major challenge for imaging these structures. The capability of OCT to nonperturbatively image deep into biological tissue makes it an ideal technology to overcome these challenges and track the effects of PDT in real time. In a recent study by Evans et al., a time-lapse OCT (TLOCT) imaging system was used to follow the treatment response (Figure 24) of ovarian cancer micronodules to BPD PDT over the course of several days.<sup>301</sup> After only 12 h post-treatment, the ovarian nodules showed evidence of structural breakdown. One day following treatment, massive structural degradation was seen, with the formation of highly scattering



**Figure 23.** Comparison of Doppler OCT images of a Dunning prostate tumor before (top panels), during (middle panels), and after (bottom panels) exposure to light. The cross-sectional area of the blood vessels was reduced during the treatment, with some vasodilation observed after treatment. The leftmost blood vessel was seen to constrict first and did not recover after the treatment was completed. Reprinted with permission from ref 294. Copyright 2006 Wiley-Liss.



**Figure 24.** Application of TLOCT for studying the basic tumor biology of the PDT response, demonstrating a series of OCT cross-sectional images of ovarian cancer acini taken from a full 3D data set at time points following BPD PDT. Ovarian cancer acini appeared as small, solid, and spherical structures immediately following treatment. Twelve hours post-PDT, signs of structural breakdown were seen. One day after PDT, the acini showed large-scale structural deformation with the appearance of apoptotic cell clusters at the nodules' periphery. Few structural differences can be seen between 24 and 48 h following treatment. Reprinted with permission from ref 301. Copyright 2010 SPIE.

apoptotic cell clusters<sup>10</sup> at the nodules' peripheries. Interestingly, very few structural changes were observed between 24 and 48 h post-PDT, indicating that the majority of cellular death occurred in the first 24 h. TLOCT studies promise to

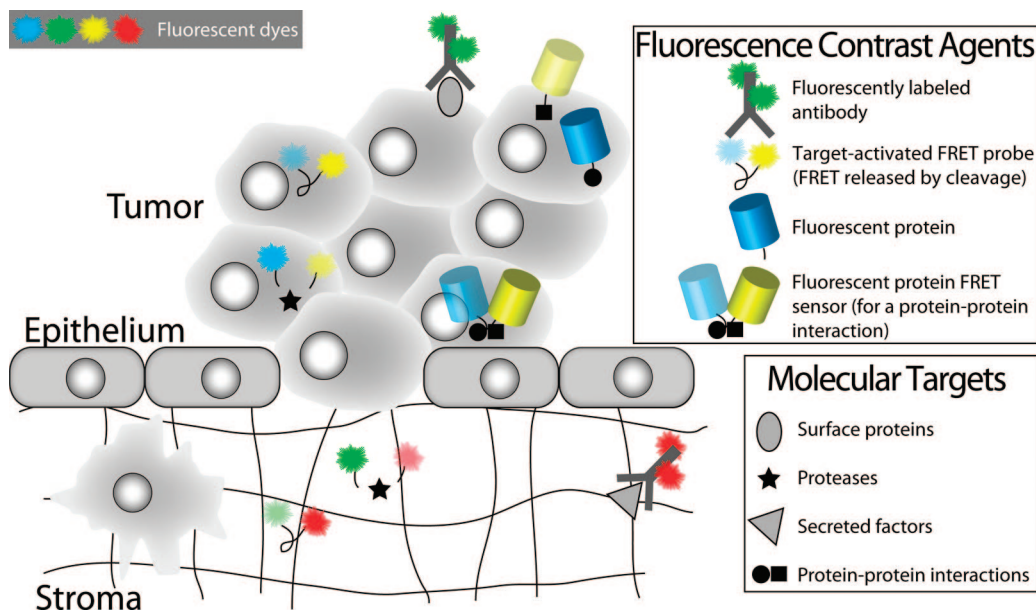
provide valuable insight into the structural dynamics that govern cell death and resistance in PDT.

## 5. Molecular Imaging of Dynamic Molecular Mechanisms Induced by PDT

### 5.1. Overview

As described by Massoud and Gambhir<sup>302</sup> and Weissleder,<sup>303</sup> molecular imaging refers to the visualization, characterization, and quantification of biological targets and processes at the cellular and molecular level. Over the past decade, molecular imaging has been increasingly used to diagnose diseased tissue, to visualize dynamic therapeutic effects, and to monitor therapeutic outcomes using specific biological and molecular targets. On the basis of the improved characterization of the diverse biological mechanisms involved in PDT, molecular imaging now provides new opportunities for *in vivo* monitoring of tumor responses to PDT in near real time. The focus of this section is emerging molecular imaging techniques that are currently applicable to PDT research. Some of these techniques utilize exogenous contrast agents that hold promise for clinical application.

A number of *in vivo* imaging modalities and molecular-targeted contrast agents are coming of age and provide a versatile platform on which to design and implement molecular imaging. This section focuses on fluorescence imaging: intravital fluorescence microscopy,<sup>304</sup> fiber-optic fluorescence microendoscopy,<sup>305–308</sup> hyperspectral fluorescence imaging,<sup>147,309,310</sup> fluorescence lifetime imaging,<sup>311–315</sup> and fluorescence diffuse optical tomography.<sup>316–319</sup> However, it is important to note that molecular imaging encompasses a number of imaging modalities and molecular-targeted contrast agents (as discussed in section 5.4 below, which



**Figure 25.** Fluorescence contrast agents relevant for molecular imaging of biological responses to PDT. Fluorescently labeled antibodies, target-activated probes, and genetically encoded fluorescent proteins are examples of fluorescence contrast agents that have been applied for molecular imaging of biological responses to PDT. This figure highlights the use of these contrast agents for detecting molecular factors in both the intracellular and extracellular spaces. The natural clearance of unbound antibody–fluorophore conjugates from the extracellular space enables their use for labeling cell surface proteins and extracellular secreted factors. Target-activated probes based on FRET (as shown here) or ground-state quenching are applicable for imaging both intracellular and extracellular factors. Fluorescent proteins (an endogenous labeling scheme) are useful for monitoring protein expression levels and protein–protein interactions and for visualizing protein trafficking. Fluorescent protein FRET sensors also exist and can be used to detect protein–protein interactions. Examples of the application of these contrast agents for studying PDT-induced molecular mechanisms are shown in Figure 26 and are discussed in the text.

includes several references to PET<sup>180,320,321</sup>). The multitude of molecular imaging techniques includes PET, MRI, ultrasound, and other modes of optical imaging (such as light scattering and reflectance).

Examples of molecular-targeted contrast agents for fluorescence imaging can be found in Figure 25. The molecular targeting strategies used to design molecular imaging agents include receptor–ligand binding, small-molecule or peptide targeting, site-activatable markers, and multitargeted agents, as discussed in section 3. Figure 26 illustrates PDT-induced molecular mechanisms that can be imaged using the fluorescence contrast agents presented in Figure 25. One of the major advances in PDT has been the elucidation of the molecular mechanisms involved in cellular responses to acute stress and damage resulting from the photogeneration of reactive oxygen species (ROS). A tremendous opportunity now exists to apply molecular-targeted therapies (e.g., inhibitors of specific enzymes and pathological signaling cascades) to enhance the treatment outcome by leveraging the growing knowledge base of PDT-activated signal transduction events. Combination therapies, where PDT is combined with a molecular-targeted therapy, have already shown promise for enhancing the treatment outcome following PDT.<sup>322–325</sup>

In recent years there have been major advances in the understanding of PDT-related molecular mechanisms.<sup>326–329</sup> In the context of PDT, molecular imaging is in its infancy, but appears to hold great potential for online monitoring of key biomarkers associated with cancer progression and responses to PDT. The following discussion presents promising developments toward *in vivo* molecular imaging of dynamic biological responses to PDT, focusing on the following specific molecular mechanisms related to cancer treatment: (1) PDT-activated apoptotic signal transduction, (2) biomarkers of the treatment response to PDT, and (3)

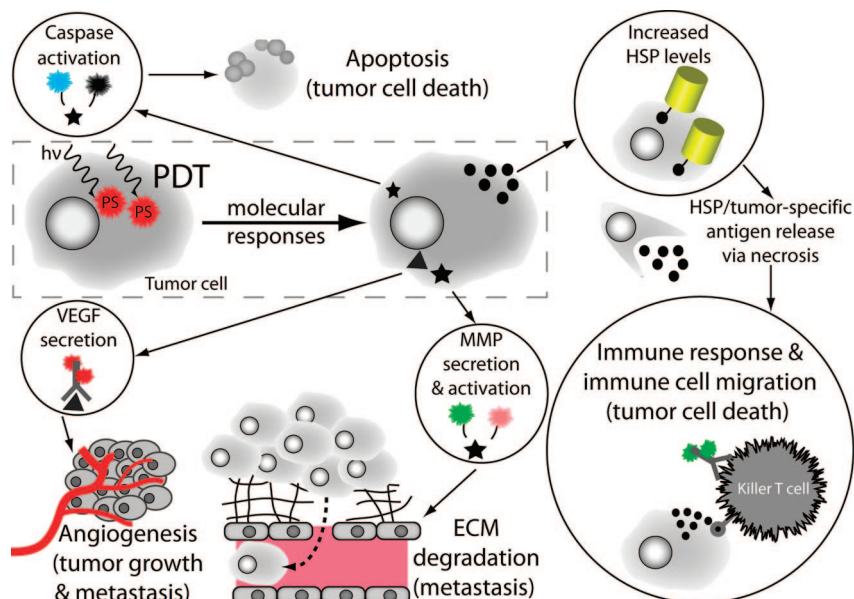
secreted factors that promote tumor metastasis and recurrence following subcurative PDT.

## 5.2. Imaging Molecular Pathways Involved in PDT-Induced Apoptosis

Apoptosis, or programmed cell death, is one mechanism by which toxicity is conferred to the target tissue following PDT.<sup>330</sup> Apoptosis involves a cascade of molecular events leading to orderly cellular death without an inflammatory response.<sup>331–334</sup> The initiation of apoptosis involves a complex network of signaling pathways, both intrinsic and extrinsic to the individual cell, which are regulated in part by pro- and antiapoptotic factors.<sup>334</sup> Two of the mechanisms explored by molecular imaging in the context of PDT-induced apoptosis are discussed here: (1) the release of proapoptotic factors from the mitochondrial inner membrane space, which amplifies proapoptotic cell death signaling upstream of apoptosome formation and procaspase activation and (2) the activation of cysteine–aspartic acid proteases (caspases) to carry out cleavage of key cellular proteins to degrade the cytoskeleton and cellular organelles as well as to activate other enzymes important for apoptosis. Here we review the use of genetically encoded green fluorescence protein (GFP) sensors to track the spatial localization and activation of proapoptotic factors and the use of a target-activated probe to monitor the activation of an effector (executioner) caspase.

### 5.2.1. Green Fluorescent Protein Sensors for Visualizing Proapoptotic Factor Activation and Trafficking

The Oleinick group has shown that phthalocyanine 4 (Pc4)-mediated PDT (Pc4 PDT) causes mitochondrial damage and induces apoptosis through the release of cytochrome



**Figure 26.** Imaging of molecular mechanisms induced by PDT using the fluorescence contrast agents introduced in Figure 25. The ability to image critical molecular responses in tumors and proximal tissue following PDT is crucial for the development of effective therapeutic strategies designed to abrogate tumor survival and to enhance proapoptotic and immune-based responses. Examples of specific molecular targets and fluorescence contrast agents for imaging each of these mechanisms are shown in circles. The specific mechanisms shown here are executioner caspase activation, increased expression of HSPs, immune cell migration, and secretion of VEGF and MMPs. These biological responses include both cellular death and prosurvival signaling pathways. Cellular death signaling includes the induction of the apoptotic cascade (see section 5.2) and, separately, the activation of an immune response to tumor-specific antigens and inflammation. Prosurvival signaling includes increased production of certain proteins as part of the cellular stress response for repairing damage resulting from the generation of ROS during PDT (see section 5.3.1) and the secretion of cytokines and enzymes to manipulate the tumor microenvironment. The secreted factors VEGF and MMP are important for tumor growth and metastasis (and are discussed in sections 5.3.2–5.3.3).

*c* into the cytosol.<sup>335</sup> In a subsequent study, Usada et al. applied molecular imaging to investigate the mechanism of this release in GFP-transfected human breast cancer cells positive for Bcl-2-associated X protein (Bax) and mutated prostate cancer cells in which the Bax gene was deleted. A GFP fusion protein was used to image the mitochondrial protein Smac/DIABLO (second mitochondrion-derived activator of caspase/direct inhibitor of apoptosis binding protein with low pI) and the dependence of its release into the cytosol on the proapoptotic factor Bax in Pc4-PDT-induced apoptosis.<sup>336</sup> Smac/DIABLO is localized in the mitochondrial intermembrane space, and once it is released into the cytoplasm, it can promote caspase activation through binding the IAPs (inhibitor of apoptosis proteins) and blocking their antiapoptotic activity. Confocal imaging 3 h following Pc4 PDT showed a concomitant release of cytochrome *c* and Smac/DIABLO from the mitochondria, but only in the Bax-positive cell line.<sup>336</sup> Furthermore, apoptosis was enhanced in the GFP–Smac/DIABLO-transfected cells compared with cells transfected only with GFP.

In this study, molecular imaging provided clear evidence that Smac/DIABLO plays an important role in PDT-induced apoptosis and suggests that the release of both cytochrome *c* and Smac/DIABLO from the mitochondria is dependent on Bax. This is a good example of how imaging can be applied to understand the role of a particular molecule. Further experiments could be done to establish the hierarchical temporal release of cytochrome *c* and Smac/DIABLO.

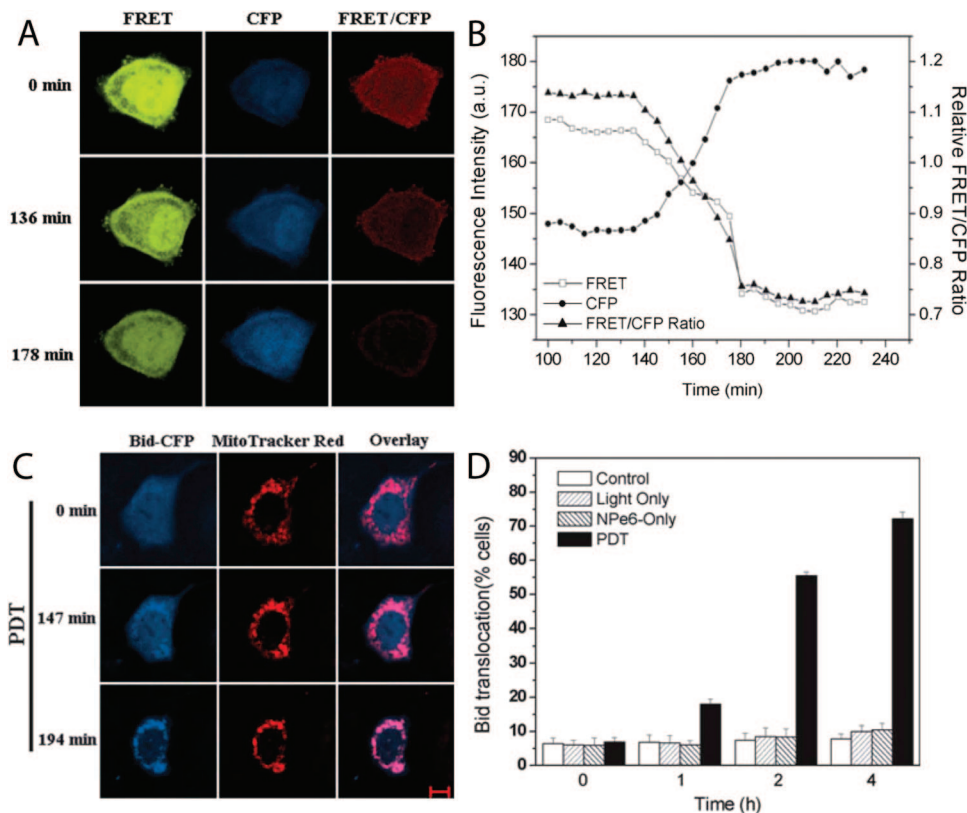
The following is an example where imaging helped resolve a controversy regarding the role of BH3 interacting domain death agonist (Bid) cleavage in NPe6-PDT-induced apoptosis. Wan et al. investigated the molecular mechanisms of PDT-induced apoptosis by *N*-aspartyl-Ce6, NPe6, which localizes to lysosomes.<sup>337</sup> NPe6 PDT had been shown

previously to induce apoptosis through liposome disruption and Bid cleavage.<sup>338</sup> This finding, however, is somewhat controversial, since some studies based on other liposomal-localizing PS molecules did not find that Bid contributed to apoptosis.<sup>339,340</sup>

Wan et al. monitored Bid activation by confocal fluorescence imaging of a genetically encoded FRET probe in live cells (termed a “Bid FRET sensor”). The Bid FRET sensor<sup>341,342</sup> consisted of a fusion protein with a FRET donor (cyan fluorescent protein, CFP) and acceptor fluorescent protein (yellow fluorescent protein, YFP) pair attached to the opposing ends of Bid (YFP–Bid–CFP). In this implementation, Bid cleavage/activation is visualized by a release of FRET quenching (i.e., increased CFP fluorescence emission and decreased YFP emission upon selective excitation of CFP). Translocation of the activated, truncated form of Bid (tBid) to the mitochondria was visualized by colocalization of CFP–tBid with Mitotracker Red dye, which stains the mitochondria. Wan et al. showed the temporal kinetics of Bid cleavage to form tBid and the translocation of tBid from the cytoplasm to the mitochondria following Npe6 PDT (Figure 27). Interestingly, the study found that Bid cleavage following Npe6 PDT was not mediated by caspase 8 (the normal mechanism of Bid cleavage).

### 5.2.2. Caspase-Activated Fluorescent Reporter of Apoptosis

Stefflova and colleagues have synthesized a PMB (see section 3) that serves a dual role as a PDT agent and a target-activated fluorescent indicator of apoptosis, which they have termed a “PDT agent with a built-in apoptosis sensor” (PDT-BIAS).<sup>343</sup> PDT-BIAS is a target-activated probe with a design similar to that of the site-activated contrast agent depicted



**Figure 27.** Imaging the activation dynamics of a proapoptotic factor and its cellular trafficking during PDT-induced apoptosis. A genetically encoded FRET sensor reports the dynamics of Bid (a key proapoptotic protein) activation and trafficking of tBid to the mitochondria during NPe6-PDT-induced apoptosis. (A, B) The temporal dynamics of Bid activation are visualized as a loss of FRET quenching of CFP fluorescence emission (i.e., increased CFP fluorescence, labeled as the “CFP” channel) and as a concomitant loss of YFP fluorescence due to FRET (labeled as the “FRET” channel) using the Bid FRET fluorescent protein sensor described in the text. (C, D) Time-lapse images and quantification of tBid–CFP (activated Bid) trafficking from the cytosol into the mitochondria are shown, following cleavage of the Bid FRET sensor. The bars represent the percentage of cells showing Bid translocation to mitochondria at the indicated time points. The scale bar is 10  $\mu\text{m}$ . Adapted with permission from ref 337. Copyright 2008 Wiley.

in Figure 19B of section 3.3. In this implementation of a PMB, a dark, nonfluorescent quencher (black hole quencher, BHQ) is used as the FRET acceptor molecule and is held in close proximity to the PS molecule (Pyro) by a caspase 3 cleavable peptide linker sequence. Upon digestion of the linker by the executioner caspase 3, FRET quenching is abolished, and the fluorescence quantum yield of PDT-BIAS increases. Confocal live cell imaging experiments demonstrated the successful use of PDT-BIAS for detecting PDT-induced apoptosis in a proof-of-principle study.<sup>343</sup> Increased fluorescence was observed in light-irradiated cells incubated with PDT-BIAS in comparison to a scrambled linker sequence. However, much more work is needed for this sensor to be applied routinely for in vivo imaging.

The quenched PS will have lower production of singlet oxygen than the free PS, which must be accounted for by increasing either the concentration of the PS or the administered light dose (or both). FRET quenching depopulates the singlet electronic excited state of the PS in competition with the intersystem-crossing pathway, effectively reducing the triplet-state and singlet oxygen yields of the PS. Since photobleaching of the PS and changes in its local concentration will influence the measured fluorescence intensity, one must be careful when using intensity-based imaging to detect caspase activity using PDT-BIAS. One powerful approach is to use time-resolved techniques to image the fluorescence lifetime of the PS for unambiguous detection of caspase 3 cleavage, as the fluorescence lifetime is generally a robust measure of FRET.<sup>344</sup> Despite these potential limitations,

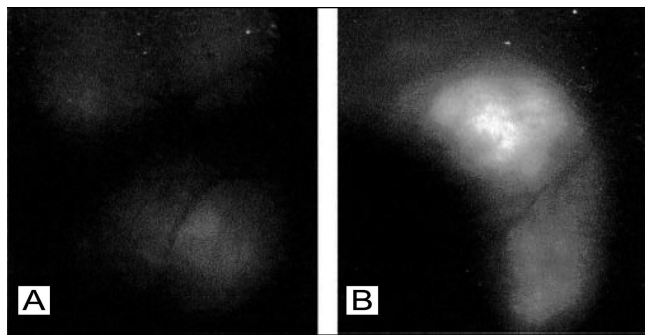
PDT-BIAS and other PMB designs stemming from its general concept (see section 3 and the MMP-activated PMB presented section 5.3.2) hold great potential for in vivo therapeutic monitoring applications.

### 5.3. Imaging Biomarkers of Therapeutic Responses to PDT

An interesting molecular mechanism of tumor response to PDT is the change in the expression levels of certain proteins. There are numerous such molecules that have been established and include both cell-associated and secreted molecules. In this section we discuss the following biomarkers: (1) heat shock protein 70 (HSP70)—an exemplary intracellular protein, (2) MMP-7—a secreted proteinase that is activated extracellularly to degrade the ECM, and (3) VEGF—a secreted cytokine that is a critical regulator of tumor growth and angiogenesis. The latter two biomarkers of PDT responses (MMP-7 and VEGF) are both critical to tumorigenesis and metastasis.

#### 5.3.1. Heat Shock Protein 70

HSP70 is strongly up-regulated following PDT and apparently accounts for the greatest increase in expression of all genes, on the basis of a cDNA microarray study.<sup>345</sup> Mitra and colleagues have applied GFP to monitor the expression of HSP70 following subcurative PDT both in vitro and in an animal model.<sup>346</sup> In this pioneering molecular imaging



**Figure 28.** In vivo molecular imaging of a cellular stress response to PDT: (A) before and (B) 6 h after PDT. The figure shows images of increased heat shock protein expression in an EMT6 (mouse mammary carcinoma) tumor, a molecular response to acute cellular stress during PDT. In this experiment, GFP-transfected EMT6 cells were implanted into mice subcutaneously, where GFP expression is driven by the activation of the HSP70 promoter and GFP fluorescence is used to visualize the HSP70 expression level. The GFP fluorescence increases substantially following PDT, indicating an up-regulation in HSP70 expression. Reprinted with permission from ref 346. Copyright 2003 Wiley.

study, the activation of HSP70 was imaged within EMT6 mouse mammary carcinoma cells that were stably transfected with a plasmid containing GFP. In this experiment, GFP expression was under the control of an HSP70 promoter sequence, such that GFP fluorescence acted as a reporter of the expression level of HSP70. PDT was carried out for a range of light doses following incubation of the cells with the PS, mTHPC (or Foscan). Subsequently, fluorescence images of GFP emission were collected. Mitra et al. found the expression of HSP70 to increase 4–5-fold following subcurative PDT in live cells.<sup>346</sup> In addition, they demonstrated in vivo imaging of increased HSP70 expression within a mouse model, as shown in Figure 28, within 6 h of subcurative PDT. The characterization of maximal HSP70 expression in response to sublethal PDT doses may hold clinical relevance for applying low-dose PDT to stimulate an antitumor immune response,<sup>346</sup> which remains an exciting prospect.

A significant proportion of HSP molecules localize to the cell surface following PF PDT and are released into the extracellular space following necrosis.<sup>347</sup> For this reason, HSP70 has generated interest as a biomarker for PDT-induced cellular damage and as a potential antigen for antitumor immune responses activated by PDT,<sup>348</sup> which have recently been exploited to dramatically improve the treatment outcome in J774 tumors (a highly metastatic reticulum cell sarcoma line) within mice.<sup>349</sup> It will be important to extend this work in the future for the identification of potential tumor antigens released during PDT, which may lead to novel combination therapies. For instance, PDT could be applied alongside cancer immunotherapy, where dendritic cells are harvested from the patient, activated with the tumor-specific antigen, and reintroduced to the patient for treatment.

### 5.3.2. Matrix Metalloproteinase

MMPs are a family of extracellular enzymes that facilitate tumor growth, cancer cell motility, and metastasis through degradation of the extracellular matrix (ECM) and the release of growth factors, cell surface markers, and other nonmatrix substrates (see the MMP imaging review by Scherer et al.<sup>350</sup> and references therein). MMP imaging has attracted a great

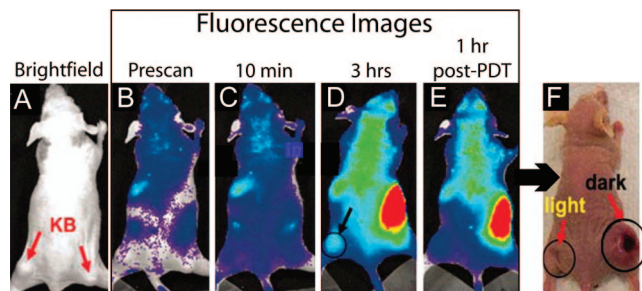
deal of interest and excitement as a means for sensitive tumor detection and as a biomarker for therapeutic monitoring and for drug delivery targeting. As mentioned above, tumoral MMP secretion and activation can be stimulated by tumor cell autocrine and paracrine signaling mediated by secreted cytokines. Both tumor cells and surrounding stromal cells are known to contribute to the MMP pool.<sup>351</sup> In the context of PDT, the expression of certain MMPs has been found to be increased following PDT and the use of MMP inhibitors increases the tumoricidal activity of PDT in vivo.<sup>352</sup>

Synthetic small-molecule MMP inhibitors have been developed on the basis of endogenous tissue inhibitor of MMP (TIMP) molecules, which naturally regulate MMP activation.<sup>350</sup> One approach to MMP imaging is to conjugate a contrast agent to an MMP inhibitor, and radiolabeled MMP inhibitor probes have been synthesized for PET imaging.<sup>353,354</sup> Unfortunately, this strategy has not yet proved effective primarily due to high levels of nonspecific binding.<sup>350</sup> As MMPs are secreted to the extracellular space, where they are activated, another approach has emerged in optical imaging that achieves exquisite selectivity for activated MMP enzymes. MMP-activated fluorescent probes utilize MMP-digestible linkers that, upon cleavage, release a FRET pair from quenching. In some cases, the FRET acceptor molecule's fluorescence can be used as an internal fluorescence standard to determine the ratio of cleaved to total substrate.<sup>355,356</sup> As mentioned in section 3.3, these target-activated probe designs stem from the work of Weissleder et al. to develop protease-activated NIR molecular probes<sup>151</sup> and apply them for monitoring MMP inhibition.<sup>357</sup> This strategy represents a highly selective platform for detecting the presence of MMPs.

Applying the above strategy to PDT, Zheng et al. have developed a “PMB” (“photodynamic molecular beacon”) activated by MMP-7, an MMP commonly expressed by epithelial cancer cells as discussed in detail in section 3.3 and shown schematically in Figure 19B.<sup>154</sup> This strategy of target-activated PDT agents for tumor cells represents a promising breakthrough for enhancing the selectivity of PDT and could be further developed for molecular imaging. Figure 29 shows in vivo images by Zheng et al. for a single mouse, which suggest that the PMB holds promise for selective treatment of MMP-7-positive tumors. With further development, this PMB could be applied as a molecular imaging contrast agent to monitor MMP-7 expression in response to PDT and to design targeted combination therapies. Further work is warranted to investigate the use of this beacon as a dual PDT and therapeutic monitoring agent to determine whether it can be used as a quantitative measure of MMP concentrations in vivo.

### 5.3.3. Vascular Endothelial Growth Factor

VEGF exists in several isoforms and is an archetypal cytokine that correlates with poor prognosis and disease recurrence for a number of cancers.<sup>358</sup> Moreover, tumoral up-regulation of VEGF expression has been observed in response to a number of treatment modalities, including radiotherapy,<sup>359,360</sup> cytoreductive surgery,<sup>361</sup> chemotherapy,<sup>362,363</sup> and PDT.<sup>12,147,325</sup> All of the VEGF isoforms bind and activate the tyrosine kinase receptors VEGFR-1 and VEGFR-2, which in turn activate a number of signaling cascades. These cascades stimulate the sprouting of neovasculature and ECM degradation to facilitate cancer cell motility and metastasis.<sup>358</sup> Aberrant VEGF signaling leads to disorganized neovasculature and leaky

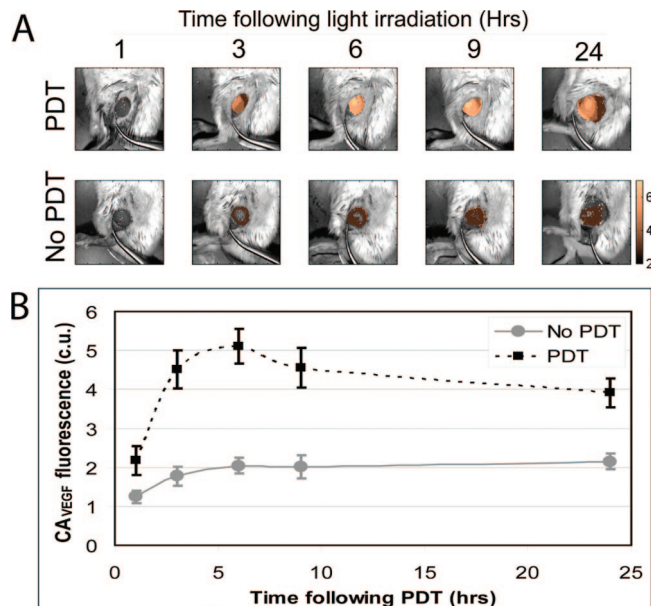


**Figure 29.** Preliminary demonstration of in vivo molecular imaging of a secreted, proteolytic enzyme important for metastasis. The fluorescence images are of an MMP-7-activated dual probe and PS agent. (A) Bright-field image of a mouse bearing two KB (human nasopharyngeal epidermoid carcinoma, an MMP-7+ cancer cell line) tumors, one in each flank as indicated by the arrows. (B–E) Whole-body fluorescence images of the mouse before and after administration of the MMP-7-activated probe/PS (B, prescan before iv injection of the target-activated fluorescent probe; C, 10 min postinjection of the probe; D, 3 h postinjection; E, 1 h following PDT). Note that the circle in (D) demarks the tumor in the left flank, which received light irradiation, while the right flank served as a “no light” control. (F) Photograph of the same mouse 30 days following PDT. Note that the left flank tumor exhibits reduced tumor burden in comparison to the right flank tumor. This represents a promising outcome, although only a single mouse was tested. Adapted with permission from ref 154. Copyright 2007 National Academy of Sciences of the U.S.A.

blood vessels, which facilitates metastasis and the accumulation of ascites<sup>358</sup> and carries tremendous implications for drug delivery to tumors.<sup>364</sup> VEGF and its receptors are concomitantly overexpressed by some cancer cells,<sup>365,366</sup> and VEGF stimulates cancer cell proliferation in vitro.<sup>367</sup> Given these factors, it is critical to develop strategies to image VEGF so that aberrant VEGF signaling following therapeutic intervention can be mitigated to improve the treatment outcome and patient survival.

Because VEGF is a secreted factor and dynamic in nature, imaging VEGF is a particular challenge and there are only a few reports of VEGF imaging. Radiolabeled anti-VEGF antibodies for PET imaging have been developed and applied in vivo,<sup>368,369</sup> however, a general weakness of radiolabeled probes is their short half-lives, which conflict with the longer time periods needed for the clearance of unbound antibody contrast agent from the target tissue. A more promising approach has been developed by Chang et al., which applies a small animal hyperspectral fluorescence imaging system in conjunction with a fluorophore-conjugated anti-VEGF antibody (and a VEGF inhibitor known as Avastin) as the contrast agent ( $CA_{VEGF}$ ).<sup>147</sup> This technique is the first real-time, quantitative molecular imaging strategy to monitor secreted VEGF and the transient elevation in VEGF expression and secretion following PDT.

The hyperspectral VEGF imaging strategy described above builds on the work of Ferrario et al.,<sup>322</sup> Solban et al.,<sup>12</sup> and Kosharsky et al.<sup>325</sup> to develop strategies to mitigate aberrant VEGF signaling following subcurative PDT. Figure 30 shows transient, elevated VEGF expression levels following subcurative PDT in orthotopic prostate tumors recorded using this imaging approach. Due to the complexity of tissue autofluorescence, linear spectral unmixing image analysis<sup>309,310</sup> was applied to produce background-free VEGF images. In these experiments,  $CA_{VEGF}$  was administered intravenously 24 h prior to imaging. During that time, the antibody–dye conjugate circulated in the bloodstream, bound to extracellular VEGF, and gradually accumulated within the tumor.



**Figure 30.** In vivo molecular imaging of cytokine secretion dynamics in response to PDT. Here, fluorescence hyperspectral imaging has been applied to acquire a secreted VEGF level time course in subcutaneous prostate cancer tumors (PC-3 human prostate cancer cells) following PDT. (A) Overlay of Avastin–AF488 conjugate (contrast agent for secreted VEGF,  $CA_{VEGF}$ ) fluorescence images (after spectral unmixing and calibration to a dye standard) and monochromatic reflectance images for a PDT-treated and a nontreated tumor. The  $CA_{VEGF}$  fluorescence amplitude is false colored gold. (B) Average calibrated fluorescence intensity of PDT-treated and nontreated tumors at 1, 3, 6, 9, and 24 h following PDT. The  $CA_{VEGF}$  fluorescence stabilizes after 24 h. Full time courses reveal a peak in VEGF secretion 24 h post-PDT, which returns to its pre-PDT baseline value after 3–7 days. The peak in secreted VEGF levels represents an opportune/critical time period for inhibiting VEGF activity. Reprinted with permission from ref 147. Copyright 2008 American Association for Cancer Research.

At approximately 24 h postinjection, the  $CA_{VEGF}$  reached its maximum accumulation and its concentration stabilized within the tumor tissue. At this time the tumor was surgically exposed for imaging. Using this protocol, Chang et al. observed that the secreted VEGF levels increase approximately 2-fold (a dramatic increase for a cytokine growth factor) within 24 h following subcurative PDT (Figure 30) and return to, or below, their baseline value within 3–7 days following PDT.

In contrast to the MMP-activated probes described above, fluorescently labeled antibody imaging relies on the specificity of the antibody for its molecular target and the clearance of unbound antibody from the tissue of interest. The accuracy of the spectral unmixing analysis for quantifying relative changes in tumoral VEGF concentration was confirmed by an ex vivo biochemical assay performed on pulverized tumor tissue following the imaging sessions.<sup>147</sup> The specificity of VEGF imaging was further demonstrated by in vivo competition assays that included antigen blocking by unlabeled Avastin and pretreatment with antibodies that do not bind VEGF.<sup>147</sup> These results are encouraging for applying VEGF imaging for therapeutic monitoring, though future work is warranted using fluorescence microendoscopy to visualize bound and released pools of VEGF and the spatial localization of VEGF and to image the potential pools of VEGF within the tissue that currently escape Avastin binding. Furthermore, fluorescence diffuse optical tomography may

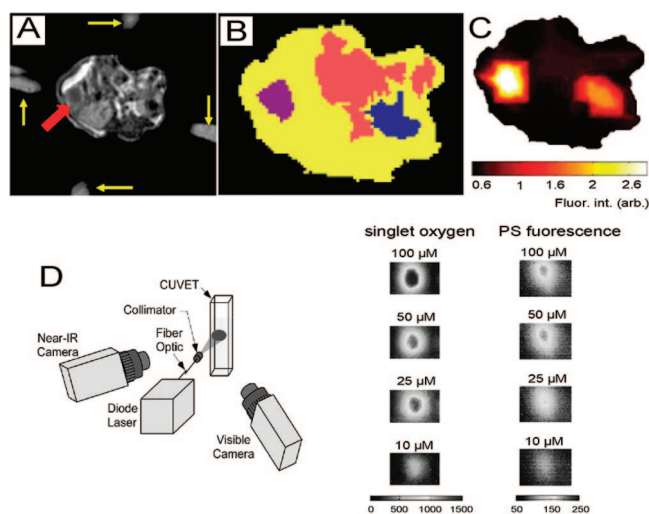


provide a method to extend these measurements deeper into the tissue for determining VEGF concentrations for a greater percentage of the tumor volume.

#### 5.4. PET and MRI for Molecular Imaging of Biological Responses to PDT

Thus far, we have highlighted the use of fluorescence imaging techniques and contrast agents in imaging therapeutic responses to PDT. Fluorescence imaging fits naturally with PDT since PS molecules are fluorescent themselves. Moreover, optical imaging and PDT generally share the advantage of possessing low systemic toxicity. On the other hand, it is important to realize that optical techniques are generally limited to surface imaging due to the limited penetration depth of visible and NIR light into tissue. Thus, optical imaging of deep tissues requires fiber-optic light guides and/or invasive surgical methods to access internal tissue sites. While the use of NIR light can increase the imaging depth substantially (as discussed in section 6.2 below) and fluorescence diffuse optical tomography<sup>316–319</sup> shows promise for noninvasive optical imaging, optical penetration depths are still, at most, a few centimeters, and a trade-off ultimately exists between spatial resolution and imaging depth. The limited penetration may be addressed using noninvasive modalities such as PET and MRI. Multimodal approaches that combine high-resolution optical imaging with guidance from whole-body imaging techniques such as PET and MRI may be implemented to take advantage of the strengths of the individual techniques. Examples of PS conjugates and molecular contrast agents for PET and MRI relevant to monitoring PS localization, PDT-induced apoptosis, and other molecular responses are given in the following.

A good example of noninvasive molecular imaging is provided by Subbarayan et al.,<sup>370</sup> who used autoradiography imaging to monitor apoptosis after PDT with the compound <sup>99m</sup>Tc-annexin V as the contrast agent. <sup>99m</sup>Tc-annexin V has a high affinity for phosphatidylserine, a molecule that is redistributed from the inner to outer cell membrane in the early stages of apoptosis. Autoradiography images demonstrated that, while untreated tumors did not take up the radiolabeled compound, PDT-treated tumors did. A similar study undertaken by Cauchon et al.<sup>320</sup> using PET scanning to detect <sup>64</sup>Cu-labeled streptavidin binding to previously injected biotinylated annexin V molecules observed apoptosis as early as 30 min following PDT with a phthalocyanine PS. A further example of PET-based molecular imaging is the use of a PET contrast agent to monitor gene expression following PDT. Dong et al. monitored the activation of the suicide gene herpes simplex virus thymidine kinase (HSV-tk) in xenograft breast carcinomas during PDT through the use of a PET imaging agent that is metabolized by HSV-tk and subsequently trapped intracellularly.<sup>371</sup> Finally, ligand–receptor targeting for MRI-guided fluorescence molecular tomography has been demonstrated by the Pogue group to monitor EGFR expression levels before and after PDT.<sup>201</sup> A commercially available fluorophore conjugated to epidermal growth factor (EGF, a ligand for EGFR) produced by LICOR Biosciences (EGF-conjugated IRDye 800CW) was used to demonstrate that EGFR expression levels can be monitored noninvasively and can report on the current status of the tumor (Figure 31). In this case, gadolinium contrast-enhanced MRI was used to guide placement of the fibers for fluores-



**Figure 31.** Examples of multimodal molecular imaging for PDT. MRI-guided fluorescence molecular tomography with EGF-labeled IRDye 800CW (LI-COR Biosciences). (A)–(C) provide both structural and functional information about the target tissue, in this case a pancreatic tumor. Singlet oxygen phosphorescence and PS fluorescence monitoring (D, E) can be used for dosimetry, treatment monitoring, and assessment. (A) Axial T1-weighted gadolinium contrast-enhanced MR image of a mouse. The yellow arrows indicate fiducials that mark the placement of the optical fibers for fluorescence detection, and the red arrow indicates the tumor. (B) Segmentation of the abdomen in relevant tissues based on significant fluorophore localization, absorption, and scattering properties. The tumor is in purple, the intestine in pink, the right kidney in blue, and the remaining abdomen in yellow. (C) EGF-IRDye 800CW fluorescence reconstruction of the mouse abdomen based on the segmentation in (B) and the assumption that there are heterogeneous distributions of the optical properties within each of the segments, i.e., soft priors. EGF-IRDye 800CW was injected intravenously 48 h prior to imaging. (D) The combined singlet oxygen phosphorescence and photosensitizer fluorescence imager developed by PSI is shown. (E) Simultaneous phosphorescence and fluorescence images can be produced. In this case solutions of the PS Ce6 were used. Reprinted with permission from refs 201 and 408. Copyright 2009 SPIE.

cence diffuse optical tomography of EGFR using the fluorescence contrast provided by the IRDye 800CW–EGF conjugate.

Multimodal contrast agents based on PS conjugates have also been investigated thoroughly by the Pandey group at Roswell Park Cancer Institute (Buffalo, NY).<sup>21,155</sup> These PS conjugates can serve as PDT agents, medical imaging (MRI or PET) contrast agents, and/or fluorescence imaging agents (multimodal contrast agents), allowing visualization before, during, and after PDT to assess therapy success. For example, a construct created by conjugating the MRI contrast agent Gd(III)–aminobenzyl–diethylenetriaminepentaacetic acid (DTPA) to the PS 3-vinyl-3-[1-(hexyloxy)ethyl]pyropheophorbide a (HPPH) via a tris(polyethylene glycol) monomethyl ether (PEG methyl ether) in a liposomal formulation<sup>155</sup> enhanced tumor localization by MRI while maintaining its PDT efficacy. Another agent introduced by the Pandey group was a PET-active PS created by labeling HPPH with <sup>124</sup>I that demonstrated 100% tumor-free progression 60 days after PDT.<sup>21</sup> Koo et al. developed nanoparticles with the ability to incorporate PDT agents by encapsulation or covalent attachment that have shown high therapeutic efficacy in a 9L rat gliosarcoma model. Multimodal nanoplatforms containing MRI agents and PS molecules that incorporate targeting ligands on the outer surface have been shown to improve both MRI contrast and PDT efficacy.<sup>19</sup> Similar

multimodality and targeted agents have also been developed by other groups.<sup>19,372,373</sup>

### 5.5. Summary of Molecular Imaging To Elucidate Biological Mechanisms Induced by PDT

The molecular mechanisms involved in biological responses to PDT are diverse and range in scale from intracellular signaling to the induction of coordinated physiological responses through intercellular communication among tumor cells, host cells within the tumor microenvironment, and the immune system. The imaging of molecular mechanisms is in the early stages of development, and there remains a great deal of work to further develop a toolbox of *in vivo* imaging platforms relevant for therapeutic monitoring of PDT. Thus far, there have been noteworthy advances: (1) the use of GFP-transfected cells to investigate intracellular signal transduction pathways and gene up-regulation, (2) the development of molecular target-activated probes, and (3) quantitative *in vivo* imaging of extracellular factors using fluorescently labeled antibodies. We anticipate that these promising directions will be expanded to investigate the hierarchy of pertinent signal transduction and regulatory pathways involved in cell death and prosurvival signaling in response to PDT. The development of such molecular imaging platforms is an important step toward enabling real-time therapeutic optimization.

The apoptosis signaling imaging studies presented here are of great interest for understanding the precise cellular death signal transduction pathways activated by PDT. Until recently, models of the molecular mechanisms of PDT-induced apoptosis have largely been derived from indirect observations, based on PS intracellular localization, the PS's affinity for certain molecules, and the use of inhibitors to block the action of certain molecules. Imaging spatiotemporal dynamics will help to elucidate the hierarchical order of signaling pathways that lead to apoptotic death. This line of research is critical for studying tumor cells that have survived sublethal PDT and for determining if they are better able to cope with further rounds of PDT.

These studies further demonstrate the power of imaging GFP-tagged proteins and GFP FRET sensors for visualizing the spatiotemporal dynamics of molecular-level events during apoptosis. A wide array of GFP-based biosensors have been developed for imaging calcium concentration, kinase phosphorylation, protease activation, redox potential, and many other processes involved in signal transduction.<sup>374–377</sup> In addition, GFP-tagged fusion proteins can generally be used to track protein expression and trafficking, as done recently for hypoxia-inducible factor 1 $\alpha$  following PDT.<sup>378</sup> Although transfection in humans is not yet acceptable, these sensors are applicable for cell culture and mouse models of disease and could be applied more often for imaging molecular mechanisms induced by PDT responses in preclinical mouse models of disease.

Site-activated contrast agents for MMP imaging are of great interest for the specific targeting of a particular tumor or tissue, and they may be used as "PDT molecular beacons" to cause very precise, local tissue death.

While imaging of molecular pathways has been underutilized thus far, it is expected to play a critical role in the development of novel combination therapeutic regimens. Until now, most combination regimens have relied on fixed protocols, such as chronic systemic administration of a predetermined dosage. By applying imaging to monitor

dynamic molecular events *in vivo*, critical parameters such as optimal delivery time and optimal dosage and the appropriate delivery vehicle for molecular-targeted therapeutic agents can be determined in real time. Real-time imaging of cytokines and other secreted factors (such as MMPs) will point the way to more effective combination therapies. *In vivo* imaging enables the characterization of opportune time periods during treatment response to inhibit the activity of secreted factors. Efficient use of these drugs will also help limit their intrinsic systemic toxicity. Thus far it appears that the spatiotemporal dynamics of secreted factors are germane to their role in recurrent cancer and for the rational design of strategies to mitigate the signaling cascades they induce.

### 6. Perspective and Future Directions

Imaging plays an essential role at every stage of PDT, from disease detection to treatment planning, dosimetry, therapy monitoring, and outcome assessment. Figure 35 depicts this perspective of the essential elements of the role of imaging in PDT. Currently, imaging techniques such as endoscopy, MRI, CT, and PET are widely used in PDT planning and assessment. Imaging with these mainstream medical techniques provides a familiar environment for medical staff, encouraging the incorporation of PDT into treatment regimens. However, there has been a surge of interest in newer, less conventional techniques such as intravital fluorescence microscopy, multiphoton excitation imaging, Doppler OCT, diffuse optical tomography, and multimodal imaging technologies. These techniques will likely play a major role in combining pretreatment dosimetry with outcome assessment, which will further our current knowledge about tissue response to PDT, and will be therefore essential in creating more standardized treatment parameters and enabling therapeutic advances. Broadly speaking, imaging combined with PDT has the potential to revolutionize therapeutic strategies. By providing individualized dosimetry and therapy monitoring at the molecular level, it could provide an opportunity for patient customized treatments, enhancement of other existing treatment modalities, and impact on healthcare costs.

Ultimately, multimodality imaging combined with PDT will be most useful where both structural and functional images may be obtained. As already mentioned, established techniques such as CT and MRI for assessment of treatment response have already been incorporated in PDT.<sup>171–175,191–201</sup> However, other than OCT in ophthalmology, the newer developments in imaging are far from being a routine component of PDT implementation so that the full impact of imaging on PDT is yet to come. Advances in imaging technologies and a better understanding of the PDT process in general, and mechanisms in particular, offer an unprecedented opportunity to enhance patient care by improving treatment outcomes and providing the potential for individualized treatments. Some of these opportunities have been discussed in preceding sections of this review. For example, PFD (section 2), where the PS (the therapeutic agent) is also the imaging agent, is fairly unique to PDT (perhaps with the exception of certain situations in radiation therapy) and has already altered treatment strategies for guided resections in bladder and brain cancers. PFD-guided resections combined with PDT have the potential of providing "mop up" of residual disease at many sites (e.g., brain cancer, dis-

seminated ovarian cancer, etc.) and is under investigation both clinically and preclinically.

A successful outcome of these investigations may be predicted to have a high positive impact on patient care in terms of both survival and the quality of life and perhaps on cost. The potential for the impact of imaging and PDT on healthcare cost may be exemplified by Mohs surgery of cutaneous cancers. This cumbersome procedure could be accelerated by the development of targeted, highly sensitive imaging combined with targeted PDT to ensure the removal of any residual cancer cells. Although this topic of delineating margins of resection for Mohs surgery has been investigated using standard PS,<sup>110,114</sup> the results have not been convincing enough for the standard of care to be altered or even for the approach to be adopted by physicians broadly. Targeted imaging or therapy strategies for augmenting Mohs procedures have not been reported and may be key to achieving the sensitivity and selectivity required for routine application in the clinic. The clinical management of bladder cancer is another application which is associated with a significant economic burden due to the high costs of treatment and monitoring of the disease over the lifetime of the patient.<sup>59</sup> Although there has not yet been sufficiently wide implementation of PFD to predict the long-term impact, the superior sensitivity of this approach allowing for more timely intervention indicates that it could have an impact on patient care in economic terms as well as survival and quality of life.

Laboratory research will also be a beneficiary of developments in molecular imaging by enhancing an understanding of molecular mechanisms, which in turn provides opportunities for investigations of rational, mechanism-based treatment regimens. As the effect of PDT on molecular entities such as heat shock proteins, prosurvival or prodeath molecules, and secreted cytokines are better understood, novel combination regimens may be tested and individualized patient response may also be modeled as discussed in section 5. Biological responses to PDT are complex because of the variety of molecular signaling cascades involved and the variety of parameters involved in PDT dosimetry. Monitoring these responses in real time, both structurally and molecularly, is a challenge, particularly when secreted factors or intracellular molecules are involved, but does have the potential for being a high-gain endeavor. An excellent example of this exists with spectroscopy, where Zhou et al. showed that active, real-time monitoring of PS photobleaching was a much better reporter of treatment response prediction of individual mice than simply the light or the initial PS dose.<sup>379</sup> A similar paradigm using imaging might be even more powerful as it will provide spatial resolution and thus the degree of heterogeneity of target response that might need to be considered in interpretation of data and treatment planning. As these approaches of online image-guided monitoring evolve, it will make the evaluation of new therapeutic regimens in the laboratory more economical and expeditious for translation into the clinic. For example, in the specific case of ovarian cancer, appropriate models of the disease are complicated, cumbersome to produce, and expensive. Evaluating a series of therapeutic strategies in the laboratory would then become a daunting task if every animal were to represent a single data point. As shown in recent studies and discussed in section 2, molecular imaging may be useful in overcoming this hurdle and reporting the efficacy of a particular therapy such that individualized

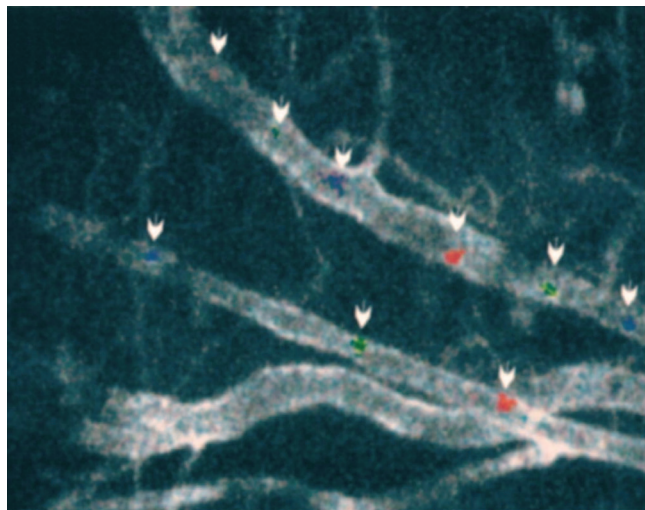
treatment design may be tested.<sup>12,147</sup> An area that has not received particular attention in PDT research is the application of PDT to appropriate models of disease both *in vitro* and *in vivo*. Imaging can play a very important role as was demonstrated recently in a study using OCT in the development of a 3D *in vitro* model of ovarian cancer.<sup>10</sup> The use of genetically modified cells exhibiting luminescence or fluorescence is now frequently used to circumvent some of these issues and is discussed in, for example, section 5.2. However, the problem with genetic modifications to introduce fluorescent proteins or the luciferase gene is that it often alters the biological behavior of cells so that fidelity to disease being modeled is lost,<sup>380</sup> and of course, the genetic modifications will not be translatable to humans.

Molecularly targeted imaging is an area of tremendous growth and promise that has received sizable attention but has not made a significant headway into the clinic perhaps due to the fact that the differences between target disease tissues and normal tissues can be modest. However, molecular imaging is particularly relevant to PDT as the fluorescent entity can be the same as the therapeutic one and any molecular targeting that is done for therapy can also be exploited for imaging. Here the choice of molecular targets becomes critical, and perhaps the best results will be achieved when the molecular expression of host tissue is maximally different from the disease being monitored or treated. An excellent example of this is the site-specific cleavage of a fluorophore construct by a bacterial enzyme in bacteria located in/on human cells and tissue.<sup>13</sup> In principle, the difference in the human and the bacterial genome offers a rare opportunity identifying a unique target for the treatment of infections, without damaging normal host tissue. Similar approaches are being pursued in imaging of cancers,<sup>151</sup> where the difference in molecular expression between target and nontarget tissues is typically one of degree rather than of content and therefore much more challenging. These challenges may be mitigated by the exciting developments in nanotechnology where the modest differential between normal and target tissues may be enhanced by appropriate targeted packaging, delivering high payloads of contrast agents.

Recent advances in imaging technology have opened a wide arena of potential areas of future development that impact PDT and other therapies. In the following subsections we focus on three specific examples of imaging techniques particularly relevant to PDT that hold promise for the future and are currently being developed: (i) *in vivo* tracking of cell migration in response to PDT to optimize short- and long-term treatment effects, (ii) multiphoton excitation for deep tissue imaging to improve the ability of PFD to reliably identify margins of diseased tissues below the surface of the lesion, and (iii) monitoring molecular oxygen for customized PDT dosimetry during treatment.

### 6.1. In Vivo Tracking of Cell Migration in Response to Photodynamic Therapy

*In vivo* imaging of cell trafficking is of great interest for therapeutic monitoring and carries particular importance in the context of PDT as a major prognostic indicator of survival following therapeutic intervention. Monitoring tumor cell trafficking *in vivo* will be tremendously beneficial for the real-time visualization of metastasis and the extent of its mitigation using combination therapies, such as anti-VEGF and/or anti-MMP therapy in combination with PDT. Another



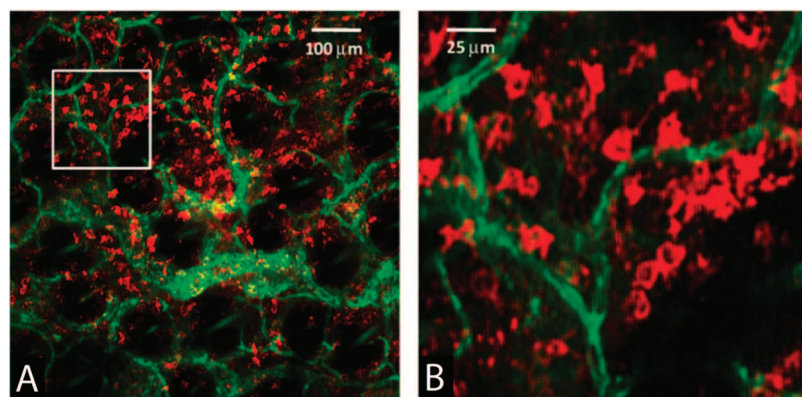
**Figure 32.** In vivo imaging of fluorescently labeled, circulating tumor cells for the detection of metastatic disease. Combined image of three still frames, spanning 200 ms, acquired at video rate showing fluorescently labeled rat prostate cancer cells (MLL cells) traveling through an artery vein pair. Two cells are highlighted along the vein (top vessel) and one cell is highlighted along the artery (bottom vessel) using blue, green, and red for the same cells as they are imaged in the first, second, and third frames, respectively. The vascular endothelium is labeled with antiplatelet/endothelial cell adhesion molecule 1 (CD31) conjugated to Cy5. As discussed in the text, the in vivo detection of circulating cancer cells is a powerful approach for the early assessment of response to therapy (e.g., detection of metastasis and/or its mitigation using combination therapies). Reprinted with permission from ref 11. Copyright 2004 American Association for Cancer Research.

powerful application is in vivo imaging of immune cell trafficking, which could be applied following PDT to investigate PDT-activated immune responses.

Novak et al. and Boutrus et al. applied in vivo flow cytometry (IVFC)<sup>381,382</sup> to monitor the depletion kinetics of circulating prostate cancer cells in mice and rats following tail vein injection of  $10^6$  cells to examine the dependence of the circulation kinetics on the cell line and the host environment.<sup>11</sup> Figure 32 shows images of circulating tumor cells flowing through the peripheral vasculature. The IVFC

technique uses a shaped laser beam to form an illumination slit across an artery of interest, and bursts in fluorescence are detected as fluorescently labeled cells traverse the slit. In the study by Georgakoudi et al., a strong heterogeneity in the interaction of tumor cells (seed) and their host microenvironment (soil) was highlighted in the cell depletion kinetics.<sup>11</sup> A more recent study by He et al. demonstrated IVFC quantification of circulating tumor cells as an emerging tool for the diagnosis and staging of cancer, assessment of response to therapy, and evaluation of residual disease after surgery.<sup>383</sup> Their IVFC method noninvasively counted rare circulating tumor cells in vivo as they flowed through the peripheral vasculature using an in vivo labeling strategy to stain FR-expressing circulating tumor cells with a fluorescent conjugate. Studies in mice with metastatic tumors demonstrated that circulating tumor cells could be detected weeks before metastatic disease was detected by other means.<sup>383</sup> Such an approach could be used to study changes in circulating metastatic tumor cells before, during, and after PDT intervention, providing valuable insight into treatment efficacy and post-PDT-related metastasis.

Imaging cell trafficking outside of the vasculature in tissues such as tumors also has considerable potential. For instance, Georgakoudi et al. developed and applied in vivo confocal and multiphoton imaging to study the spatiotemporal dynamics of cell populations<sup>384</sup> such as hematopoietic stem and progenitor cells.<sup>385</sup> The Foster laboratory has demonstrated in vivo confocal imaging of dendritic cells (antigen-presenting cells and key mediators of the immune response to tumor antigens) stained with fluorescently labeled antibodies directed against the major histocompatibility complex class II (Figure 33).<sup>386</sup> Following radiotherapy, these dendritic cells were observed to undergo migration in response to the ionizing radiation.<sup>387</sup> These breakthroughs in imaging of in vivo cell trafficking will undoubtedly play a role in future PDT studies monitoring, studying, and targeting tumor cells. Visualizing cell trafficking in tissues, especially in response to therapeutic intervention, will be essential in PDT studies that seek to understand, and potentially eliminate, post-treatment effects.



**Figure 33.** Imaging of immune cell populations in living specimens, which may potentially be applied for online monitoring of immune responses to PDT. In vivo confocal fluorescence images of immune cells are shown using an antibody–fluorescent dye conjugate injected into a tumor, after allowing 2 h for unbound conjugate to clear. Here, an antibody–dye conjugate targeted to MHC-II (major histocompatibility complex class II) labels dendritic MHC-II+ cells in an EMT6 (mouse mammary carcinoma) tumor grown intradermally in a mouse ear. (A) Positively stained dendritic MHC-II+ cells are labeled with a fluorescent antibody conjugate (red) at a depth of  $80\ \mu\text{m}$  in the tumor in the presence of a highly vascularized tumor microenvironment (green color indicates the CD31–fluorophore conjugate, which labels the vasculature). (B) Expanded views of the region of interest indicated by the white box superimposed on (A). In vivo imaging of immune cell trafficking is an exciting prospect for therapeutic monitoring (e.g., to optimize protocols for PDT-induced antitumor immune response). Reprinted with permission from ref 386. Copyright 2008 SPIE.

## 6.2. Multiphoton Excitation for Deep Tissue Imaging

A major drawback of conventional imaging strategies using one-photon excitation is the limited penetration of visible light into tissue. Visible light of the wavelengths required for efficient fluorescence excitation of PS typically penetrates only a few hundred micrometers into tissue, thus restricting the utility of PFD to superficial tumor identification (as described in section 2). One way to mitigate this inherent limitation of PFD may lie in the implementation of multiphoton excitation (MPE), an approach which has not yet seen significant development relevant to imaging and PDT.

In MPE, a molecule can be promoted into the same excited state as in single photon excitation through the simultaneous absorption of two or more lower energy photons, provided their energy sum equals the energy of the electronic transition (Figure 4).<sup>388,389</sup> The advantages of MPE for imaging applications in general have been reviewed extensively in the literature,<sup>390</sup> and the characteristic features of MPE imaging are applicable for many aspects of the PFD, PDT, and in vivo molecular imaging applications discussed in this review. As lower energy NIR photons between 800 and 1000 nm experience less scattering in the turbid tissue environment and reduced tissue absorption, MPE can intrinsically probe deeper in a sample than visible light—up to centimeter depths. The probability of simultaneous absorption scales with the number of photons required to reach a given state, meaning that multiphoton absorption only occurs when there is high photon flux, as available at the focus of a microscope objective during an ultrafast femtosecond laser pulse. This nonlinear effect gives rise to MPE only in the femtoliter-size laser focus (i.e., subcellular volumes), allowing for precise, three-dimensional control of the excitation volume and providing optically sectioned images without the need for a confocal pinhole. The tightly confined excitation volume intrinsic to MPE could have tremendous implications for PFD, where fluorescence emission would arise only from the femtoliter-sized excitation volume. In this manner MPE PFD would still offer the same potent capability for highly sensitive tumor recognition as in the traditional implementation, but instead of being primarily a superficial imaging modality, it would allow for 3D tumor margins to be precisely defined far below the surface of the tissue. This would also have implications for the molecular imaging applications described in section 5 with microscopic resolution carried out to visualize distributions of molecular factors within the tissue and their precise spatial localization (e.g., intracellular versus extracellular localizations). In addition, the pulsed, near-infrared light used for multiphoton excitation can be used for second harmonic generation microscopy, which is useful for imaging collagen fibers<sup>390</sup> and their rearrangements by tumor-associated fibroblasts.<sup>391</sup>

Although we are not aware of any published studies using MPE PFD, there have been investigations of MPE PDT using HpD<sup>392,393</sup> and PF,<sup>35</sup> offering the same advantages of deeper tissue penetration and more localized selection of photoactivation as described above in the context of imaging implementation. However, a major challenge in these studies is that the traditional porphyrin photosensitizers which are widely used in single-photon absorption PDT, have very low two-photon absorption cross-sections. Wilson and colleagues reported that the two-photon cross-section of PF is about 10 Göppert-Mayer units (GM; 1 GM =  $10^{-50}$  (cm<sup>4</sup> s)/photon), thus requiring an impractical light dose of 6300 J/cm<sup>2</sup> to

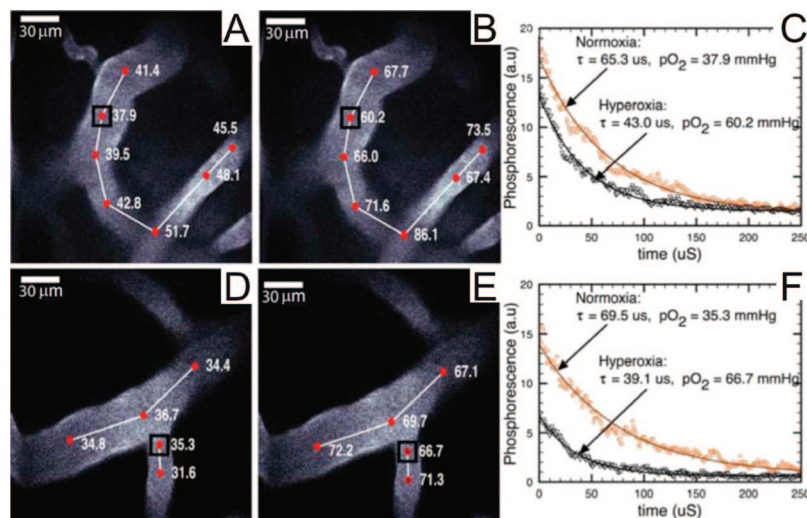
achieve 50% cell killing. To address this challenge, which currently limits the implementation of both MPE PFD and PDT, there have been efforts to design new PSs with enhanced two-photon cross-sections and evaluate them in preclinical PDT studies.<sup>394–399</sup> Another approach that has been proposed to achieve two-photon PS imaging involves the use of chromophores with strong two-photon absorption conjugated to the PS and used to transfer energy (via FRET) to the PS.<sup>393</sup> This idea continues to be developed<sup>400</sup> and has been recently implemented in a nanoparticle construct.<sup>401</sup> The continued development of new PSs with enhanced two-photon cross-sections is an exciting research direction and one that could allow for practical implementation of MPE PFD. As these new PSs are developed, it will be critical to determine how their intrinsic biodistribution in vivo compares with that of other PSs and their suitability for MPE PFD and PDT.

## 6.3. Monitoring Molecular Oxygen for Photodynamic Therapy Dosimetry

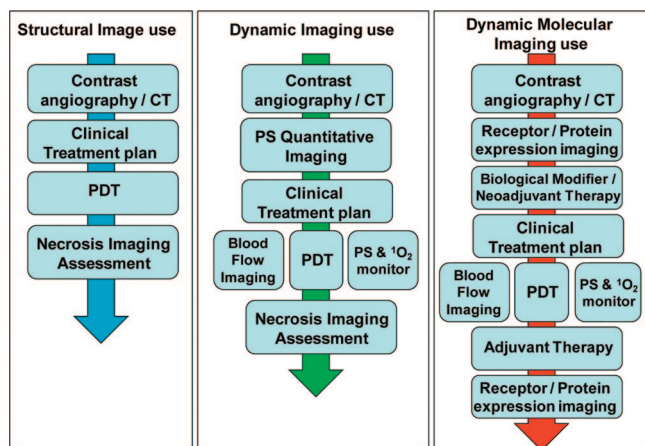
Dosimetry remains a formidable challenge for advancing the clinical use of PDT. Because most PDT regimens require the presence of light, a PS, and molecular oxygen to produce targeted killing, PDT dosimetry is inherently complex and difficult to quantify, as discussed in section 4.4. Attempts to monitor the deposited light dose and PS concentration have already improved PDT dosimetry significantly,<sup>379</sup> with a great deal of excitement surrounding new methods for imaging oxygen perfusion and direct imaging of PDT-generated cytotoxic species. Because the PS, light penetration, and oxygen perfusion vary from patient to patient (and for various tissue types), the ability to record the precise PDT dose is a crucial step in achieving effective, custom-tailored treatment regimens that can overcome natural biological heterogeneity. Here we expand on the possibility of visualizing these regions of hypoxia using the PS itself. PSs derive their photodynamic effect from their triplet state, a long-lived excited state that is sensitive to the molecule's surroundings. Once in the triplet state, the branching ratio between available relaxation pathways (as discussed briefly in section 1) is dependent on the local environment. One potential useful pathway is through phosphorescence (Figure 4), where a photon is emitted as the molecule returns from the triplet state to its ground state. This phosphorescence, however, can be quenched if the molecule leaves the triplet state through a nonradiative path, such as reacting with molecular oxygen.

This effect can be exploited in porphyrin-based and phthalocyanine-based PSs to measure the local oxygen tension. Using this approach, pO<sub>2</sub> has been monitored directly by measuring the phosphorescence lifetime.<sup>402</sup> An exciting future imaging direction relevant to PDT is in the use of MPE for deep measurements and three-dimensional imaging of blood vessel oxygenation in both healthy and tumor tissue (Figure 34).<sup>403</sup> Other areas that hold promise for the future in this area include the measurement of the triplet-state lifetime of the PS through delayed fluorescence alongside the singlet oxygen phosphorescence decay<sup>240</sup> to give a more complete picture of PS dosimetry. Oxygen tension can also be detected by simply measuring the ratio between the fluorescence and phosphorescence in some PSs.<sup>404</sup>

Identifying methods to directly quantify the deposited PDT dose remains an important and active area of research. As described in section 4 of this review, the PDT dose is



**Figure 34.** In vivo monitoring of oxygen tension by time-resolved PS phosphorescence imaging, which has potential implications for PDT dosimetry. The images are of arteries 120 and 100  $\mu\text{m}$  below the surface experiencing both normoxia (A, D) and hyperoxia (B, E), respectively. The phosphorescence decay data and best fit curves (C, F) are given for the points in (A), (B), (D), and (E). Regions under hypoxia have shorter lifetimes due to increased oxygen concentration. The monitoring of oxygen tension may be applied to record the consumption of molecular oxygen during PDT, to help determine the deposited PDT dose, and to identify hypoxic regions that may be resistant to PDT.  $p\text{O}_2$  values are given in units of mmHg. Reprinted with permission from ref 403. Copyright 2008 The Optical Society of America.



**Figure 35.** Examples of imaging workflow paradigms in PDT based on structural, dynamic, and molecular imaging. The left panel shows a simplified scenario in which structural imaging is used to design the treatment plan, including the PDT regimen, which is followed by postprocedural imaging to assess treatment efficacy. The middle panel depicts implementations of dynamic imaging for online monitoring of blood flow and generation of singlet oxygen during PDT treatment. The right-hand panel incorporates the additional level of sophistication that can be achieved if the treatment planning, monitoring, and assessment workflow includes techniques for measurement of dynamic biological responses, such as levels of activation of receptors and/or secretion of key cytokines before and after treatment.

extrapolated from numerous indirect means, including PS photobleaching, oxygen perfusion, and computer simulations based on assumptions regarding light penetration into tissue. However, for many PSs, the  $^1\text{O}_2$ -mediated pathway is critical for achieving the photodynamic effect. Hence, it has been suggested that a direct quantification of the cytotoxic  $^1\text{O}_2$  produced during PDT would circumvent these measures, giving researchers and clinicians the ability to deliver precise PDT doses. It is possible to directly observe the cytotoxic molecular singlet oxygen by imaging its luminescent emission. Jarvi et al.<sup>405</sup> comprehensively reviewed  $^1\text{O}_2$  luminescence dosimetry in 2006, in which they discuss challenges and promising progress in this area.

Notwithstanding the inherent challenges of obtaining spectroscopic measurements from the weak  $^1\text{O}_2$  phosphorescence signal,<sup>406</sup> these measurements have been correlated with treatment response in a recently conducted clinical study.<sup>240,407</sup> However, imaging of  $^1\text{O}_2$  still remains elusive. Recently, an imaging system that can monitor both  $^1\text{O}_2$  phosphorescence and PS fluorescence (Figure 31) has been reported.<sup>201,408</sup> This technique offers a unique method to measure the PDT effect before, during, and after treatment. The utility of this recently developed system, however, remains to be fully demonstrated, and further research is needed for this approach to be implemented broadly in the laboratory or the clinic.

Breakthroughs in detector technology likely hold the key for further developing and implementing singlet oxygen-based PDT dosimetry imaging. As there are many sources of background and the singlet oxygen signal is low, spectral detection in combination with time-resolved measurements would be ideal for future instrumentation, where linear spectral unmixing could be applied to extract the singlet oxygen luminescence signal. Perhaps most importantly, the engineering of higher quantum efficiency NIR detectors is desperately needed.

In conclusion, the combination of imaging and PDT is in early development, but recent advances have already made an impact on patient management, as in the case of brain and bladder cancers and PS-guided resections<sup>56,78</sup> and in laboratory science.<sup>10,14,343,346</sup> Progress in imaging technologies, targeting chemistries, and nanotechnology combined with a detailed understanding of PDT-related molecular mechanisms provides optimism for the future of imaging in PDT and may be an important conduit for new applications of PDT and for the development of patient individualized treatments.

## 7. List of Abbreviations

ALA	aminolevulinic acid
AIS2Pc	disulfonated aluminum phthalocyanine
AMD	age-related macular degeneration
Bax	Bcl-2-associated X protein
Bid	BH3 interacting domain death agonist

BPD	benzoporphyrin derivative (monoacid ring A)
Ce6	chlorin e6
CFD	combined fluorescence diagnosis
CFP	cyan fluorescent protein
CNV	choroidal neovascularization
CT	computed tomography
DTPA	Gd(III)-aminobenzyl-diethylenetriaminepenta-acetic
EGF	epidermal growth factor
EGFR	epidermal growth factor receptor
FR	folate receptor
FRET	Förster resonance energy transfer
GFP	green fluorescent protein
GM	Göppert-Mayer (1 GM = 10 <sup>-50</sup> (cm <sup>4</sup> s)/photon)
HAL	hexyl ester of aminolevulinic acid
HER2	human epidermal growth factor receptor 2
HP	hematoporphyrin
HpD	hematoporphyrin derivative
HPPH	3-vinyl-3-[1-(hexyloxy)ethyl]pyropheophorbide a
HSV-tk	herpes simplex virus thymidine kinase
IVFC	in vivo flow cytometry
MAL	methyl ester of aminolevulinic acid
MMP	matrix metalloproteinase
MRI	magnetic resonance imaging
MRS	magnetic resonance spectroscopy
mTHPC	tetrakis( <i>m</i> -hydroxyphenyl)chlorin
NIR	near-infrared
PDD	photodynamic diagnosis
PDT	photodynamic therapy
PDT-BIAS	PDT agent with a built-in apoptosis sensor
PF	Photofrin
PIC	photoimmunoconjugate
PMB	photomolecular beacon
PpIX	protoporphyrin IX
PS	photosensitizer
PET	positron emission tomography
PFD	photosensitizer fluorescence detection
Pyro	pyropheophorbide a
ROS	reactive oxygen species
TPC	5-(4-carboxyphenyl)-10,15,20-triphenyl-2,3-dihydroxychlorin
VEGF	vascular endothelial growth factor
VEGFR	vascular endothelial growth factor receptor
VIP	verteporfin in photodynamic therapy
YFP	yellow fluorescent protein

## 8. Acknowledgments

We are grateful to the late Dr. Thomas F. Deutsch for first introducing T.H. to the tremendous potential of imaging in PDT, almost 2 decades ago. This work was supported by National Institutes of Health Grant Number P01 CA084203-06, National Cancer Institute/National Institutes of Health Grant Number R01 CA119388, the Department of Defense Medical Free Electron Laser Program, and Wellman Center for Photomedicine core funds.

## 9. References

- Fitzpatrick, T. B.; Pathak, M. A. *J. Invest. Dermatol.* **1959**, *32*, 229.
- Epstein, J. H. *N. Engl. J. Med.* **1990**, *322*, 1149.
- Lipson, R. L.; Baldes, E. J.; Olsen, A. M. *J. Natl. Cancer Inst.* **1961**, *26*, 1.
- Kessel, D. *Photochem. Photobiol.* **1986**, *44*, 193.
- Dougherty, T. J. *J. Clin. Laser Med. Surg.* **1996**, *14*, 219.
- Huang, Z. *Technol. Cancer Res. Treat.* **2005**, *4*, 283.
- Schmidt-Erfurth, U.; Miller, J. W.; Sickenberg, M.; Laqua, H.; Barbazetto, I.; Gragoudas, E. S.; Zografos, L.; Piguat, B.; Pourmaras, C. J.; Donati, G.; Lane, A. M.; Birngruber, R.; van den Berg, H.; Strong, H. A.; Manjuri, U.; Gray, T.; Fsadni, M.; Bressler, N. M. *Arch. Ophthalmol.* **1999**, *117*, 1177.
- Ackroyd, R.; Kelty, C.; Brown, N.; Reed, M. *Photochem. Photobiol.* **2001**, *74*, 656.
- Polcard, C. R. *Soc. Biol.* **1924**, *91*, 1423.
- Evans, C. L.; Rizvi, I.; Hasan, T.; de Boer, J. F. *Opt. Express* **2009**, *17*, 8892.
- Georgakoudi, I.; Solban, N.; Novak, J.; Rice, W.; Wei, X.; Hasan, T.; Lin, C. *Cancer Res.* **2004**, *64*, 5044.
- Solban, N.; Pal, S. K.; Alok, S. K.; Sung, C. K.; Hasan, T. *Cancer Res.* **2006**, *66*, 5633.
- Zheng, X.; Sallum, U. W.; Verma, S.; Athar, H.; Evans, C. L.; Hasan, T. *Angew. Chem., Int. Ed.* **2009**, *48*, 2148.
- Soukos, N. S.; Hamblin, M. R.; Keel, S.; Fabian, R. L.; Deutsch, T. F.; Hasan, T. *Cancer Res.* **2001**, *61*, 4490.
- Zhong, W.; Celli, J. P.; Rizvi, I.; Mai, Z.; Spring, B. Q.; Yun, S. H.; Hasan, T. *Br. J. Cancer* **2009**, *101*, 2015.
- Gibbs-Strauss, S. L.; O'Hara, J. A.; Hoopes, P. J.; Hasan, T.; Pogue, B. W. *J. Biomed. Opt.* **2009**, *14*, 014007.
- Borle, F.; Radu, A.; Monnier, P.; van den Bergh, H.; Wagnieres, G. *Photochem. Photobiol.* **2003**, *78*, 377.
- Bouree, L.; Thibaut, S.; Briffaud, A.; Rousset, N.; Eleouet, S.; Lajat, Y.; Patrice, T. *J. Photochem. Photobiol., B* **2002**, *67*, 23.
- Koo, Y.-E. L.; Fan, W.; Hah, H.; Xu, H.; Orringer, D.; Ross, B.; Rehemtulla, A.; Philbert, M. A.; Kopelman, R. *Appl. Opt.* **2007**, *46*, 1924.
- McCarthy, J. R.; Weissleder, R. *Adv. Drug Delivery Rev.* **2008**, *60*, 1241.
- Pandey, S. K.; Gryshuk, A. L.; Sajjad, M.; Zheng, X.; Chen, Y.; Abouzeid, M. M.; Morgan, J.; Charamisinau, I.; Nabi, H. A.; Oseroff, A.; Pandey, R. K. *J. Med. Chem.* **2005**, *48*, 6286.
- Reddy, G. R.; Bhojani, M. S.; McConville, P.; Moody, J.; Moffat, B. A.; Hall, D. E.; Kim, G.; Koo, Y.-E. L.; Woolliscroft, M. J.; Sugai, J. V.; Johnson, T. D.; Philbert, M. A.; Kopelman, R.; Rehemtulla, A.; Ross, B. D. *Clin. Cancer Res.* **2006**, *12*, 6677.
- Shea, C. R.; Hefetz, Y.; Gillies, R.; Wimberly, J.; Dalickas, G.; Hasan, T. *J. Biol. Chem.* **1990**, *265*, 5977.
- Smith, G.; McGimpsey, W. G.; Lynch, M. C.; Kochevar, I. E.; Redmond, R. W. *Photochem. Photobiol.* **1994**, *59*, 135.
- Karotki, A.; Khurana, M.; Lepock, J.; Wilson, B. *Photochem. Photobiol.* **2006**, *82*, 443.
- Kuimova, M. K.; Collins, H. A.; Balaz, M.; Dahlstedt, E.; Levitt, J. A.; Sergent, N.; Suhling, K.; Drobizhev, M.; Makarov, N. S.; Rebane, A.; Anderson, H. L.; Phillips, D. *Org. Biomol. Chem.* **2009**, *7*, 889.
- Scherer, J. *Ann. Chem. Pharm.* **1841**, *40*, 1.
- Auler, H.; Banzer, G. *J. Cancer Res. Clin. Oncol.* **1942**, *53*, 65.
- Figge, F. J.; Wieland, G. S.; Manganiello, L. O. *J. Proc. Soc. Exp. Biol. Med.* **1948**, *68*, 640.
- Rassmussen-Taxdal, D. S.; Ward, G. E.; Figge, F. J. *Cancer* **1955**, *8*.
- Schwartz, S. K.; Absolon, K.; Vermund, H. *Univ. Minn. Med. Bull.* **1955**, *27*, 7.
- Lipson, R. L.; Baldes, E. J. *Arch. Dermatol.* **1960**, *82*, 508.
- Lipson, R. L.; Baldes, E. J.; Olsen, A. M. *J. Thorac. Cardiovasc. Surg.* **1961**, *42*, 623.
- Gray, M. J.; Lipson, R.; Maeck, J. V.; Parker, L.; Romeyn, D. *Am. J. Obstet. Gynecol.* **1967**, *99*, 766.
- Kyriazis, G. A.; Balin, H.; Lipson, R. L. *Am. J. Obstet. Gynecol.* **1973**, *117*, 375.
- Lipson, R. L.; Baldes, E. J.; Gray, M. J. *Cancer* **1967**, *20*, 2255.
- Kinsey, J. H.; Cortese, D. A.; Sanderson, D. R. *Mayo Clin. Proc.* **1978**, *53*, 594.
- Cortese, D. A.; Kinsey, J. H.; Woolner, L. B.; Payne, W. S.; Sanderson, D. R.; Fontana, R. S. *Mayo Clin. Proc.* **1979**, *54*, 635.
- Kato, H.; Cortese, D. A. *Clin. Chest Med.* **1985**, *6*, 237.
- Leonard, J. R.; Beck, W. L. *Laryngoscope* **1971**, *81*, 365.
- Benson, R. C., Jr.; Farrow, G. M.; Kinsey, J. H.; Cortese, D. A.; Zincke, H.; Utz, D. C. *Mayo Clin. Proc.* **1982**, *57*, 548.
- Gregorie, H. B., Jr.; Horger, E. O.; Ward, J. L.; Green, J. F.; Richards, T.; Robertson, H. C., Jr.; Stevenson, T. B. *Ann. Surg.* **1968**, *167*, 820.
- Gomer, C. J.; Dougherty, T. J. *Cancer Res.* **1979**, *39*, 146.
- Jori, G.; Pizzi, G.; Reddi, E.; Tomio, L.; Salvato, B.; Zorat, P.; Calzavara, F. *Tumori* **1979**, *65*, 425.
- Kessel, D. *Cancer Res.* **1982**, *42*, 1703.
- Unsöld, E.; Ell, C.; Jocham, D.; Sroka, R.; Stocker, S. *Lasers Med. Sci.* **1990**, *5*, 309.
- Kennedy, J. C.; Pottier, R. H. *J. Photochem. Photobiol., B* **1992**, *14*, 275.
- Kennedy, J. C.; Pottier, R. H.; Pross, D. C. *J. Photochem. Photobiol., B* **1990**, *6*, 143.
- Berlin, N. I.; Neuberger, A.; Scott, J. J. *Biochem. J.* **1956**, *64*, 80.
- Krieg, R. *Photochem. Photobiol.* **2002**, *76*, 518.

- (51) van den Boogert, J.; van Hillegersberg, R.; de Rooij, F. W.; de Bruin, R. W.; Edixhoven-Bosdijk, A.; Houtsmuller, A. B.; Siersema, P. D.; Wilson, J. H.; Tilanus, H. W. *J. Photochem. Photobiol., B* **1998**, *44*, 29.
- (52) Inuma, S.; Bachor, R.; Flotte, T.; Hasan, T. *J. Urol.* **1995**, *153*, 802.
- (53) Wyss-Desserich, M. T.; Sun, C. H.; Wyss, P.; Kurlawalla, C. S.; Haller, U.; Berns, M. W.; Tadir, Y. *Biochem. Biophys. Res. Commun.* **1996**, *224*, 819.
- (54) Hua, Z.; Gibson, S. L.; Foster, T. H.; Hilf, R. *Cancer Res.* **1995**, *55*, 1723.
- (55) Ortel, B.; Chen, N.; Brissette, J.; Dotto, G. P.; Maytin, E.; Hasan, T. *Br. J. Cancer* **1998**, *77*, 1744.
- (56) Witjes, J. A.; Douglass, J. *Nat. Clin. Pract. Urol.* **2007**, *4*, 542.
- (57) Kirkali, Z. *Urology* **2005**, *66*, 4.
- (58) Sylvester, R. *Eur. Urol.* **2006**, *49*, 466.
- (59) Botteman, M. *Pharmacoeconomics* **2003**, *21*, 1315.
- (60) Kriegmair, M.; Ehsan, A.; Baumgartner, R.; Lumper, W.; Knuechel, R.; Hofstädter, F.; Steinbach, P.; Hofstetter, A. *Urology* **1994**, *44*, 836.
- (61) Kriegmair, M. *J. Urol.* **1996**, *155*, 105.
- (62) Koenig, F.; McGovern, F. J.; Larne, R.; Enquist, H.; Schomacker, K. T.; Deutsch, T. F. *BJU Int.* **1999**, *83*, 129.
- (63) Zaak, D. *Urology* **2001**, *57*, 690.
- (64) Riedl, C. R.; Daniltchenko, D.; Koenig, F.; Simak, R.; Loening, S. A.; Pflueger, H. *J. Urol.* **2001**, *165*, 1121.
- (65) Kriegmair, M. *J. Urol.* **2002**, *168*, 475.
- (66) Lange, N.; Jichlinski, P.; Zellweger, M.; Forrer, M.; Marti, A.; Guillou, L.; Kucera, P.; Wagnieres, G.; van den Bergh, H. *Br. J. Cancer* **1999**, *80*, 185.
- (67) Jichlinski, P. *J. Urol.* **2003**, *170*, 226.
- (68) Schmidbauer, J. *J. Urol.* **2004**, *171*, 135.
- (69) Jocham, D. *J. Urol.* **2005**, *174*, 862.
- (70) Fradet, Y. *J. Urol.* **2007**, *178*, 68.
- (71) Grossman, H. *J. Urol.* **2007**, *178*, 62.
- (72) Kah, J. C.; Lau, W. K.; Tan, P. H.; Sheppard, C. J.; Olivo, M. *J. Biomed. Opt.* **2008**, *13*, 054022.
- (73) Lacroix, M.; Abi-Said, D.; Fournay, D. R.; Gokaslan, Z. L.; Shi, W.; DeMonte, F.; Lang, F. F.; McCutcheon, I. E.; Hassenbusch, S. J.; Holland, E.; Hess, K.; Michael, C.; Miller, D.; Sawaya, R. *J. Neurosurg.* **2001**, *95*, 190.
- (74) Albert, F. K.; Forsting, M.; Sartor, K.; Adams, H. P.; Kunze, S. *Neurosurgery* **1994**, *34*, 45.
- (75) Stummer, W.; Stocker, S.; Novotny, A.; Heimann, A.; Sauer, O.; Kempfski, O.; Plesnila, N.; Wietzorrek, J.; Reulen, H. J. *J. Photochem. Photobiol., B* **1998**, *45*, 160.
- (76) Stummer, W.; Stocker, S.; Wagner, S.; Stepp, H.; Fritsch, C.; Goetz, C.; Goetz, A. E.; Kieffmann, R.; Reulen, H. J. *Neurosurgery* **1998**, *42*, 518.
- (77) Stummer, W.; Novotny, A.; Stepp, H.; Goetz, C.; Bise, K.; Reulen, H. J. *J. Neurosurg.* **2000**, *93*, 1003.
- (78) Stummer, W.; Pichlmeier, U.; Meinel, T.; Wiestler, O. D.; Zanella, F.; Reulen, H.-J.; Group, A. L.-G. *S. Lancet Oncol.* **2006**, *7*, 392.
- (79) Barker, F. G., 2nd; Chang, S. M. *Lancet Oncol.* **2006**, *7*, 359.
- (80) Zimmermann, A.; Ritsch-Martel, M.; Kostron, H. *Photochem. Photobiol.* **2001**, *74*, 611.
- (81) Bogaards, A.; Sterenborg, H. J.; Trachtenberg, J.; Wilson, B. C.; Lilge, L. *Lasers Surg. Med.* **2007**, *39*, 605.
- (82) Kostron, H.; Rossler, K. *Wien. Med. Wochenschr.* **2006**, *156*, 338.
- (83) Stepp, H.; Beck, T.; Pongratz, T.; Meinel, T.; Kreth, F.-W.; Tonn, J. C.; Stummer, W. *J. Environ. Pathol., Toxicol. Oncol.* **2007**, *26*, 157.
- (84) Yang, V. X.; Muller, P. J.; Herman, P.; Wilson, B. C.; Yang, V. X. D.; Muller, P. J.; Herman, P.; Wilson, B. C. *Lasers Surg. Med.* **2003**, *32*, 224.
- (85) Olivo, M.; Wilson, B. C. *Int. J. Oncol.* **2004**, *25*, 37.
- (86) Bogaards, A.; Varma, A.; Zhang, K.; Zach, D.; Bisland, S. K.; Moriyama, E. H.; Lilge, L.; Muller, P. J.; Wilson, B. C. *Photochem. Photobiol. Sci.* **2005**, *4*, 438.
- (87) Bogaards, A.; Varma, A.; Collens, S. P.; Lin, A. H.; Giles, A.; Yang, V. X. D.; Bilbao, J. M.; Lilge, L. D.; Muller, P. J.; Wilson, B. C. *Lasers Surg. Med.* **2004**, *35*, 181.
- (88) Jemal, A.; Siegel, R.; Ward, E.; Hao, Y.; Xu, J.; Thun, M. J. *Ca-Cancer J. Clin.* **2009**, *59*, 225.
- (89) Cho, K. R.; Shih, I. M. *Annu. Rev. Pathol.* **2009**, *4*, 287.
- (90) Berek, J. S.; Bast, R. C. J. In *Cancer Medicine*; Kufe, D. W., Pollack, R. E., Weichselbaum, R. R., Bast, R. C. J., Gansler, T. S., Holland, J. F., Frei, E. I., Eds.; BC Decker Inc.: Hamilton, Ontario, Canada, 2003.
- (91) Davila, G. W.; Estape, R. *Surg. Oncol. Clin. N. Am.* **2001**, *10*, 557.
- (92) Tammela, J.; Lele, S. *Curr. Opin. Obstet. Gynecol.* **2004**, *16*, 5.
- (93) Chan, J. K.; Monk, B. J.; Cuccia, D.; Pham, H.; Kimel, S.; Gu, M.; Hammer-Wilson, M. J.; Liaw, L. H. L.; Osann, K.; DiSaia, P. J. *Gynecol. Oncol.* **2002**, *87*, 64.
- (94) Ludicke, F.; Gabrecht, T.; Lange, N.; Wagnieres, G.; Van Den Bergh, H.; Berclaz, L.; Major, A. L. *Br. J. Cancer* **2003**, *88*, 1780.
- (95) Loning, M.; Diddens, H.; Kupker, W.; Diedrich, K.; Huttmann, G. *Cancer* **2004**, *100*, 1650.
- (96) Hendren, S. K.; Hahn, S. M.; Spitz, F. R.; Bauer, T. W.; Rubin, S. C.; Zhu, T.; Glatstein, E.; Fraker, D. L. *Ann. Surg. Oncol.* **2001**, *8*, 65.
- (97) Hahn, S. M.; Fraker, D. L.; Mick, R.; Metz, J.; Busch, T. M.; Smith, D.; Zhu, T.; Rodriguez, C.; Dimofte, A.; Spitz, F. *Clin. Cancer Res.* **2006**, *12*, 2517.
- (98) Sindelar, W. F.; DeLaney, T. F.; Tochner, Z.; Thomas, G. F.; Dachoswki, L. J.; Smith, P. D.; Friauf, W. S.; Cole, J. W.; Glatstein, E. *Arch. Surg.* **1991**, *126*, 318.
- (99) Ericson, M. B.; Sandberg, C.; Gudmundson, F.; Rosen, A.; Larko, O.; Wennberg, A. M. *J. Photochem. Photobiol., B* **2003**, *69*, 121.
- (100) Hemming, A. W.; Davis, N. L.; Dubois, B.; Quenville, N. F.; Finley, R. J. *Surg. Oncol.* **1993**, *2*, 187.
- (101) Megerian, C. A.; Zaidi, S. I.; Sprecher, R. C.; Setrakian, S.; Stepnick, D. W.; Oleinick, N. L.; Mukhtar, H. *Laryngoscope* **1993**, *103*, 967.
- (102) Andrejevic-Blant, S.; Hadjur, C.; Ballini, J. P.; Wagnieres, G.; Fontollet, C.; van den Bergh, H.; Monnier, P. *Br. J. Cancer* **1997**, *76*, 1021.
- (103) Allison, R. R.; Mang, T. S.; Wilson, B. D. *Semin. Cutaneous Med. Surg.* **1998**, *17*, 153.
- (104) Chang, C. J.; Lai, Y. L.; Wong, C. J. *Chang Keng I Hsueh* **1998**, *21*, 13.
- (105) Svanberg, K.; Andersson, T.; Killander, D.; Wang, I.; Stenram, U.; Andersson-Engels, S.; Berg, R.; Johansson, J.; Svanberg, S. *Br. J. Dermatol.* **1994**, *130*, 743.
- (106) Fijan, S.; Honigsmann, H.; Ortel, B. *Br. J. Dermatol.* **1995**, *133*, 282.
- (107) Harth, Y.; Hirshowitz, B.; Kaplan, B. *Dermatol. Surg.* **1998**, *24*, 723.
- (108) Gupta, G.; Morton, C. A.; Whitehurst, C.; Moore, J. V.; MacKie, R. M. *Br. J. Dermatol.* **1999**, *141*, 385.
- (109) Fritsch, C.; Lang, K.; Neuse, W.; Ruzicka, T.; Lehmann, P. *Skin Pharmacol. Appl. Skin Physiol.* **1998**, *11*, 358.
- (110) Redondo, P.; Marquina, M.; Pretel, M.; Aguado, L.; Iglesias, M. E. *Arch. Dermatol.* **2008**, *144*, 115.
- (111) Andersson-Engels, S.; Elner, Å.; Johansson, J.; Karlsson, S.; Salford, L.; Strömblad, L.; Svanberg, K.; Svanberg, S. *Lasers Med. Sci.* **1991**, *6*, 415.
- (112) Andersson-Engels, S.; Berg, R.; Svanberg, K.; Svanberg, S. *Bioimaging* **1995**, *3*, 134.
- (113) Hewett, J.; Nadeau, V.; Ferguson, J.; Moseley, H.; Ibbotson, S.; Allen, J. W.; Sibbett, W.; Padgett, M. *Photochem. Photobiol.* **2001**, *73*, 278.
- (114) Martin, A.; Tope, W. D.; Grevelink, J. M.; Starr, J. C.; Fewkes, J. L.; Flotte, T. J.; Deutsch, T. F.; Anderson, R. R. *Arch. Dermatol. Res.* **1995**, *287*, 665.
- (115) Fritsch, C.; Homey, B.; Stahl, W.; Lehmann, P.; Ruzicka, T.; Sies, H. *Photochem. Photobiol.* **1998**, *68*, 218.
- (116) Juzeniene, A.; Juzenas, P.; Ma, L. W.; Iani, V.; Moan, J. *Br. J. Dermatol.* **2006**, *155*, 791.
- (117) Kuijpers, D. I.; Thissen, M. R.; Thissen, C. A.; Neumann, M. H. *J. Drugs Dermatol.* **2006**, *5*, 642.
- (118) Wiegell, S. R.; Wulf, H. C. *J. Am. Acad. Dermatol.* **2006**, *54*, 647.
- (119) Leunig, A.; Rick, K.; Stepp, H.; Gutmann, R.; Alwin, G.; Baumgartner, R.; Feyh, J. *Am. J. Surg.* **1996**, *172*, 674.
- (120) Leunig, A.; Betz, C. S.; Mehlmann, M.; Stepp, H.; Arbogast, S.; Grevers, G.; Baumgartner, R. *Laryngoscope* **2000**, *110*, 78.
- (121) Betz, C. S.; Stepp, H.; Janda, P.; Arbogast, S.; Grevers, G.; Baumgartner, R.; Leunig, A. *Int. J. Cancer* **2002**, *97*, 245.
- (122) Ebihara, A.; Krasieva, T. B.; Liaw, L.-H. L.; Fago, S.; Messadi, D.; Osann, K.; Wilder-Smith, P. *Lasers Surg. Med.* **2003**, *32*, 17.
- (123) Baumgartner, R.; Huber, R. M.; Schulz, H.; Stepp, H.; Rick, K.; Gamarra, F.; Leberig, A.; Roth, C. *J. Photochem. Photobiol., B* **1996**, *36*, 169.
- (124) Endlicher, E.; Knuechel, R.; Hauser, T.; Szeimies, R.-M.; Schölmacher, J.; Messmann, H. *Gut* **2001**, *48*, 314.
- (125) Stepinac, T.; Felley, C.; Jornod, P.; Lange, N.; Gabrecht, T.; Fontollet, C.; Grosjean, P.; vanMelle, G.; van den Bergh, H.; Monnier, P.; Wagnieres, G.; Dorta, G. *Endoscopy* **2003**, *35*, 663.
- (126) Hillemanns, P.; Korell, M.; Schmitt-Sody, M.; Baumgartner, R.; Beyer, W.; Kimmig, R.; Untch, M.; Hepp, H. *Int. J. Cancer* **1999**, *81*, 34.
- (127) Hillemanns, P.; Untch, M.; Prove, F.; Baumgartner, R.; Hillemanns, M.; Korell, M. *Obstet. Gynecol.* **1999**, *93*, 71.
- (128) Hillemanns, P.; Weingandt, H.; Baumgartner, R.; Diebold, J.; Xiang, W.; Stepp, H. *Cancer* **2000**, *88*, 2275.
- (129) Duska, L. R.; Wimberly, J.; Deutsch, T. F.; Ortel, B.; Haas, J.; Houck, K.; Hasan, T. *Gynecol. Oncol.* **2002**, *85*, 125.
- (130) Henderson, B. W.; Bellnier, D. A.; Greco, W. R.; Sharma, A.; Pandey, R. K.; Vaughan, L. A.; Weishaupt, K. R.; Dougherty, T. J. *Cancer Res.* **1997**, *57*, 4000.



- (131) Mojzisoava, H.; Bonneau, S.; Brault, D. *Eur. Biophys. J.* **2007**, *36*, 943.
- (132) Jori, G. *J. Photochem. Photobiol., B* **1996**, *36*, 87.
- (133) Berg, K.; Selbo, P. K.; Weyergang, A.; Dietze, A.; Prasmickaite, L.; Bonsted, A.; Engesaeter, B. O.; Angell-Petersen, E.; Warloe, T.; Frandsen, N.; Hogset, A. *J. Microsc.* **2005**, *218*, 133.
- (134) Pandey, R. K.; James, N.; Chen, Y.; Dobhal, M. P. *Top. Heterocycl. Chem.* **2008**, *14*, 41.
- (135) Yaghini, E.; Seifalian, A. M.; MacRobert, A. J. *Nanomedicine* **2009**, *4*, 353.
- (136) Sun, Y.; Chen, Z. L.; Yang, X. X.; Huang, P.; Zhou, X. P.; Du, X. X. *Nanotechnology* **2009**, *20*, 135102.
- (137) Verma, S.; Watt, G. M.; Mai, Z.; Hasan, T. *Photochem. Photobiol.* **2007**, *83*, 996.
- (138) Stefflova, K.; Chen, J.; Zheng, G. *Front Biosci.* **2007**, *12*, 4709.
- (139) Chang, S. K.; Errabelli, D.; Rizvi, I.; Solban, N.; O'Riordan, K.; Hasan, T. *Proc. SPIE—Int. Soc. Opt. Eng.* **2006**, *6097*, 609701.
- (140) Savellano, M. D.; Hasan, T. *Clin. Cancer Res.* **2005**, *11*, 1658.
- (141) Kuimova, M. K.; Bhatti, M.; Deonarain, M.; Yahioglu, G.; Levitt, J. A.; Stamatii, I.; Suhling, K.; Phillips, D. *Photochem. Photobiol. Sci.* **2007**, *6*, 933.
- (142) Choi, Y.; McCarthy, J. R.; Weissleder, R.; Tung, C. H. *ChemMedChem* **2006**, *1*, 458.
- (143) Stefflova, K.; Li, H.; Chen, J.; Zheng, G. *Bioconjugate Chem.* **2007**, *18*, 379.
- (144) Stefflova, K.; Chen, J.; Zheng, G. *Curr. Med. Chem.* **2007**, *14*, 2110.
- (145) Hamblin, M. R.; Miller, J. L.; Ortel, B. *Photochem. Photobiol.* **2000**, *72*, 533.
- (146) Tawakol, A.; Castano, A. P.; Gad, F.; Zahra, T.; Bashian, G.; Migrino, R. Q.; Ahmadi, A.; Stern, J.; Anatelli, F.; Chirico, S.; Shirazi, A.; Syed, S.; Fischman, A. J.; Muller, J. E.; Hamblin, M. R. *Photochem. Photobiol. Sci.* **2008**, *7*, 33.
- (147) Chang, S. K.; Rizvi, I.; Solban, N.; Hasan, T. *Clin. Cancer Res.* **2008**, *14*, 4146.
- (148) *Handbook of Biological Confocal Microscopy*, 3rd ed.; Springer Science: New York, 2006.
- (149) Lakowicz, J. R. *Principles of Fluorescence Spectroscopy*, 3rd ed.; Springer: New York, 2006.
- (150) Valeur, B. *Molecular Fluorescence*; Wiley-VCH: New York, 2002.
- (151) Weissleder, R.; Tung, C. H.; Mahmood, U.; Bogdanov, A., Jr. *Nat. Biotechnol.* **1999**, *17*, 375.
- (152) Choi, Y.; Weissleder, R.; Tung, C. H. *Cancer Res.* **2006**, *66*, 7225.
- (153) Lovell, J. F.; Chen, J.; Jarvi, M. T.; Cao, W. G.; Allen, A. D.; Liu, Y.; Tidwell, T. T.; Wilson, B. C.; Zheng, G. *J. Phys. Chem. B* **2009**, *113*, 3203.
- (154) Zheng, G.; Chen, J.; Stefflova, K.; Jarvi, M.; Li, H.; Wilson, B. C. *Proc. Natl. Acad. Sci. U.S.A.* **2007**, *104*, 8989.
- (155) Li, G.; Slansky, A.; Dobhal, M. P.; Goswami, L. N.; Graham, A.; Chen, Y.; Kanter, P.; Alberico, R. A.; Sperryak, J.; Morgan, J.; Mazurchuk, R.; Oseroff, A.; Grossman, Z.; Pandey, R. K.; Li, G.; Slansky, A.; Dobhal, M. P.; Goswami, L. N.; Graham, A.; Chen, Y.; Kanter, P.; Alberico, R. A.; Sperryak, J.; Morgan, J.; Mazurchuk, R.; Oseroff, A.; Grossman, Z.; Pandey, R. K. *Bioconjugate Chem.* **2005**, *16*, 32.
- (156) Weigel, T. L.; Yousem, S.; Dacic, S.; Kosco, P. J.; Siegfried, J.; Luketich, J. D. *Ann. Surg. Oncol.* **2000**, *7*, 176.
- (157) Zargi, M.; Fajdiga, I.; Smid, L. *Eur. Arch. Oto-Rhino-Laryngol.* **2000**, *257*, 17.
- (158) Zellweger, M.; Goujon, D.; Conde, R.; Forrer, M.; van den Bergh, H.; Wagnieres, G. *Appl. Opt.* **2001**, *40*, 3784.
- (159) Sibille, A.; Lambert, R.; Souquet, J.-C.; Sabben, G.; Descos, F. *Gastroenterology* **1995**, *108*, 337.
- (160) Miyazu, Y.; Miyazawa, T.; Kurimoto, N.; Iwamoto, Y.; Kanoh, K.; Kohno, N. *Am. J. Respir. Crit. Care Med.* **2002**, *165*, 832.
- (161) Haringsma, J.; Tytgat, G. N.; Yano, H.; Iishi, H.; Tatsuta, M.; Ogiwara, T.; Watanabe, H.; Sato, N.; Marcon, N.; Wilson, B. C.; Cline, R. W. *Gastrointest. Endosc.* **2001**, *53*, 642.
- (162) Dacosta, R. S.; Wilson, B. C.; Marcon, N. E. *J. Gastroenterol. Hepatol.* **2002**, *17* (Suppl.), S85.
- (163) Treatment of Age-Related Macular Degeneration with Photodynamic Therapy (TAP) Study Group. *Arch. Ophthalmol.* **1999**, *117*, 1329.
- (164) Treatment of Age-Related Macular Degeneration with Photodynamic Therapy (TAP) Study Group. *Arch. Ophthalmol.* **2001**, *119*, 198.
- (165) Arnold, J.; Kilmartin, D.; Olson, J.; Neville, S.; Robinson, K.; Laird, A.; Richmond, C.; Farrow, A.; McKay, S.; Saperstein, D. A.; Aaberg, T. M.; Johnson, J. B.; Waldron, R.; Loupe, D.; Gillman, J.; Myles, B.; Schachat, A. P.; Bressler, N. M.; Bressler, S. B.; Nesbitt, P.; Porter, T.; Hawse, P.; Hartnett, M.; Eager, A.; Belt, J.; Cain, D.; Emmert, D.; George, T.; Herring, M.; McDonald, J.; Mones, J.; Corcostegui, B.; Gilbert, M.; Duran, N.; Sisquella, M.; Nolla, A.; Margalef, A.; Miller, J. W.; Gragoudas, E. S.; Lane, A. M.; Emmanuel, N.; Holbrook, A.; Evans, C.; Lord, U. S.; Walsh, D. K.; Callahan, C. D.; DuBois, J. L.; Lewis, H.; Kaiser, P. K.; Holody, L. J.; Lesak, E.; Lichterman, S.; Siegel, H.; Fattori, A.; Ambrose, G.; Fecko, T.; Ross, D.; Burke, S.; Singerman, L.; Zegarra, H.; Novak, M.; Bartel, M.; Tilocco-DuBois, K.; Ilic, M.; Schura, S.; Mayes, S. J.; Tanner, V.; Rowe, P.; Smith-Brewer, S.; Kukula, D.; Greanoff, G.; Daley, G.; DuBois, J.; Lehnhardt, D.; Fish, G. E.; Jost, B. F.; Anand, R.; Callanan, D.; Arceneaux, S.; Arnwine, J.; Ellenich, P.; King, J.; Aguado, H.; Rollins, R.; Jurklics, B.; Pauleikhoff, D.; Hintzmann, A.; Fischer, M.; Sowar, C.; Behne, E.; Pournaras, C. J.; Donati, G.; Kapetanios, A. D.; Cavaliere, K.; Guney-Wagner, S.; Gerber, N.; Sickenberg, M.; Sickenberg, V.; Gans, A.; Hosner, B. *Ophthalmology* **2001**, *108*, 841.
- (166) Barbazetto, I.; Burdan, A.; Bressler, N. M.; Bressler, S. B.; Haynes, L.; Kapetanios, A. D.; Lukas, J.; Olsen, K.; Potter, M.; Reaves, A.; Rosenfeld, P.; Schachat, A. P.; Strong, H. A.; Wenkstern, A.; Burdan, M.; Reaves, D. *Arch. Ophthalmol.* **2003**, *121*, 1253.
- (167) Schmidt-Erfurth, U.; Miller, J.; Sickenberg, M.; Bunse, A.; Laqua, H.; Gragoudas, E.; Zografos, L.; Birngruber, R.; van den Bergh, H.; Strong, A.; Manjuris, U.; Fsadni, M.; Lane, A. M.; Piguet, B.; Bressler, N. M. *Graefes Arch. Clin. Exp. Ophthalmol.* **1998**, *236*, 365.
- (168) Schmidt-Erfurth, U.; Miller, J. W.; Sickenberg, M.; Laqua, H.; Barbazetto, I.; Gragoudas, E. S.; Zografos, L.; Piguet, B.; Pournaras, C. J.; Donati, G.; Lane, A.-M.; Birngruber, R.; van den Berg, H.; Strong, H. A.; Manjuris, U.; Gray, T.; Fsadni, M.; Bressler, N. M. *Arch. Ophthalmol.* **1999**, *117*, 1177.
- (169) Schmidt-Erfurth, U. M.; Michels, S.; Kusserow, C.; Jurklics, B.; Augustin, A. J. *Ophthalmology* **2002**, *109*, 2284.
- (170) Harding, S. *Eye* **2001**, *15*, 407.
- (171) Bown, S. G.; Rogowska, A. Z.; Whitelaw, D. E.; Lees, W. R.; Lovat, L. B.; Ripley, P.; Jones, L.; Wyld, P.; Gillams, A.; Hatfield, A. W. R. *Gut* **2002**, *50*, 549.
- (172) Jocham, D.; Baumgartner, R.; Stepp, H.; Unsold, E. J. *Photochem. Photobiol., B* **1990**, *6*, 183.
- (173) Jocham, D.; Beer, M.; Baumgartner, R.; Staehler, G.; Unsold, E. *Ciba Found. Symp.* **1989**, *146*, 198.
- (174) Ono, R.; Ikeda, S.; Suemasu, K. *Cancer* **1992**, *69*, 1696.
- (175) Powers, S. K.; Cush, S. S.; Walstad, D. L.; Kwock, L. *Neurosurgery* **1991**, *29*, 688.
- (176) Chan, H. H.; Nishioka, N. S.; Mino, M.; Lauwers, G. Y.; Puricelli, W. P.; Collier, K. N.; Brugge, W. R. *Gastrointest. Endosc.* **2004**, *59*, 95.
- (177) Cubeddu, R.; Canti, G.; Taroni, P.; Valentini, G. *Lasers Med. Sci.* **1997**, *12*, 200.
- (178) Cubeddu, R.; Pifferi, A.; Taroni, P.; Torricelli, A.; Valentini, G.; Comelli, D.; D'Andrea, C.; Angelini, V.; Canti, G. *Photochem. Photobiol.* **2000**, *72*, 690.
- (179) Berard, V.; Rousseau, J. A.; Cadorette, J.; Hubert, L.; Bentourkia, M. h.; van Lier, J. E.; Lecomte, R. *J. Nucl. Med.* **2006**, *47*, 1119.
- (180) Lapointe, D.; Brasseur, N.; Cadorette, J.; La Madeleine, C.; Rodrigue, S.; van Lier, J. E.; Lecomte, R. *J. Nucl. Med.* **1999**, *40*, 876.
- (181) Kruijt, B.; de Bruijn, H. S.; van der Ploeg-van den Heuvel, A.; Sterenberg, H. J. C. M.; Robinson, D. J. *Lasers Med. Sci.* **2006**, *21*, 208.
- (182) Chen, Z.; Milner, T. E.; Wang, X.; Srinivas, S.; Nelson, J. S. *Photochem. Photobiol.* **1998**, *67*, 56.
- (183) Mariampillai, A.; Standish, B. A.; Moriyama, E. H.; Khurana, M.; Munce, N. R.; Leung, M. K. K.; Jiang, J.; Cable, A.; Wilson, B. C.; Vitkin, I. A.; Yang, V. X. D. *Opt. Lett.* **2008**, *33*, 1530.
- (184) Standish, B. A.; Jin, X.; Smolen, J.; Mariampillai, A.; Munce, N. R.; Wilson, B. C.; Vitkin, I. A.; Yang, V. X. D. *J. Biomed. Opt.* **2007**, *12*, 034022.
- (185) Standish, B. A.; Yang, V. X. D.; Munce, N. R.; Song, L.; Gardiner, G.; Lin, A.; Mao, Y. I.; Vitkin, A.; Marcon, N. E.; Wilson, B. C. *Gastrointest. Endosc.* **2007**, *66*, 326.
- (186) Yu, G. Q.; Durduran, T.; Zhou, C.; Wang, H. W.; Putt, M. E.; Saunders, H. M.; Sehgal, C. M.; Glatstein, E.; Yodh, A. G.; Busch, T. M. *Clin. Cancer Res.* **2005**, *11*, 3543.
- (187) Mason, C.; Markusen, J. F.; Town, M. A.; Dunnill, P.; Wang, R. K. *Biosens. Bioelectron.* **2004**, *20*, 414.
- (188) Major, A.; Kimel, S.; Mee, S.; Milner, T.; Smithies, D.; Srinivas, S.; Chen, Z.; Nelson, J. *IEEE J. Sel. Top. Quantum Electron.* **1999**, *5*, 1168.
- (189) Khurana, M.; Moriyama, E. H.; Mariampillai, A.; Wilson, B. C. *J. Biomed. Opt.* **2008**, *13*, 040502.
- (190) Moore, J. V.; Waller, M. L.; Zhao, S.; Dodd, N. J.; Acton, P. D.; Jeavons, A. P.; Hastings, D. L. *Eur. J. Nucl. Med.* **1998**, *25*, 1248.
- (191) Haider, M. A.; Davidson, S. R. H.; Kale, A. V.; Weersink, R. A.; Evans, A. J.; Toi, A.; Gertner, M. R.; Bogaards, A.; Wilson, B. C.; Chin, J. L.; Elhilali, M.; Trachtenberg, J. *Radiology* **2007**, *244*, 196.
- (192) Huang, Z.; Haider, M. A.; Kraft, S.; Chen, Q.; Blanc, D.; Wilson, B. C.; Hetzel, F. W. *Lasers Surg. Med.* **2006**, *38*, 672.
- (193) Trachtenberg, J.; Bogaards, A.; Weersink, R. A.; Haider, M. A.; Evans, A.; McCluskey, S. A.; Scherz, A.; Gertner, M. R.; Yue, C.;

- Appu, S.; Aprikian, A.; Savard, J.; Wilson, B. C.; Elhilali, M. J. *J. Urol.* **2007**, *178*, 1974.
- (194) Zilberstein, J.; Schreiber, S.; Bloemers, M. C.; Bendel, P.; Neeman, M.; Schechtman, E.; Kohen, F.; Scherz, A.; Salomon, Y. *Photochem. Photobiol.* **2001**, *73*, 257.
- (195) Samkoe, K. S.; Chen, A.; Rizvi, I.; O'Hara, J. A.; Hoopes, P. J.; Hasan, T.; Pogue, B. W. *Proc. SPIE—Int. Soc. Opt. Eng.* **2009**, *7164*, 71640D.
- (196) Fei, B.; Wang, H.; Meyers, J. D.; Feyes, D. K.; Oleinick, N. L.; Duerk, J. L. *Lasers Surg. Med.* **2007**, *39*, 723.
- (197) Jiang, Q.; Knight, R. A.; Chopp, M.; Helpert, J. A.; Ordidge, R. J.; Qing, Z. X.; Hetzel, F. W. *Neurosurgery* **1991**, *29*, 538.
- (198) Winsborrow, B. G.; Grondy, H.; Savoie, H.; Fyfe, C. A.; Dolphin, D. *Photochem. Photobiol.* **1997**, *66*, 847.
- (199) Dodd, N. J.; Moore, J. V.; Poppitt, D. G.; Wood, B. *Br. J. Cancer* **1989**, *60*, 164.
- (200) Liu, Y. H.; Hawk, R. M.; Ramaprasad, S. *Magn. Reson. Imaging* **1995**, *13*, 251.
- (201) Samkoe, K. S.; Davis, S. C.; Srinivasan, S.; O'Hara, J. A.; Hasan, T.; Pogue, B. W. *Proc. SPIE—Int. Soc. Opt. Eng.* **2009**, *7380*, 73803M.
- (202) Enejder, A. M.; af Klinteberg, C.; Wang, I.; Andersson-Engels, S.; Bendsoe, N.; Svanberg, S.; Svanberg, K. *Acta Derm.-Venereol.* **2000**, *80*, 19.
- (203) Wang, I.; Andersson-Engels, S.; Nilsson, G. E.; Wardell, K.; Svanberg, K. *Br. J. Dermatol.* **1997**, *136*, 184.
- (204) Hart, L.; Gonzalez, V. H.; Gragoudas, E. S.; Young, L. H. Y. *Invest. Ophthalmol. Visual Sci.* **1993**, *34*, 967.
- (205) Liu, D. L.; Svanberg, K.; Wang, I.; Andersson-Engels, S.; Svanberg, S. *Lasers Surg. Med.* **1997**, *20*, 473.
- (206) Wieman, T. J.; Mang, T. S.; Fingar, V. H.; Hill, T. G.; Reed, M. W.; Corey, T. S.; Nguyen, V. Q.; Render, E. R., Jr. *Surgery* **1988**, *104*, 512.
- (207) Channual, J.; Choi, B.; Osann, K.; Pattanachinda, D.; Lotfi, J.; Kelly, K. M. *Lasers Surg. Med.* **2008**, *40*, 644.
- (208) Smith, T. K.; Choi, B.; Ramirez-San-Juan, J. C.; Nelson, J. S.; Osann, K.; Kelly, K. M. *Lasers Surg. Med.* **2006**, *38*, 532.
- (209) Blumenkranz, M. S.; Woodburn, K. W.; Qing, F.; Verdooner, S.; Kessel, D.; Miller, R. *Am. J. Ophthalmol.* **2000**, *129*, 353.
- (210) Rogers, A. H.; Martidis, A.; Greenberg, P. B.; Puliafito, C. A. *Am. J. Ophthalmol.* **2002**, *134*, 566.
- (211) Aveline, B. M.; Redmond, R. W. *Photochem. Photobiol.* **1999**, *69*, 306.
- (212) Woodhams, J. H.; Macrobert, A. J.; Bown, S. G. *Photochem. Photobiol. Sci.* **2007**, *6*, 1246.
- (213) Wilson, B. C.; Patterson, M. S. *Phys. Med. Biol.* **2008**, *53*, R61.
- (214) Grossweiner, L. I. *Prog. Clin. Biol. Res.* **1984**, *170*, 391.
- (215) van Lier, J. E.; Spikes, J. D. *Ciba Found. Symp.* **1989**, *146*, 17.
- (216) Schmidt, R. *Photochem. Photobiol.* **2006**, *82*, 1161.
- (217) Patterson, M. S.; Madsen, S. J.; Wilson, B. C. *J. Photochem. Photobiol., B* **1990**, *5*, 69.
- (218) Weishaupt, K. R.; Gomer, C. J.; Dougherty, T. J. *Cancer Res.* **1976**, *36*, 2326.
- (219) Reed, M. W.; Mullins, A. P.; Anderson, G. L.; Miller, F. N.; Wieman, T. J. *Surgery* **1989**, *106*, 94.
- (220) Tromberg, B. J.; Orenstein, A.; Kimel, S.; Barker, S. J.; Hyatt, J.; Nelson, J. S.; Berns, M. W. *Photochem. Photobiol.* **1990**, *52*, 375.
- (221) Nichols, M. G.; Foster, T. H. *Phys. Med. Biol.* **1994**, *39*, 2161.
- (222) Foster, T. H.; Murant, R. S.; Bryant, R. G.; Knox, R. S.; Gibson, S. L.; Hilf, R. *Radiat. Res.* **1991**, *126*, 296.
- (223) Foster, T. H.; Gao, L. *Radiat. Res.* **1992**, *130*, 379.
- (224) Chen, Q.; Huang, Z.; Chen, H.; Shapiro, H.; Beckers, J.; Hetzel, F. W. *Photochem. Photobiol.* **2002**, *76*, 197.
- (225) Vaupel, P.; Mayer, A.; Briest, S.; Hockel, M. *Adv. Exp. Med. Biol.* **2005**, *566*, 333.
- (226) Foster, T. H.; Hartley, D. F.; Nichols, M. G.; Hilf, R. *Cancer Res.* **1993**, *53*, 1249.
- (227) Georgakoudi, I.; Nichols, M. G.; Foster, T. H. *Photochem. Photobiol.* **1997**, *65*, 135.
- (228) Mitra, S.; Foster, T. H. *Biophys. J.* **2000**, *78*, 2597.
- (229) Finlay, J. C.; Mitra, S.; Foster, T. H. *Photochem. Photobiol.* **2002**, *75*, 282.
- (230) Busch, T. M.; Wileyto, E. P.; Emanuele, M. J.; Del Piero, F.; Marconato, L.; Glatstein, E.; Koch, C. J. *Cancer Res.* **2002**, *62*, 7273.
- (231) Pogue, B. W.; Braun, R. D.; Lanzen, J. L.; Erickson, C.; Dewhirst, M. W. *Photochem. Photobiol.* **2001**, *74*, 700.
- (232) Yu, G.; Durduran, T.; Zhou, C.; Wang, H. W.; Putt, M. E.; Saunders, H. M.; Sehgal, C. M.; Glatstein, E.; Yodh, A. G.; Busch, T. M. *Clin. Cancer Res.* **2005**, *11*, 3543.
- (233) Henderson, B. W.; Busch, T. M.; Snyder, J. W. *Lasers Surg. Med.* **2006**, *38*, 489.
- (234) Busch, T. M. *Lasers Surg. Med.* **2006**, *38*, 494.
- (235) Wang, H. W.; Putt, M. E.; Emanuele, M. J.; Shin, D. B.; Glatstein, E.; Yodh, A. G.; Busch, T. M. *Cancer Res.* **2004**, *64*, 7553.
- (236) Schouwink, H.; Oppelaar, H.; Ruevekamp, M.; van der Valk, M.; Hart, G.; Rijken, P.; Baas, P.; Stewart, F. A. *Radiat. Res.* **2003**, *159*, 190.
- (237) Niedre, M.; Patterson, M. S.; Wilson, B. C. *Photochem. Photobiol.* **2002**, *75*, 382.
- (238) Wei, Y.; Xing, D.; Luo, S.; Xu, W.; Chen, Q. *J. Biomed. Opt.* **2008**, *13*, 024023.
- (239) Lee, S.; Zhu, L.; Minhaj, A. M.; Hinds, M. F.; Vu, D. H.; Rosen, D. I.; Davis, S. J.; Hasan, T. *J. Biomed. Opt.* **2008**, *13*, 034010.
- (240) Laubach, H.; Chang, S.; Lee, S.; Rizvi, I.; Zurakowski, D.; Davis, S.; Taylor, C.; Hasan, T. *J. Biomed. Opt.* **2008**, *13*, 050504.
- (241) Niedre, M. J.; Yu, C. S.; Patterson, M. S.; Wilson, B. C. *Br. J. Cancer* **2005**, *92*, 298.
- (242) Niedre, M. J.; Secord, A. J.; Patterson, M. S.; Wilson, B. C. *Cancer Res.* **2003**, *63*, 7986.
- (243) Sitnik, T. M.; Hampton, J. A.; Henderson, B. W. *Br. J. Cancer* **1998**, *77*, 1386.
- (244) Henderson, B. W.; Sitnik-Busch, T. M.; Vaughan, L. A. *Photochem. Photobiol.* **1999**, *70*, 64.
- (245) Robinson, D. J.; de Bruijn, H. S.; van der Veen, N.; Stringer, M. R.; Brown, S. B.; Star, W. M. *Photochem. Photobiol.* **1998**, *67*, 140.
- (246) Kruijt, B.; de Bruijn, H. S.; van der Ploeg-van den Heuvel, A.; de Bruin, R. W.; Sterenborg, H. J.; Amelink, A.; Robinson, D. J. *Photochem. Photobiol.* **2008**, *84*, 1515.
- (247) Seshadri, M.; Bellnier, D. A.; Vaughan, L. A.; Sperry, J. A.; Mazurchuk, R.; Foster, T. H.; Henderson, B. W. *Clin. Cancer Res.* **2008**, *14*, 2796.
- (248) Pogue, B. W.; Hasan, T. *Radiat. Res.* **1997**, *147*, 551.
- (249) Yuan, J.; Mahama-Relue, P. A.; Fournier, R. L.; Hampton, J. A. *Radiat. Res.* **1997**, *148*, 386.
- (250) Curnow, A.; Haller, J. C.; Bown, S. G. *J. Photochem. Photobiol., B* **2000**, *58*, 149.
- (251) Sterenborg, H.; de Wolf, J.; Koning, M.; Kruijt, B.; van den Heuvel, A.; Robinson, D. *Opt. Express* **2004**, *12*, 1873.
- (252) Sheng, C.; Hoopes, P. J.; Hasan, T.; Pogue, B. W. *Photochem. Photobiol.* **2007**, *83*, 738.
- (253) Bisland, S. K.; Lilge, L.; Lin, A.; Rusnov, R.; Wilson, B. C. *Photochem. Photobiol.* **2004**, *80*, 22.
- (254) Henderson, B. W.; Waldow, S. M.; Mang, T. S.; Potter, W. R.; Malone, P. B.; Dougherty, T. J. *Cancer Res.* **1985**, *45*, 572.
- (255) Fabre, M. A.; Fuseau, E.; FICHEUX, H. *J. Pharm. Sci.* **2007**, *96*, 3444.
- (256) Chen, B.; Pogue, B. W.; Hoopes, P. J.; Hasan, T. *Int. J. Radiat. Oncol. Biol. Phys.* **2005**, *61*, 1216.
- (257) Chen, B.; Pogue, B. W.; Hoopes, P. J.; Hasan, T. *Crit. Rev. Eukaryotic Gene Expression* **2006**, *16*, 279.
- (258) Chen, B.; Pogue, B. W.; Luna, J. M.; Hardman, R. L.; Hoopes, P. J.; Hasan, T. *Clin. Cancer Res.* **2006**, *12*, 917.
- (259) Huang, D.; Swanson, E. A.; Lin, C. P.; Schuman, J. S.; Stinson, W. G.; Chang, W.; Hee, M. R.; Flotte, T.; Gregory, K.; Puliafito, C. A. *Science* **1991**, *254*, 1178.
- (260) Tearney, G. J.; Brezinski, M. E.; Bouma, B. E.; Boppart, S. A.; Pitris, C.; Southern, J. F.; Fujimoto, J. G. *Science* **1997**, *276*, 2037.
- (261) Fercher, A. F.; Hitzinger, C. K.; Kamp, G.; El-Zaiat, S. Y. *Opt. Commun.* **1995**, *117*, 43.
- (262) Häusler, G.; Lindner, M. W. *J. Biomed. Opt.* **1998**, *3*, 21.
- (263) Wojtkowski, M.; Leitgeb, R.; Kowalczyk, A.; Fercher, A. F. *Proc. SPIE—Int. Soc. Opt. Eng.* **2002**, *4619*, 230.
- (264) de Boer, J. F.; Cense, B.; Park, B. H.; Pierce, M. C.; Tearney, G. J.; Bouma, B. E. *Opt. Lett.* **2003**, *28*, 2067.
- (265) Vakoc, B.; Yun, S.; de Boer, J.; Tearney, G.; Bouma, B. *Opt. Express* **2005**, *13*, 5483.
- (266) De Bruin, D.; Burnes, D.; Loewenstein, J.; Chen, Y.; Chang, S.; Chen, T.; Esmaili, D.; De Boer, J. *Invest. Ophthalmol. Visual Sci.* **2008**, *49*, 4545.
- (267) Lee, E. C.; de Boer, J. F.; Mujat, M.; Lim, H.; Yun, S. H. *Opt. Express* **2006**, *14*, 4403.
- (268) Huber, R.; Wojtkowski, M.; Fujimoto, J. G. *Opt. Express* **2006**, *14*, 3225.
- (269) Jang, I. K.; Bouma, B. E.; Kang, D. H.; Park, S. J.; Park, S. W.; Seung, K. B.; Choi, K. B.; Shishkov, M.; Schlendorf, K.; Pomerantsev, E. *J. Am. Coll. Cardiol.* **2002**, *39*, 604.
- (270) Poneros, J. M.; Brand, S.; Bouma, B. E.; Tearney, G. J.; Compton, C. C.; Nishioka, N. S. *Gastroenterology* **2001**, *120*, 7.
- (271) Bouma, B. E.; Tearney, G. J.; Compton, C. C.; Nishioka, N. S. *Gastrointest. Endosc.* **1999**, *49*.
- (272) De Boer, J.; Srinivas, S.; Malekafzali, A.; Chen, Z. P.; Nelson, J. *Opt. Express* **1998**, *3*, 212.
- (273) Park, B. H.; Saxer, C.; Srinivas, S. M.; Nelson, J. S.; de Boer, J. F. *J. Biomed. Opt.* **2001**, *6*, 474.
- (274) Fujimoto, J. G. *Nat. Biotechnol.* **2003**, *21*, 1361.

- (275) Nassif, N.; Cense, B.; Park, B.; Pierce, M.; Yun, S.; Bouma, B.; Tearney, G.; Chen, T.; de Boer, J. *Opt. Express* **2004**, *12*, 367.
- (276) Cense, B.; Nassif, N.; Chen, T.; Pierce, M.; Yun, S. H.; Park, B.; Bouma, B.; Tearney, G.; de Boer, J. *Opt. Express* **2004**, *12*, 2435.
- (277) Oldenburg, A. L.; Gunther, J. R.; Boppart, S. A. *Opt. Lett.* **2005**, *30*, 747.
- (278) Xu, C.; Vinegoni, C.; Ralston, T. S.; Luo, W.; Tan, W.; Boppart, S. A. *Opt. Lett.* **2006**, *31*, 1079.
- (279) Wolfensberger, T.; Gonvers, M. *Graefes Arch. Clin. Exp. Ophthalmol.* **2002**, *240*, 85.
- (280) Costello, F.; Hodge, W.; Pan, Y. I.; Freedman, M.; DeMeulemeester, C. *J. Neurol. Sci.* **2009**, *281*, 74.
- (281) Jaffe, G.; Caprioli, J. *Am. J. Ophthalmol.* **2004**, *137*, 156.
- (282) Ozdemir, H.; Karacorlu, S. A.; Karacorlu, M. *Am. J. Ophthalmol.* **2006**, *141*, 574.
- (283) Fukuchi, T.; Takahashi, K.; Shou, K. *Graefes Arch. Clin. Exp. Ophthalmol.* **2001**, *239*, 41.
- (284) Fukuchi, T.; Takahashi, K.; Ida, H.; Sho, K.; Matsumura, M. *Graefes Arch. Clin. Exp. Ophthalmol.* **2001**, *239*, 424.
- (285) Salinas-Alamán, A.; García-Layana, A.; Maldonado, M.; Sainz-Gómez, C.; Álvarez-Vidal, A. *Am. J. Ophthalmol.* **2005**, *140*, 23.
- (286) Sahni, J.; Stanga, P.; Wong, D.; Harding, S. *Br. J. Ophthalmol.* **2005**, *89*, 316.
- (287) Krebs, I.; Binder, S.; Stolba, U.; Schmid, K.; Glittenberg, C.; Brannath, W.; Goll, A. *Br. J. Ophthalmol.* **2005**, *89*, 1184.
- (288) Lai, T.; Chan, W.; Li, H.; Lai, R.; Liu, D.; Lam, D. *Br. J. Ophthalmol.* **2006**, *90*, 869.
- (289) Yu, G.; Durduran, T.; Zhou, C.; Zhu, T.; Finlay, J.; Busch, T.; Malkowicz, S. B.; Hahn, S.; Yodh, A. *Photochem. Photobiol.* **2006**, *82*, 1279.
- (290) Wang, H.; Putt, M.; Emanuele, M.; Shin, D.; Glatstein, E.; Yodh, A.; Busch, T. *Cancer Res.* **2004**, *64*, 7553.
- (291) Pogue, B. W.; O'Hara, J. A.; Demidenko, E.; Wilmot, C. M.; Goodwin, I. A.; Chen, B.; Swartz, H. M.; Hasan, T. *Cancer Res.* **2003**, *63*, 1025.
- (292) Izatt, J. A.; Kulkarni, M. D.; Yazdanfar, S.; Barton, J. K.; Welch, A. J. *Opt. Lett.* **1997**, *22*, 1439.
- (293) Chen, Z.; Milner, T.; Srinivas, S.; Wang, X.; Malekafzali, A.; van Gemert, M.; Nelson, J. *Opt. Lett.* **1997**, *22*, 1119.
- (294) Li, H.; Standish, B.; Mariampillai, A.; Munce, N.; Mao, Y.; Chiu, S.; Marcon, N.; Wilson, B. C.; Vitkin, A.; Yang, V. *Lasers Surg. Med.* **2006**, *38*, 754.
- (295) Mueller-Klieser, W. *Am. J. Physiol.* **1997**, *273*, C1109.
- (296) Kim, J. B. *Semin. Cancer Biol.* **2005**, *15*, 365.
- (297) Debnath, J.; Brugge, J. S. *Nat. Rev. Cancer* **2005**, *5*, 675.
- (298) Nelson, C. M.; Bissell, M. J. *Annu. Rev. Cell Dev. Biol.* **2006**, *22*, 287.
- (299) Smalley, K. S. M.; Lioni, M.; Herlyn, M. *In Vitro Cell. Dev. Biol.: Anim.* **2006**, *42*, 242.
- (300) Lee, G. Y.; Kenny, P. A.; Lee, E. H.; Bissell, M. J. *Nat. Methods* **2007**, *4*, 359.
- (301) Evans, C. L.; Rizvi, I.; Celli, J.; Abu-Yousif, A.; De Boer, J.; Hasan, T. *Proc. SPIE—Int. Soc. Opt. Eng.* **2010**, *7551*, 75510J.
- (302) Massoud, T.; Gambhir, S. *Genes Dev.* **2003**, *17*, 545.
- (303) Weissleder, R. *Science* **2006**, *312*, 1168.
- (304) Jain, R.; Munn, L. *Nat. Rev. Cancer* **2002**, *2*, 266.
- (305) Flusberg, B.; Cocker, E.; Piyawattanametha, W.; Jung, J.; Cheung, E.; Schnitzer, M. *Nat. Methods* **2005**, *2*, 941.
- (306) Gmitro, A.; Aziz, D. *Opt. Lett.* **1993**, *18*, 565.
- (307) Laemmel, E.; Genet, M.; Le Goualher, G.; Perchant, A.; Le Gargasson, J. F.; Vicaut, E. *J. Vasc. Res.* **2004**, *41*, 400.
- (308) MacAulay, C.; Lane, P.; Richards-Kortum, R. *Gastrointest. Endosc. Clin. N. Am.* **2004**, *14*, 595.
- (309) Mansfield, J.; Gossage, K.; Hoyt, C.; Levenson, R. *J. Biomed. Opt.* **2005**, *10*, 041207.
- (310) Zimmermann, T.; Rietdorf, J.; Pepperkok, R. *FEBS Lett.* **2003**, *546*, 87.
- (311) Bloch, S.; Lesage, F.; McIntosh, L.; Gandjbakhche, A.; Liang, K.; Achilefu, S. *J. Biomed. Opt.* **2005**, *10*, 054003.
- (312) Nothdurft, R.; Patwardhan, S.; Akers, W.; Ye, Y.; Achilefu, S.; Culver, J. *J. Biomed. Opt.* **2009**, *14*, 024004.
- (313) Skala, M. C.; Riching, K. M.; Gendron-Fitzpatrick, A.; Eickhoff, J. C.; Eliceiri, K. W.; White, J. G.; Ramanujam, N. *Proc. Natl. Acad. Sci. U.S.A.* **2007**, *104*, 19494.
- (314) Provenzano, P.; Eliceiri, K.; Keely, P. *Clin. Exp. Metastasis* **2009**, *26*, 357.
- (315) Provenzano, P.; Rueden, C.; Trier, S.; Yan, L.; Ponik, S.; Inman, D.; Keely, P.; Eliceiri, K. *J. Biomed. Opt.* **2008**, *13*, 031220.
- (316) Corlu, A.; Choe, R.; Durduran, T.; Rosen, M. A.; Schweiger, M.; Arridge, S. R.; Schnall, M. D.; Yodh, A. G. *Opt. Express* **2007**, *15*, 6696.
- (317) Koenig, A.; Hervé, L.; Josserand, V.; Berger, M.; Boutet, J.; Da Silva, A.; Dinten, J.; Peltié, P.; Coll, J.; Rizo, P. *J. Biomed. Opt.* **2008**, *13*, 011008.
- (318) Deliolanis, N.; Dunham, J.; Wurdinger, T.; Figueiredo, J.; Bakhos, T.; Ntziachristos, V. *J. Biomed. Opt.* **2009**, *14*, 030509.
- (319) Niedre, M.; de Kleine, R.; Aikawa, E.; Kirsch, D.; Weissleder, R.; Ntziachristos, V. *Proc. Natl. Acad. Sci. U.S.A.* **2008**, *105*, 19126.
- (320) Cauchon, N.; Langlois, R.; Rousseau, J. A.; Tessier, G.; Cadorette, J.; Lecomte, R.; Hunting, D. J.; Pavan, R. A.; Zeisler, S. K.; van Lier, J. E. *Eur. J. Nucl. Med. Mol. Imaging* **2007**, *34*, 247.
- (321) Sugiyama, M.; Sakahara, H.; Sato, K.; Harada, N.; Fukumoto, D.; Kakiuchi, T.; Hirano, T.; Kohno, E.; Tsukada, H. *J. Nucl. Med.* **2004**, *45*, 1754.
- (322) Ferrario, A.; von Tiehl, K. F.; Rucker, N.; Schwarz, M. A.; Gill, P. S.; Gomer, C. J. *Cancer Res.* **2000**, *60*, 4066.
- (323) Ferrario, A.; von Tiehl, K.; Wong, S.; Luna, M.; Gomer, C. *Cancer Res.* **2002**, *62*, 3956.
- (324) Ferrario, A.; Chantrain, C. F.; von Tiehl, K.; Buckley, S.; Rucker, N.; Shalinsky, D. R.; Shimada, H.; DeClerck, Y. A.; Gomer, C. J. *Cancer Res.* **2004**, *64*, 2328.
- (325) Kosharsky, B.; Solban, N.; Chang, S. K.; Rizvi, I.; Chang, Y.; Hasan, T. *Cancer Res.* **2006**, *66*, 10953.
- (326) Agostinis, P.; Buytaert, E.; Breyssens, H.; Hendrickx, N. *Photochem. Photobiol. Sci.* **2004**, *3*, 721.
- (327) Almeida, R.; Manadas, B.; Carvalho, A.; Duarte, C. *BBA—Rev. Cancer* **2004**, *1704*, 59.
- (328) Castano, A.; Demidova, T.; Hamblin, M. *Photodiagn. Photodyn. Ther.* **2005**, *2*, 1.
- (329) Buytaert, E.; Dewaele, M.; Agostinis, P. *BBA—Rev. Cancer* **2007**, *1776*, 86.
- (330) Oleinick, N.; Morris, R.; Belichenko, I. *Photochem. Photobiol. Sci.* **2002**, *1*, 1.
- (331) Kerr, J.; Wyllie, A.; Currie, A. *Br. J. Cancer* **1972**, *26*, 239.
- (332) Hengartner, M. *Nature* **2000**, *407*, 770.
- (333) Ferri, K.; Kroemer, G. *Nat. Cell Biol.* **2001**, *3*, E255.
- (334) Danial, N.; Korsmeyer, S. *Cell* **2004**, *116*, 205.
- (335) Xue, L.; Chiu, S.; Oleinick, N. *Oncogene* **2001**, *20*, 3420.
- (336) Usuda, J.; Chiu, S.; Azizuddin, K.; Xue, L.; Lam, M.; Nieminen, A.; Oleinick, N. *Photochem. Photobiol.* **2002**, *76*, 217.
- (337) Wan, Q.; Liu, L.; Xing, D.; Chen, Q. *Photochem. Photobiol.* **2008**, *84*, 250.
- (338) Reiners, J., Jr.; Caruso, J.; Mathieu, P.; Chelladurai, B.; Yin, X.; Kessel, D. *Cell Death Differ.* **2002**, *9*, 934.
- (339) Boya, P.; Andreau, K.; Poncet, D.; Zamzami, N.; Perfettini, J.; Metivier, D.; Ojcius, D.; Jaattela, M.; Kroemer, G. *J. Exp. Med.* **2003**, *197*, 1323.
- (340) Houseweart, M.; Vilaythong, A.; Yin, X.; Turk, B.; Noebels, J.; Myers, R. *Cell Death Differ.* **2003**, *10*, 1329.
- (341) Onuki, R.; Nagasaki, A.; Kawasaki, H.; Baba, T.; Uyeda, T.; Taira, K. *Proc. Natl. Acad. Sci. U.S.A.* **2002**, *99*, 14716.
- (342) Pei, Y.; Xing, D.; Gao, X.; Liu, L.; Chen, T. *Apoptosis* **2007**, *12*, 1681.
- (343) Stefflova, K.; Chen, J.; Marotta, D.; Li, H.; Zheng, G. *J. Med. Chem.* **2006**, *49*, 3850.
- (344) Pelet, S.; Previte, M.; So, P. *J. Biomed. Opt.* **2006**, *11*, 034017.
- (345) Verwanger, T.; Sanovic, R.; Aberger, F.; Frischauf, A.; Krammer, B. *Int. J. Oncol.* **2002**, *21*, 1353.
- (346) Mitra, S.; Goren, E.; Frelinger, J.; Foster, T. *Photochem. Photobiol.* **2003**, *78*, 615.
- (347) Korbelik, M.; Sun, J.; Cecic, I. *Cancer Res.* **2005**, *65*, 1018.
- (348) Castano, A. P.; Mroz, P.; Hamblin, M. R. *Nat. Rev. Cancer* **2006**, *6*, 535.
- (349) Castano, A.; Mroz, P.; Wu, M.; Hamblin, M. *Proc. Natl. Acad. Sci. U.S.A.* **2008**, *105*, 5495.
- (350) Scherer, R.; McIntyre, J.; Matrisian, L. *Cancer Metastasis Rev.* **2008**, *27*, 679.
- (351) McKerrow, J.; Bhargava, V.; Hansell, E.; Huling, S.; Kuwahara, T.; Matley, M.; Coussens, L.; Warren, R. *Mol. Med.* **2000**, *6*, 450.
- (352) Ferrario, A.; Chantrain, C.; von Tiehl, K.; Buckley, S.; Rucker, N.; Shalinsky, D.; Shimada, H.; DeClerck, Y.; Gomer, C. *Cancer Res.* **2004**, *64*, 2328.
- (353) Zheng, Q.; Fei, X.; Liu, X.; Wang, J.; Bin Sun, H.; Mock, B.; Lee Stone, K.; Martinez, T.; Miller, K.; Sledge, G. *Nucl. Med. Biol.* **2002**, *29*, 761.
- (354) Fei, X.; Zheng, Q.; Liu, X.; Wang, J.; Sun, H.; Mock, B.; Stone, K.; Miller, K.; Sledge, G.; Hutchins, G. *Bioorg. Med. Chem. Lett.* **2003**, *13*, 2217.
- (355) McIntyre, J.; Fingleton, B.; Wells, K.; Piston, D.; Lynch, C.; Gautam, S.; Matrisian, L. *Biochem. J.* **2004**, *377*, 617.
- (356) Scherer, R.; Vansaun, M.; McIntyre, J.; Matrisian, L. *Mol. Imaging* **2008**, *7*, 118.
- (357) Bremer, C.; Tung, C.; Weissleder, R. *Nat. Med.* **2001**, *7*, 743.
- (358) Hicklin, D.; Ellis, L. *J. Clin. Oncol.* **2005**, *23*, 1011.

- (359) Gorski, D.; Beckett, M.; Jaskowiak, N.; Calvin, D.; Mauceri, H.; Salloum, R.; Seetharam, S.; Koons, A.; Hari, D.; Kufe, D. *Cancer Res.* **1999**, *59*, 3374.
- (360) Abdollahi, A.; Lipson, K.; Han, X.; Krempien, R.; Trinh, T.; Weber, K.; Hahnfeldt, P.; Hlatky, L.; Debus, J.; Howlett, A. *Cancer Res.* **2003**, *63*, 3755.
- (361) Justinger, C.; Schlüter, C.; Oliviera-Frick, V.; Kopp, B.; Rubie, C.; Schilling, M. *Oncol. Rep.* **2008**, *20*, 1527.
- (362) Tran, J.; Master, Z.; Yu, J.; Rak, J.; Dumont, D.; Kerbel, R. *Proc. Natl. Acad. Sci. U.S.A.* **2002**, *99*, 4349.
- (363) Wild, R.; Dings, R.; Subramanian, I.; Ramakrishnan, S. *Int. J. Cancer* **2004**, *110*, 343.
- (364) Fukumura, D.; Jain, R. *Microvasc. Res.* **2007**, *74*, 72.
- (365) Itakura, J.; Ishiwata, T.; Shen, B.; Kornmann, M.; Korc, M. *Int. J. Cancer* **2000**, *85*, 27.
- (366) Garcea, G.; Neal, C.; Pattenden, C.; Steward, W.; Berry, D. *Eur. J. Cancer* **2005**, *41*, 2213.
- (367) von Marschall, Z.; Cramer, T.; Höcker, M.; Burde, R.; Plath, T.; Schirmer, M.; Heidenreich, R.; Breier, G.; Riecken, E.; Wiedenmann, B. *Gastroenterology* **2000**, *119*, 1358.
- (368) Collingridge, D.; Carroll, V.; Glaser, M.; Aboagye, E.; Osman, S.; Hutchinson, O.; Barthel, H.; Luthra, S.; Brady, F.; Bicknell, R. *Cancer Res.* **2002**, *62*, 5912.
- (369) Jayson, G.; Zweit, J.; Jackson, A.; Mulatero, C.; Julyan, P.; Ranson, M.; Broughton, L.; Wagstaff, J.; Hakansson, L.; Groenewegen, G. *J. Natl. Cancer Inst.* **2002**, *94*, 1484.
- (370) Subbarayan, M.; Hafeli, U. O.; Feyes, D. K.; Unnithan, J.; Emancipator, S. N.; Mukhtar, H.; Subbarayan, M.; Hafeli, U. O.; Feyes, D. K.; Unnithan, J.; Emancipator, S. N.; Mukhtar, H. *J. Nucl. Med.* **2003**, *44*, 650.
- (371) Dong, D.; Dubeau, L.; Bading, J.; Nguyen, K.; Luna, M.; Yu, H.; Gazit-Bornstein, G.; Gordon, E. M.; Gomer, C.; Hall, F. L.; Gambhir, S. S.; Lee, A. S. *Hum. Gene Ther.* **2004**, *15*, 553.
- (372) Hamblin, M. R.; O'Donnell, D. A.; Murthy, N.; Contag, C. H.; Hasan, T. *Photochem. Photobiol.* **2002**, *75*, 51.
- (373) Moriyama, E. H.; Bisland, S. K.; Lilge, L.; Wilson, B. C.; Moriyama, E. H.; Bisland, S. K.; Lilge, L.; Wilson, B. C. *Photochem. Photobiol.* **2004**, *80*, 242.
- (374) Zaccolo, M. *Circ. Res.* **2004**, *94*, 866.
- (375) Giepmans, B.; Adams, S.; Ellisman, M.; Tsien, R. *Science* **2006**, *312*, 217.
- (376) Goedhart, J.; Gadella, T. *J. R. Soc. Interface* **2009**, *6*, S27.
- (377) Wang, Y.; John, Y.; Chien, S. *Annu. Rev. Biomed. Eng.* **2008**, *10*, 1.
- (378) Mitra, S.; Cassar, S.; Niles, D.; Puskas, J.; Frelinger, J.; Foster, T. *Mol. Cancer Ther.* **2006**, *5*, 3268.
- (379) Zhou, X.; Pogue, B.; Chen, B.; Demidenko, E.; Joshi, R.; Hoopes, J.; Hasan, T. *Int. J. Radiat. Oncol., Biol., Phys.* **2006**, *64*, 1211.
- (380) Castano, A.; Liu, Q.; Hamblin, M. *Br. J. Cancer* **2006**, *94*, 391.
- (381) Novak, J.; Georgakoudi, I.; Wei, X.; Prossin, A.; Lin, C. *Opt. Lett.* **2004**, *29*, 77.
- (382) Boutrus, S.; Greiner, C.; Hwu, D.; Chan, M.; Kuperwasser, C.; Lin, C.; Georgakoudi, I. *J. Biomed. Opt.* **2007**, *12*, 020507.
- (383) He, W.; Wang, H.; Hartmann, L.; Cheng, J.; Low, P. *Proc. Natl. Acad. Sci. U.S.A.* **2007**, *104*, 11760.
- (384) Sackstein, R.; Merzaban, J.; Cain, D.; Dagia, N.; Spencer, J.; Lin, C.; Wohlgemuth, R. *Nat. Med.* **2008**, *14*, 181.
- (385) Celso, C.; Fleming, H.; Wu, J.; Zhao, C.; Miake-Lye, S.; Fujisaki, J.; Côté, D.; Rowe, D.; Lin, C.; Scadden, D. *Nature* **2008**, *457*, 92.
- (386) Cummings, R.; Mitra, S.; Lord, E.; Foster, T. *J. Biomed. Opt.* **2008**, *13*, 044041.
- (387) Cummings, R.; Mitra, S.; Foster, T.; Lord, E. *Radiat. Res.* **2009**, *171*, 687.
- (388) Göppert-Mayer, M. *Ann. Phys.* **1931**, *9*, 273.
- (389) Göppert-Mayer, M. *Ann. Phys.* **2009**, *18*, 466 (reprint of 1931 paper).
- (390) Helmchen, F.; Denk, W. *Nat. Methods* **2005**, *2*, 932.
- (391) Perentes, J.; McKee, T.; Ley, C.; Mathiew, H.; Dawson, M.; Padera, T.; Munn, L.; Jain, R.; Boucher, Y. *Nat. Methods* **2009**, *6*, 143.
- (392) Fisher, W.; Partridge, W.; Dees, C.; Wachter, E. *Photochem. Photobiol.* **1997**, *66*, 141.
- (393) Bhawalkar, J.; Kumar, N.; Zhao, C.; Prasad, P. *J. Clin. Laser Med. Surg.* **1997**, *15*, 201.
- (394) Karotki, A.; Kruk, M.; Drobizhev, M.; Rebane, A.; Nickel, E.; Spangler, C. *IEEE J. Sel. Top. Quantum Electron.* **2001**, *7*, 971.
- (395) Spangler, C.; Starkey, J.; Rebane, A.; Meng, F.; Gong, A.; Drobizhev, M. *Proc. SPIE—Int. Soc. Opt. Eng.* **2006**, *6139*, 61390X.
- (396) Starkey, J.; Rebane, A.; Drobizhev, M.; Meng, F.; Gong, A.; Elliott, A.; McInnerney, K.; Spangler, C. *Clin. Cancer Res.* **2008**, *14*, 6564.
- (397) Drobizhev, M.; Stepanenko, Y.; Dzenis, Y.; Karotki, A.; Rebane, A.; Taylor, P.; Anderson, H. *J. Am. Chem. Soc.* **2004**, *126*, 15352.
- (398) Drobizhev, M.; Stepanenko, Y.; Dzenis, Y.; Karotki, A.; Rebane, A.; Taylor, P.; Anderson, H. *J. Phys. Chem. B* **2005**, *109*, 7223.
- (399) Drobizhev, M.; Meng, F.; Rebane, A.; Stepanenko, Y.; Nickel, E.; Spangler, C. *J. Phys. Chem. B* **2006**, *110*, 9802.
- (400) Oar, M.; Dichtel, W.; Serin, J.; Frechet, J.; Rogers, J.; Slagle, J.; Fleitz, P.; Tan, L.; Ohulchanskyy, T.; Prasad, P. *Chem. Mater.* **2006**, *18*, 3682.
- (401) Kim, S.; Ohulchanskyy, T.; Pudavar, H.; Pandey, R.; Prasad, P. *J. Am. Chem. Soc.* **2007**, *129*, 2669.
- (402) Vanderkooi, J.; Maniara, G.; Green, T.; Wilson, D. *J. Biol. Chem.* **1987**, *262*, 5476.
- (403) Estrada, A. D.; Ponticorvo, A.; Ford, T. N.; Dunn, A. K. *Opt. Lett.* **2008**, *33*, 1038.
- (404) Sterenborg, H.; de Wolf, J.; Koning, M.; Kruijt, B.; van den Heuvel, A.; Robinson, D. *Opt. Express* **2004**, *12*, 1873.
- (405) Jarvi, M.; Niedre, M.; Patterson, M.; Wilson, B. *Photochem. Photobiol.* **2006**, *82*, 1198.
- (406) Snyder, J.; Skovsen, E.; Lambert, J.; Poulsen, L.; Ogilby, P. *Phys. Chem. Chem. Phys.* **2006**, *8*, 4280.
- (407) Lee, S.; Vu, D.; Hinds, M.; Davis, S.; Liang, A.; Hasan, T. *J. Biomed. Opt.* **2008**, *13*, 064035.
- (408) Lee, S.; Galbally-Kinney, K.; Hinds, M.; O'Hara, J.; Pogue, B.; Liang, A.; Hasan, T.; Davis, S. *Proc. SPIE—Int. Soc. Opt. Eng.* **2009**, *7380*, 738046.

CR900300P